

David Taylor Research Center

Bethesda, Maryland 20884-5000

AD-A203 981

DTRC-88/040 November 1988

Propulsion and Auxiliary Systems Department
Research and Development Report

Studies of Liquid Metal Flows and Power Losses in Ducts With Moving Conducting Wall, Slanted Magnetic Field, and Applied External Electric Potential

by
John S. Walker
Samuel H. Brown
Neal A. Sondergaard

Studies of Liquid Metal Flows and Power Losses in Ducts With Moving Conducting Wall,
Slanted Magnetic Field, and Applied External Electric Potential

DTRC-88/040



DTIC
ELECTE
JAN 30 1989
S H D

Approved for public release; distribution unlimited.

Published previously in the Journal of Applied Physics 64(1),
1 July 1988; and 64(4), 15 August 1988

89 1 30 040

MAJOR DTRC TECHNICAL COMPONENTS

- CODE 011 DIRECTOR OF TECHNOLOGY, PLANS AND ASSESSMENT
 - 12 SHIP SYSTEMS INTEGRATION DEPARTMENT
 - 14 SHIP ELECTROMAGNETIC SIGNATURES DEPARTMENT
 - 15 SHIP HYDROMECHANICS DEPARTMENT
 - 16 AVIATION DEPARTMENT
 - 17 SHIP STRUCTURES AND PROTECTION DEPARTMENT
 - 18 COMPUTATION, MATHEMATICS & LOGISTICS DEPARTMENT
 - 19 SHIP ACOUSTICS DEPARTMENT
 - 27 PROPULSION AND AUXILIARY SYSTEMS DEPARTMENT
 - 28 SHIP MATERIALS ENGINEERING DEPARTMENT

DTRC ISSUES THREE TYPES OF REPORTS:

1. **DTRC reports, a formal series**, contain information of permanent technical value. They carry a consecutive numerical identification regardless of their classification or the originating department.
2. **Departmental reports, a semiformal series**, contain information of a preliminary, temporary, or proprietary nature or of limited interest or significance. They carry a departmental alphanumeric identification
3. **Technical memoranda, an informal series**, contain technical documentation of limited use and interest. They are primarily working papers intended for internal use. They carry an identifying number which indicates their type and the numerical code of the originating department. Any distribution outside DTRC must be approved by the head of the originating department on a case-by-case basis.

UNCLASSIFIED

SECURITY CLASSIFICATION OF THIS PAGE

REPORT DOCUMENTATION PAGE

1a. REPORT SECURITY CLASSIFICATION Unclassified			1b. RESTRICTIVE MARKINGS			
2a. SECURITY CLASSIFICATION AUTHORITY			3. DISTRIBUTION/AVAILABILITY OF REPORT Approved for public release; distribution unlimited.			
2b. DECLASSIFICATION/DOWNGRADING SCHEDULE						
4. PERFORMING ORGANIZATION REPORT NUMBER(S) DTRC 88/040			5. MONITORING ORGANIZATION REPORT NUMBER(S)			
6a. NAME OF PERFORMING ORGANIZATION David Taylor Research Center		6b. OFFICE SYMBOL (if applicable) 2712		7a. NAME OF MONITORING ORGANIZATION		
6c. ADDRESS (City, State, and ZIP Code) Bethesda, MD 20084-5067			7b. ADDRESS (City, State, and ZIP Code)			
8a. NAME OF FUNDING/SPONSORING ORGANIZATION		8b. OFFICE SYMBOL (if applicable)		9. PROCUREMENT INSTRUMENT IDENTIFICATION NUMBER		
8c. ADDRESS (City, State, and ZIP Code)			10. SOURCE OF FUNDING NUMBERS			
			PROGRAM ELEMENT NO 61152N	PROJECT NO ZR00001	TASK NO. ZR0230201	WORK UNIT ACCESSION NO. DN570523
11. TITLE (Include Security Classification) Studies of Liquid Metal Flows and Power Losses in Ducts with Moving Conducting Wall, Slanted Magnetic Field, and Applied External Electric Potential (Unclassified)						
12. PERSONAL AUTHOR(S) Walker, John S., Brown, Samuel H., and Sondergaard, Neal A.						
13a. TYPE OF REPORT Final		13b. TIME COVERED FROM _____ TO _____		14. DATE OF REPORT (Year, Month, Day) November 1988		15. PAGE COUNT 37
16. SUPPLEMENTARY NOTATION This work was performed in conjunction with the University of Illinois at Urbana Champaign, Urbana, Illinois 61801						
17. COSATI CODES			18. SUBJECT TERMS (Continue on reverse if necessary and identify by block number) Current Collector, Rectangular Channel, Magneto-hydrodynamics, Skewed Magnetic Field, Liquid Metal Flows, Moving Wall. (JES)			
FIELD	GROUP	SUB-GROUP				
			19. ABSTRACT (Continue on reverse if necessary and identify by block number)			
20. DISTRIBUTION/AVAILABILITY OF ABSTRACT <input type="checkbox"/> UNCLASSIFIED/UNLIMITED <input type="checkbox"/> SAME AS RPT <input type="checkbox"/> DTIC USERS				21. ABSTRACT SECURITY CLASSIFICATION		
22a. NAME OF RESPONSIBLE INDIVIDUAL Samuel H. Brown			22b. TELEPHONE (Include Area Code) (301) 26703458		22c. OFFICE SYMBOL Code 2712	

CONTENTS

	Page
Liquid-Metal Flows and Power Losses in Ducts with Moving Conducting Wall and Skewed Magnetic Field	1
I. Introduction	1
II. Rectangular Channel Configuration	2
III. Zeroth-Order Mathematical Solutions in Core Regions	4
IV. Zeroth-Order Mathematical Solutions in Free-Shear Layers	5
V. Experimental Evidence for Free-Shear Layers	11
VI. Total Current and Power Losses Between Electrodes in the Core	11
VII. Discussion and Conclusions	14
Acknowledgments	17
Appendix A: Thickness of Layers in Fully Developed Magnetohydrodynamic Channel Flows	17
Appendix B: Matching Principle Between Hartmann Layer and Core Region	18
Appendix C: Matching Principle Between the Free-Shear Layer and Hartmann Layer	19



Accession For	
NTIS GRA&I	<input checked="" type="checkbox"/>
DTIC TAB	<input type="checkbox"/>
Unannounced	<input type="checkbox"/>
Justification	
By _____	
Distribution/ _____	
Availability Codes	
Dist	Avail and/or Special
A-1	

CONTENTS

	Page
Further Studies of Liquid-Metal Flows and Power Losses in Ducts With a Moving Conducting Wall and a Skewed Magnetic Field	21
I. Introduction	21
II. Nondimensional Magnetohydrodynamic Equations.....	22
III. Free Shear Layer Analysis	23
IV. Generalized Free Shear Layer Solutions	26
V. Viscous Dissipation and Joulean Power Losses	28
VI. Conclusions	30
Acknowledgments	31
Appendix: Hunt and Stewartson's Integral Equation for a Similar Free Shear Layer	31

EXECUTIVE SUMMARY

Fully developed, laminar liquid-metal flows, currents, and power losses in a rectangular channel in a uniform, *skewed* high external magnetic field were studied for high Hartmann numbers, high interaction numbers, low magnetic Reynolds numbers, and different aspect ratios. The channel has insulated side walls that are skewed to the external magnetic field. Both the perfectly conducting moving top wall with an external potential and the stationary perfectly conducting bottom wall at zero potential act as electrodes and are also skewed to the external magnetic field. A solution is obtained for high Hartmann numbers by dividing the flow into three core regions, connected by two free-shear regions, and Hartmann layers along all the channel walls. Mathematical solutions are presented in each region in terms of singular perturbation expansions in negative powers of the Hartmann number.

Numerical calculations are presented for the total current carried by the core region between top and bottom electrodes, Joulean and viscous power losses, and channel resistance at different skewed external magnetic field angles. With the high external magnetic field, the current through the central core region between the electrodes must be parallel to the external magnetic field lines. The two side core regions carry no current to zeroth order. The two free-shear layers carry less current than the central core region. Both free shear layers are treated rigorously and in detail with fundamental magnetohydrodynamic theory. The solution for the free-shear layer velocity profiles are solved in terms of a complex integral equation. The integral equation is solved by the method of quadratures to give the velocity profiles, viscous dissipation and Joulean losses in the free shear layers.

In addition expressions for the viscous dissipation in the six Hartmann layers are presented. The best approximation to the viscous dissipation in the channel is the sum of the $O(M^{3/2})$ contributions from the two free shear layers, the $O(M^{3/2})$ contributions from the two Hartmann layers separating the free shear layers from the insulators, and the $O(M)$ contributions from three of the Hartmann layers separating core regions from the walls. The best approximation to the Joulean power losses in the channel is the sum of the $O(M^2)$ contribution from the central core region which carries an $O(1)$ current between the electrodes and the $O(M^{3/2})$ contributions from the free shear layers. The expressions for the viscous dissipation and Joulean losses in each region involved the products of universal constants electrical potentials and geometric factors. The theoretical magnetohydrodynamic model presented here was developed to provide data to help in the design of liquid-metal current collectors.

ADMINISTRATIVE INFORMATION

This work was a cooperative effort between the David Taylor Research Center and the University of Illinois of Urbana Champaign, Urbana, Illinois 61801. The work was supported by the DTRC Independent Research Program, Director of Naval Research, OCNR10, and administered by the Research Director, DTRC0113 under Program Element 61152N, Project Number ZR00001, Task Area ZR0230201, Work Unit 1-2712-125, Project Title: Orientation Effects in Liquid-Metal Collectors.

Liquid-metal flows and power losses in ducts with moving conducting wall and skewed magnetic field

John S. Walker

University of Illinois at Urbana-Champaign, Urbana, Illinois 61801

Samuel H. Brown and Neal A. Sondergaard

David Taylor Research Center, Bethesda, Maryland 20084-5000

(Received 5 January 1988; accepted for publication 26 February 1988)

Fully developed, laminar liquid-metal flows, currents, and power losses in a rectangular channel in a uniform, *skewed* high external magnetic field were studied for high Hartmann numbers, high interaction numbers, low magnetic Reynolds numbers, and different aspect ratios. The channel has insulating side walls that are skewed to the external magnetic field. Both the perfectly conducting *moving top wall* with an external potential and the stationary perfectly conducting bottom wall at zero potential act as electrodes and are also skewed to the external magnetic field. A solution is obtained for high Hartmann numbers by dividing the flow into three core regions, connected by two free-shear regions, and Hartmann layers along all the channel walls. Mathematical solutions are presented in each region in terms of singular perturbation expansions in negative powers of the Hartmann number. The free-shear layers are treated rigorously and in detail with fundamental magnetohydrodynamic theory. Numerical calculations are presented for the total current carried by the core region between top and bottom electrodes, Joulean and viscous power losses, and channel resistance at different skewed external magnetic field angles. With the high external magnetic field, the current through the central core region between the electrodes must be parallel to the external magnetic field lines. The two side core regions carry no current to the zeroth order. The two free-shear layers carry less current than the central core region. The theoretical magnetohydrodynamic model derived here was developed to provide data to help in the design of liquid-metal current collectors.

INTRODUCTION

Advanced homopolar electrical machinery is being considered for many new applications. This applied research requires the development of mechanisms for transporting high current at low voltages between rotating and stationary members of the machines with minimal losses and maximal operational stability. Thus, liquid metals rather than more conventional brush technology are often used in the sliding electric contact region. Generally, these machines have large external magnetic fields in the region of the current collector, which has a definite effect on the liquid metal by Lorentz force interactions. Thus, to obtain current collector design parameters, one is interested in liquid-metal channel flow problems with applied external magnetic fields and boundary conditions containing combinations of moving and fixed, conducting, or insulating walls. These boundary conditions then roughly correspond to a rotor, stator, or sidewall of the current collector and the liquid metal to the sliding electric contact. While many publications treat theoretical magnetohydrodynamic channel duct flow, only a very small percentage of these investigations have studied problems with moving conducting walls. Brown, Reilly, and Sondergaard¹¹ have studied fully developed, viscous liquid-metal flows and power losses in a rectangular channel with a moving conducting wall in a uniform, external transverse magnetic field for moderate Hartmann numbers. The solutions to the problem were presented in infinite series of a type discussed by Hughes and Young.¹⁰ The rectangular

channel studied had insulating side walls parallel to the magnetic field and a perfectly conducting moving top wall and stationary bottom wall perpendicular to the field. The objective of this paper is to treat rigorously and comprehensively this same problem with two major changes. The homogeneous transverse external magnetic field is changed to a high field strength, homogeneous, skewed magnetic field and an external potential is applied to the conducting moving wall, thus making the channel transport current. These changes complicate the channel problem by removing symmetry. This paper should be considered as part two to the above-mentioned paper.¹¹ Alty¹² presents solutions for a channel with all fixed walls and a skewed magnetic field. His core solutions are correct but his free-shear layer solutions are incorrect. To the authors' knowledge, no other reference in the literature addresses this particular problem.

The purpose of this paper is to present comprehensive two-dimensional analytic mathematical solutions for the flow velocity and electric potential in accordance with the principles of singular perturbation theory and matched asymptotic expansions in the different regions of the channel. For high Hartmann numbers, the channel is divided into three core regions (a central core and two side core regions), two free-shear layers, and Hartmann layers along all the walls. These solutions enable one to investigate the influence on the velocity and electrical potential of insulating side walls and of an external skewed high magnetic field. The results will enable the derivation of the equations for the quantities of technical interest. These quantities are load

Key words
on 1/4 → 3

currents, Joulean and viscous power dissipation, and channel electrical resistance as functions of the skewed external field angle. The rectangular channel problem approximately corresponds to an asymmetric liquid-metal current collector whose channel dimensions are small compared to the radius of curvature of the machine. In this paper a skewed magnetic field was chosen, as opposed to the simpler case treated earlier of a transverse magnetic field, because many current collectors have skewed magnetic fields in relationship to the walls.

In this work analytical expressions are derived for the load current between the electrodes (i.e., moving and stationary conducting wall), Joulean and viscous dissipation, and channel resistance with skewed angle. The parameters of variation are as follows: applied skewed external magnetic field, fluid electrical conductivity and viscosity, and channel aspect ratio. In the work presented herein the pressure gradients are assumed to be zero. Numerical results in nondimensional form are presented, along with the general analytic solutions which can serve as benchmarks for various numerical computation procedures.

This paper presents the first correct mathematical treatment of the free-shear layers resulting from skewed external magnetic field interacting with rectangular liquid-metal-filled channel described. In treating the magnetohydrodynamic flow due to electric current between two circular electrodes embedded in two parallel insulators, with a transverse magnetic field, Hunt and co-workers¹³⁻¹⁵ correctly treat a similar free-shear layer, although their approach is quite different from the present one.

A number of steps here are standard parts of analytical solutions for fully developed magnetohydrodynamic duct flows at high Hartmann numbers.⁹⁻¹⁵ We have reproduced a number of these standard steps here because these solutions are not widely known outside the relatively small magnetohydrodynamic community.

II. RECTANGULAR CHANNEL CONFIGURATION

A. Discussion of problem

The problem discussed in this paper consists of a rectangular channel filled with a liquid metal in a uniform, skewed, high external magnetic field¹² (see Fig. 1). The Hartmann number M is much greater than one ($M \gg 1$). The thin perfectly conducting top wall with an external mean potential is assumed to move at a velocity component U_0 , while the thin perfectly conducting bottom wall is stationary at zero potential. These conducting walls are sometimes referred to as electrodes. The side walls of the channel are insulators. We will consider the case of fully developed laminar flow of an incompressible fluid with uniform electrical conductivity σ , and uniform viscosity μ_f . The rectangular duct has a height of L and a width of $2aL$. We also assumed that no secondary flows are generated during this process, that there is no variation of the duct cross section, and that there is no distortion of the external magnetic field by the flow (low magnetic Reynolds number).

The angle between the skewed external field B_0 and the y axis is θ . In Fig. 2 a rotated coordinate system (x, η, ξ) is shown with respect to the coordinate system (x, y, z) . θ is the

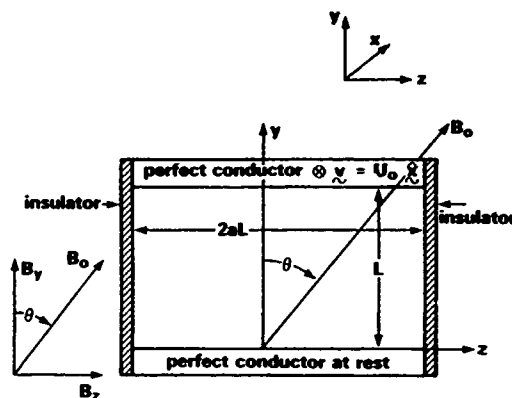


FIG 1. Rectangular channel with skewed external magnetic field and moving and stationary perfect conductor.

angle between the y axis and η axis measured positive in the clockwise direction. The three core regions $C1$, $C2$, and $C3$ are also shown in the figure. \hat{b} is the unit vector in the direction of the external field.

B. Nondimensional magnetohydrodynamic equations

The nondimensional magnetohydrodynamic equations for fully developed laminar duct flow in an external magnetic field at an angle θ with the vertical can be expressed as

$$N^{-1}(\mathbf{v} \cdot \nabla) \mathbf{v} = -\nabla P + \mathbf{j} \times \hat{\mathbf{b}} + M^{-2} \nabla^2 \mathbf{v}, \quad (1a)$$

$$\mathbf{j} = -\nabla \phi + \mathbf{v} \times \hat{\mathbf{b}}, \quad (1b)$$

$$\nabla \cdot \mathbf{v} = 0, \quad (1c)$$

$$\nabla \cdot \mathbf{j} = 0. \quad (1d)$$

In Eq. (1a), $N = \sigma B_0^2 L / \rho U_0$ represents the interaction parameter, the ratio of pondermotive force to the inertial force. $M = LB_0 \sqrt{\sigma / \mu_f}$ is the Hartmann number,¹⁰ the positive square root of the ratio of the pondermotive force¹⁰ to the viscous force. It is assumed during this work that the magnetic Reynolds number¹⁰ $R_m = U_0 L \sigma \mu$ (ratio of induced magnetic field to external magnetic field) is $\ll 1$. The nondimensional variables in Eqs. (1a)–(1d) are defined as

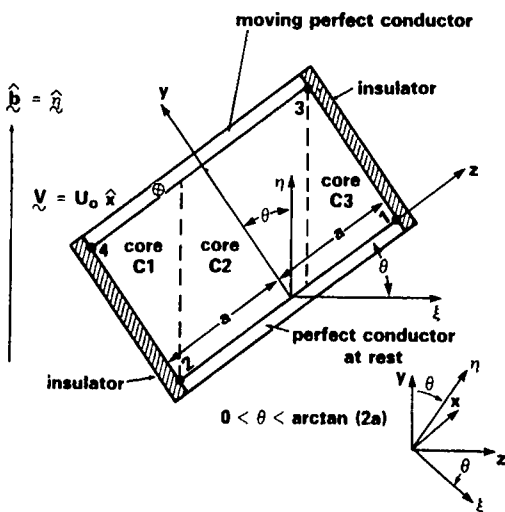


FIG 2 Rectangular channel with coordinate systems (x, y, z) and (x, η, ξ)

\mathbf{v} = fluid velocity vector normalized

$$\text{by } U_0 = \mathbf{V}/U_0, \quad (2a)$$

P = pressure normalized

$$\text{by } \sigma U_0 B_0^2 L = P^*/\sigma U_0 B_0^2 L, \quad (2b)$$

\mathbf{j} = electric current density vector

$$\text{normalized by } \sigma U_0 B_0 = \mathbf{J}/\sigma U_0 B_0, \quad (2c)$$

ϕ = electric potential normalized

$$\text{by } U_0 B_0 L = \phi^*/U_0 B_0 L, \quad (2d)$$

∇ = gradient normalized by $L = L\nabla$,

$\hat{\mathbf{b}}$ = unit vector parallel to the external

$$\text{magnetic field} = \cos \theta \hat{\mathbf{y}} + \sin \theta \hat{\mathbf{z}} \quad (\mathbf{B}_0 = B_0 \hat{\mathbf{b}}), \quad (2e)$$

$\hat{\mathbf{x}}, \hat{\mathbf{y}}, \hat{\mathbf{z}}$ = unit vectors in

$$\text{Cartesian coordinates (see Fig. 1)}. \quad (2f)$$

In the Cartesian system of coordinates (see Fig. 1) the y, z coordinates are normalized by L . The moving, perfectly conducting wall with velocity $U_0 \hat{\mathbf{x}}$ is at $y = 1$; the stationary conducting wall is at $y = 0$. The insulating walls are at $z = \pm a$. The aspect ratio of the channel is represented by $2a$. The magnitude of the external magnetic field B_0 and the angle θ between the field and the vertical is represented in terms of the field components as

$$B_0 = (B_y^2 + B_z^2)^{1/2}, \quad (3a)$$

$$\theta = \arctan(B_z/B_y). \quad (3b)$$

Equation (1a) is the nondimensional Navier-Stoke's equation with an external $\mathbf{j} \times \hat{\mathbf{b}}$ magnetic force. Also, Eq. (1b) is the usual nondimensional expression for the current density in the channel (ohms law), and Eq. (1c) is the nondimensional expression for the incompressibility of the fluid. Equation (1d) is the equation for the conservation of charge.

We define a rotated nondimensional Cartesian coordinate system (x, η, ξ) with the η axis parallel to the external field \mathbf{B}_0 . Therefore, $\hat{\boldsymbol{\eta}}$ equals the unit vector $\hat{\mathbf{b}}$ (see Fig. 2). The coordinate ξ is shown in the figure where $\hat{\boldsymbol{\xi}}$ is the unit vector in the direction ξ . Also note that $\hat{\mathbf{x}}$ is the unit vector in the axial direction along the channel into the plane of the figure. Therefore, in our rotated, right-handed coordinate system the equations describing the locus of the top, bottom, left, and right walls are, respectively,

$$\eta = \sec \theta + (\tan \theta)\xi, \quad (4a)$$

where $-a \cos \theta - \sin \theta \leq \xi \leq a \cos \theta - \sin \theta$,

$$\eta = \tan \theta \xi, \quad (4b)$$

where $-a \cos \theta \leq \xi \leq a \cos \theta$,

$$\eta = -a \csc \theta - (\cot \theta)\xi, \quad (4c)$$

where $-a \cos \theta - \sin \theta \leq \xi \leq -a \cos \theta$,

$$\eta = a \csc \theta - \cot \theta \xi, \quad (4d)$$

where $a \cos \theta - \sin \theta \leq \xi \leq a \cos \theta$. These relationships were derived from geometric considerations.

It should be noted that the unit vectors in the two systems have the relationships:

$$\hat{\mathbf{z}} = \sin \theta \hat{\boldsymbol{\eta}} + \cos \theta \hat{\boldsymbol{\xi}}, \quad (5a)$$

$$\hat{\mathbf{y}} = \cos \theta \hat{\boldsymbol{\eta}} - \sin \theta \hat{\boldsymbol{\xi}}. \quad (5b)$$

In our rotated coordinate system (x, η, ξ) the physically realizable variables for fully developed laminar flow¹⁶ can be expressed as

$$\mathbf{v} = u(\eta, \xi) \hat{\mathbf{x}}, \quad (6a)$$

$$P = P(\eta, \xi), \quad (\text{no axial pressure gradient}), \quad (6b)$$

$$\phi = \phi(\eta, \xi), \quad (6c)$$

$$\mathbf{j} = j_\eta(\eta, \xi) \hat{\boldsymbol{\eta}} + j_\xi(\eta, \xi) \hat{\boldsymbol{\xi}}. \quad (6d)$$

Substituting these variables in Eqs. (1a)–(1d) results in the following convenient system of magnetohydrodynamic equations in terms of the velocity and electrical potential. The electrical potential and flow velocity are variables that are measured in experimental work where

$$j_\xi = M^{-2} \left(\frac{\partial^2 u}{\partial \eta^2} + \frac{\partial^2 u}{\partial \xi^2} \right), \quad (7a)$$

$$j_\eta = -\frac{\partial \phi}{\partial \eta}, \quad j_\xi = -\frac{\partial \phi}{\partial \xi} + u(\eta, \xi), \quad (7b)$$

$$\frac{\partial j_\eta}{\partial \eta} + \frac{\partial j_\xi}{\partial \xi} = 0. \quad (7c)$$

We must now consider the moving perfectly conducting top wall in regard to the current density \mathbf{j}_w and potential ϕ_w . The nondimensional current density in the wall is

$$\mathbf{j}_w = \sigma_w / \sigma (-\nabla \phi_w + \hat{\boldsymbol{\xi}}), \quad (8a)$$

where

$$\hat{\boldsymbol{\xi}} = \mathbf{v}_w \times \hat{\mathbf{b}} = \hat{\mathbf{x}} \times \hat{\boldsymbol{\eta}}. \quad (8b)$$

Since the wall is a perfect conductor, the conductivity of the wall $\sigma_w \gg \sigma$, where σ is the conductivity of the conducting fluid in the channel. For ohms law in the magnetohydrodynamic approximation, it can be shown as $\sigma_w \rightarrow \infty$ that $\nabla \phi_w$ must equal $\hat{\boldsymbol{\xi}}$ for a finite current in a perfect conductor. Maxwell's equation $\nabla \times \mathbf{H} = \mathbf{j}$ determines the induced current in the system. Therefore, in the top wall $\phi_w = \phi_0 + \xi$, where ϕ_0 is the electrode potential at $\xi = 0$ and $\nabla = (\partial/\partial \eta) \hat{\boldsymbol{\eta}} + (\partial/\partial \xi) \hat{\boldsymbol{\xi}}$. Similarly, in the bottom wall $\nabla \phi = 0$ and $\phi_w = 0$ in the bottom conducting wall of the channel.

It is now necessary to specify the boundary conditions on the four walls of the rectangular channel. The top moving perfectly conducting wall of the channel has the following boundary conditions on the nondimensional velocity $u(\eta, \xi)$ and the potential $\phi(\eta, \xi) = \phi$:

$$u(\eta, \xi) = 1, \quad (9a)$$

$$\phi(\eta, \xi) = \phi = \phi_0 + \xi \text{ at } \eta = \sec \theta + (\tan \theta)\xi, \quad (9b)$$

where

$$-a \cos \theta - \sin \theta \leq \xi \leq a \cos \theta - \sin \theta.$$

The bottom perfectly conducting wall has the boundary conditions

$$u(\eta, \xi) = 0, \quad \phi = 0 \text{ at } \eta = (\tan \theta)\xi, \quad (9c)$$

where

$$-a \cos \theta \leq \xi \leq a \cos \theta.$$

The left-hand insulating wall has the boundary conditions

$$u(\eta, \xi) = 0, \quad \sin \theta j_\eta + \cos \theta j_\xi = 0, \text{ at } \eta = -a \csc \theta - (\cot \theta) \xi, \quad (9d)$$

where

$$-a \cos \theta - \sin \theta \leq \xi \leq -a \cos \theta.$$

Here it must be remembered that the current density lines must be parallel to the insulating wall. Similarly, the right-hand insulating wall has the boundary condition

$$u(\eta, \xi) = 0, \quad (10a)$$

$$\sin \theta j_\eta + \cos \theta j_\xi = 0, \text{ at } \eta = a \csc \theta - \cot \theta \xi \quad (10b)$$

for $a \cos \theta - \sin \theta \leq \xi \leq a \cos \theta$.

In this work the Hartmann number M is always assumed to be high (i.e., $M \gg 1$). In this case it can be shown that distinct subregions of flow exist in the channel and are shown in Fig. 3. In Appendix A is a derivation of the order of thickness of the various regions in the channel. The angle θ has the range of values $0 < \theta < \arctan(2a)$.

In the inertialess core regions $C1$, $C2$, and $C3$, the first partial derivatives $\partial/\partial \xi$ and $\partial/\partial \eta$ are of $O(1)$. In the inertialess Hartmann layers $h1-h6$, the layers are of approximately $O(M^{-1})$ thickness and have $O(M)$ normal derivatives. f_1 and f_2 are inertialess free-shear layers (or interior regions) which have the following characteristics:

- (1) The layers separate the different core regions.
- (2) The layers lie along magnetic field lines through the corners and are driven by current singularities at the corners.
- (3) The layers have $O(M^{-1/2})$ thickness (see Appendix A for detailed derivation).
- (4) The first partial derivatives are of orders $\partial/\partial \xi = O(M^{1/2})$, while $\partial/\partial \eta = O(1)$.

III. ZEROth ORDER MATHEMATICAL SOLUTIONS IN CORE REGIONS

A. Development of theory

The generalized mathematical solutions in the cores, where the magnetic field angle θ has the limits $0 < \theta < \arctan(2a)$

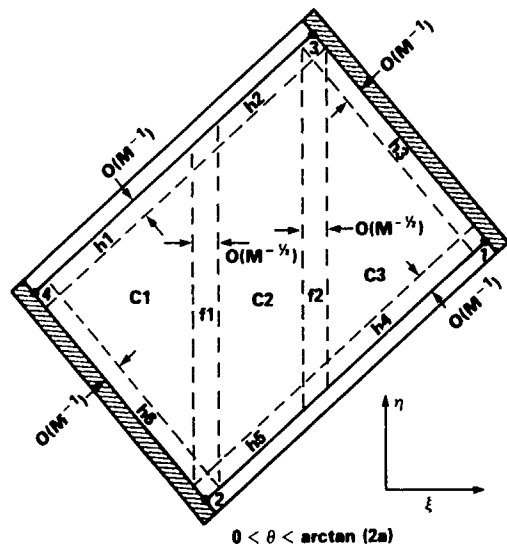


FIG. 3. Subregions in magnetohydrodynamic channel at high external magnetic fields

$\tan(2a)$, can be obtained from Eqs. (7b) and (7c) if the term of $O(M^{-2})$ is neglected [i.e., $j_\xi = M^{-2}(\partial^2 u/\partial \eta^2 + \partial^2 u/\partial \xi^2)$], the generalized core solutions can be expressed as

$$\phi_C(\eta, \xi) = -\eta j_{\eta C}(\xi) + \psi_C(\xi), \quad (11a)$$

$$u_C(\eta, \xi) = \frac{\partial \phi}{\partial \xi} = -\eta \frac{dj_{\eta C}(\xi)}{d\xi} + \frac{d\psi_C(\xi)}{d\xi}, \quad (11b)$$

and the current density components are

$$j_{\xi C} = 0, \quad j_{\eta C} = j_{\eta C}(\xi). \quad (11c)$$

The methods of singular perturbation expansions and matched asymptotic expansions at the boundaries between the Hartmann layer and core region are applied to the complex system of coupled equations to obtain the core solutions in the different core regions to zeroth order.

For continuity, the well-known matching principle between the core and Hartmann boundary layer will be stated here to the zeroth order.¹⁷ If a physically realizable function $u_C(x; M)$ at high Hartmann number can be expanded in the core as

$$u_C(x; M) = u_{C0}(x) + M^{-1}u_{C1}(x) + M^{-2}u_{C2}(x) + \dots, \quad (12)$$

where x is an independent variable, and the function $u_b(X; M)$ can be expanded at high Hartmann number M in the Hartmann layer as

$$u_b(X; M) = u_{b0}(X) + M^{-1}u_{b1}(X) + M^{-2}u_{b2}(X), \quad (13)$$

where X is a stretched coordinate,¹⁶ then

$$u_{C0}(0) = \lim_{X \rightarrow \infty} [u_{b0}(X)], \quad (14)$$

where $u_{C0}(0)$ is the value of the zeroth order function at the wall. The boundary layer value in the Hartmann layer in stretched coordinates is the value away from the wall as $X \rightarrow \infty$ (see Appendix B for details).

Cook, Ludford, and Walker¹⁸ proved that if there is a jump to $O(1)$ in the velocity u across the Hartmann layer, then the jumps in $j \cdot \hat{\eta}$ and ϕ are at most $O(M^{-1})$. The jump in ϕ is $O(M^{-2})$ for an insulator or a perfect conductor with a normal magnetic field, but it is $O(M^{-1})$ for a perfect conductor with a skewed magnetic field. Therefore, to zeroth order, we shall assume that the potential throughout the boundary is the same as the wall potential. The asymptotic expansions for the potential ϕ_C in the core area C are assumed to have the form¹⁶

$$\phi_C(\eta, \xi, M) = \phi_{C0}(\eta, \xi) + M^{-1}\phi_{C1}(\eta, \xi) + M^{-2}\phi_{C2}(\eta, \xi). \quad (15)$$

Thus, the matching condition on the bottom and top perfect conductor of the channel for the potential $\phi_{C2,0}$ in the core $C2$ to zeroth order is

$$0 = \phi_{C2,0}(\eta = \tan \theta \xi) = -(\tan \theta) \xi j_{\eta C2,0}(\xi) + \psi_{C2,0}(\xi) \quad (16a)$$

for $-a \cos \theta \leq \xi \leq a \cos \theta$ (stationary perfect conductor),

$$\begin{aligned} (\phi_0 + \xi) &= \phi_{C2,0}[\eta = \sec \theta + (\tan \theta) \xi] \\ &= -(\sec \theta + \tan \theta \xi) j_{\eta C2,0}(\xi) + \psi_{C2,0}(\xi) \end{aligned} \quad (16b)$$

for $-a \cos \theta - \sin \theta \leq \xi \leq a \cos \theta - \sin \theta$ (moving perfect conductor). The zeroth-order solution for the potential in the Hartmann layers along each perfect conductor was not needed because the change in ϕ across the layer is only $O(M^{-1})$, and using the value of the potential at the wall was sufficient.

Solving these two simple simultaneous boundary value equations (16a) and (16b) and simple algebraic manipulation of the magnetohydrodynamic equations (7a)–(7c) for core C2 results in the expressions

$$j_{\xi C2,0} = 0, \quad j_{\eta C2,0} = -\cos \theta (\phi_0 + \xi), \quad (17a)$$

$$\phi_{C2,0} = \cos \theta (\phi_0 + \xi) \eta - \sin \theta (\phi_0 + \xi) \xi, \quad (17b)$$

$$u_{C2,0} = (\cos \theta) \eta - \sin \theta (\phi_0 + 2\xi), \quad (17c)$$

$$u_{C2,0} = -\sin \theta (\phi_0 + \xi) \text{ for } \eta \\ = (\tan \theta) \xi \text{ (bottom wall),} \quad (17d)$$

$$u_{C2,0} = 1 - \sin \theta (\phi_0 + \xi) \text{ for } \eta = \sec \theta + \tan \theta \xi. \quad (17e)$$

It is interesting to note that to zeroth order there is a jump in u_{C2} across each Hartmann layer for $\theta \neq 0$.

From similar arguments the zeroth order solutions in core C1 are

$$j_{\eta C1,0} = j_{\xi C1,0} = 0, \quad (18a)$$

$$\phi_{C1,0} = \xi, \quad u_{C1,0} = 1, \quad (18b)$$

and the zeroth-order solutions in core C3 are

$$j_{\eta C3,0} = 0, \quad j_{\xi C3,0} = 0, \quad (19a)$$

$$\phi_{C3,0} = 0, \quad u_{C3,0} = 0. \quad (19b)$$

B. Discussion of core solutions of zeroth order

To zeroth order in the core C1 the velocity is $u_{C1,0} = 1$ throughout the region. Thus, the core has the same velocity throughout the core region as the moving wall. The two components of current density in core C1 to zeroth order $j_{\xi C1,0}$ and $j_{\eta C1,0}$ both equal zero. Also, the potential to zeroth order throughout core C1 is $\phi_{C1,0} = \phi_0 + \xi$.

To zeroth order in core C2 the current density follows the external magnetic field \mathbf{B}_0 and thus $j_{\xi C2,0} = 0$ and $j_{\eta C2,0} = -\cos \theta (\phi_0 + \xi)$. The potential $\phi(\eta, \xi)$ and $u(\eta, \xi)$ to zeroth order are functions of η, ξ [see Eqs. (17b) and (17c)]. It is interesting to note that to zeroth order there is a jump in u_{C2} across each Hartmann layer at the top and bottom wall when $\theta \neq 0$.

In core C3 to zeroth order $u_{C3,0}$ equals zero throughout the region. The core C3 flow thus has no velocity throughout the region. Both components of current density in core C3, $j_{\eta C3,0}$ and $j_{\xi C3,0}$ are zero as in core C1. The potential $\phi_{C3,0}$ is also zero throughout the core to zeroth order.

IV. ZERO-ORDER MATHEMATICAL SOLUTIONS IN FREE-SHEAR LAYERS

A. Development of basic theoretical concepts

The free-shear layers¹² in regions $f1$ and $f2$ in coordinates (x, t, ξ) are shown in Fig. 4. The corner region of the free-shear layer $f1$ between the insulating wall and the perfect conductor is at $(t = 0, \xi = -a \cos \theta)$. The free-shear

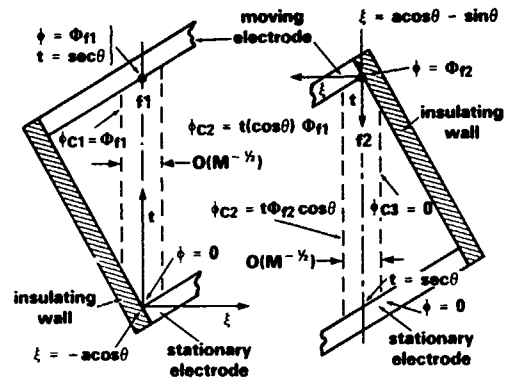


FIG. 4. Free-shear layers in regions $f1$ and $f2$ in coordinates (x, t, ξ) for $f1$, $t = \eta + a \sin \theta$, $\Phi = \phi_m + \sin \theta - a \cos \theta$ and for $f2$, $t = \sec \theta - \sin \theta (\tan \theta - a) - \eta$

layer $f2$ has the corner region between the insulating wall and the perfect conductor at $(t = 0, \xi = a \cos \theta - \sin \theta)$.

We shall work out the fundamental mathematical theory for shear layer $f1$; the theory for shear layer $f2$ can be performed in a similar manner. To develop the theory, the stretched coordinate ζ will be used. It is defined as follows:

$$\zeta = M^{1/2} (\xi + a \cos \theta), \quad \xi = -a \cos \theta + M^{-1/2} \zeta, \quad (20a)$$

$$\frac{\partial}{\partial \xi} = \frac{d\zeta}{d\xi} \frac{\partial}{\partial \zeta} = M^{1/2} \frac{\partial}{\partial \zeta}. \quad (20b)$$

Using Eqs. (7a)–(7c), the fundamental magnetohydrodynamic equations in the free-shear layer $f1$ for fully developed flow in stretched coordinate ζ and regular coordinate η are

$$j_{\xi}(\eta, \zeta) = \frac{1}{M^2} \left(\frac{\partial^2 u}{\partial \eta^2} + M \frac{\partial^2 u}{\partial \zeta^2} \right), \\ j_{\eta} = -\frac{\partial \phi(\eta, \zeta)}{\partial \eta}, \quad (21a)$$

$$j_{\xi}(\eta, \zeta) = -M^{1/2} \frac{\partial \phi}{\partial \zeta} + u(\eta, \zeta), \quad (21b)$$

$$\frac{\partial j_{\eta}(\eta, \zeta)}{\partial \eta} + M^{1/2} \frac{\partial j_{\xi}(\eta, \zeta)}{\partial \zeta} = 0. \quad (21c)$$

The first terms in the series solutions in the free-shear layer $f1$ are

$$j_{\eta}(\eta, \zeta) = j_{\eta f1,0}(\eta, \zeta), \quad (22a)$$

$$\phi(\eta, \zeta) = \phi_{f1,0}(\eta, \zeta), \quad (22b)$$

$$j_{\xi} = M^{-1/2} j_{\xi f1,0}(\eta, \zeta), \quad (22c)$$

$$u = M^{1/2} u_{f1,0}(\eta, \zeta). \quad (22d)$$

From Eqs. (22a)–(22d) the following relationships can be developed for the potential function $\phi_{f1,0}(\eta, \zeta)$

$$u_{f1,0}(\eta, \zeta) = \frac{\partial \phi_{f1,0}(\eta, \zeta)}{\partial \zeta}, \quad (23a)$$

$$j_{\eta f1,0}(\eta, \zeta) = -\frac{\partial \phi_{f1,0}(\eta, \zeta)}{\partial \eta}, \quad (23b)$$

$$j_{\xi f1,0}(\eta, \zeta) = \frac{\partial^3 \phi_{f1,0}(\eta, \zeta)}{\partial \zeta^3}. \quad (23c)$$

Using the conservation of charge, Eq. (21c), and Eqs. (22a) and (22c), the following fourth-order partial differential equation is derived:

$$\frac{\partial^2 \phi_{f1,0}(\eta, \zeta)}{\partial \eta^2} = \frac{\partial^4 \phi_{f1,0}(\eta, \zeta)}{\partial \zeta^4}, \quad (24)$$

for $-a \sin \theta \leq \eta \leq -a \sin \theta + \sec \theta$ and $-\infty < \zeta < \infty$ for free-shear layer $f1$ (see Fig. 5).

The stretch coordinate ζ must extend from $-\infty$ to ∞ in accordance with the definition of stretched coordinates. This figure also shows the core potentials ϕ_{C1} and ϕ_{C2} , which must be matched by the sides of the free-shear layer. $\phi_{f1,0}(\eta, \zeta)$ must satisfy the following boundary conditions:

(1) Boundary condition at core C 2:

$$\phi_{f1,0} \rightarrow \cos \theta (\phi_0 - a \cos \theta) (\eta + a \sin \theta) \text{ as } \zeta \rightarrow \infty. \quad (25a)$$

(2) Boundary condition at core C 1:

$$\phi_{f1,0} \rightarrow \phi_0 - a \cos \theta \text{ as } \zeta \rightarrow -\infty. \quad (25b)$$

(3) Boundary condition at moving perfect conductor:

$$\phi_{f1,0} = \phi_0 - a \cos \theta, \quad \text{at } \eta = \sec \theta - a \sin \theta \text{ for } -\infty < \zeta < \infty. \quad (25c)$$

(4) Boundary condition at fixed perfect:

$$\phi_{f1,0} = 0 \text{ at } \eta = -a \sin \theta \text{ for } 0 < \zeta < \infty. \quad (25d)$$

(5) Boundary condition at Hartmann layer between free-shear layer $f1$ and insulating wall (see Fig. 6):

$$j_{\eta f1}(-a \sin \theta, \zeta) = \text{sgn}(\sin \theta) \frac{\partial^2 \phi_{f1,0}}{\partial \zeta^2}(-a \sin \theta, \zeta). \quad (25e)$$

Boundary condition (5) will be derived in the following subsection.

B. Boundary condition on Hartmann layer and free-shear layer

For external magnetic field angles in the range of $0 < \theta < \arctan(2a)$, the Hartmann layers play a relatively passive role except when they are adjacent to free-shear layer

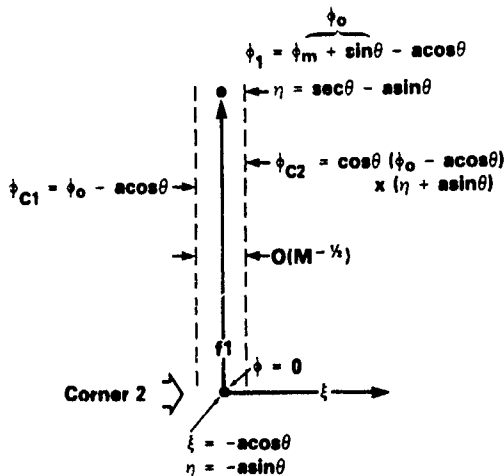


FIG 5. Free-shear layer at $\xi = -a \cos \theta$, $f1$

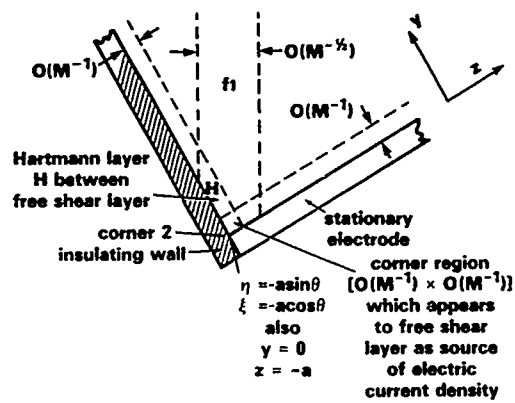


FIG. 6. Free-shear layer at region $f1$.

ers (see Fig. 7). For Hartmann layers adjacent to core regions, the layer matches any core velocity and satisfies $u = 0$ or 1, depending on the wall. The change in u across the Hartmann layer to the wall has a simple exponential structure.

Figures 3 and 6 show the Hartmann layer along the insulating wall. To treat the Hartmann layer, we will return to the original Cartesian coordinates (x, y, z) . Equations (1a)–(1d) for magnetohydrodynamic fully developed flow in the original coordinates are

$$0 = \sin \theta j_y - \cos \theta j_z + M^{-2} \left(\frac{\partial^2 u}{\partial y^2} + \frac{\partial^2 u}{\partial z^2} \right), \quad (26a)$$

$$j_y = -\frac{\partial \phi}{\partial y} - (\sin \theta) u, \quad (26b)$$

$$j_z = -\frac{\partial \phi}{\partial z} + (\cos \theta) u, \quad (26c)$$

$$\frac{\partial j_y}{\partial y} + \frac{\partial j_z}{\partial z} = 0, \quad (26d)$$

where

$$\mathbf{j} = j_y(y, z) \hat{y} + j_z(y, z) \hat{z}, \quad (26e)$$

$$\mathbf{v} = u(y, z) \hat{x}, \quad (26f)$$

$$\phi = \phi(y, z). \quad (26g)$$

The stretching coordinate for the y direction in the Hartmann layer (tangential direction along insulating wall) is approximately

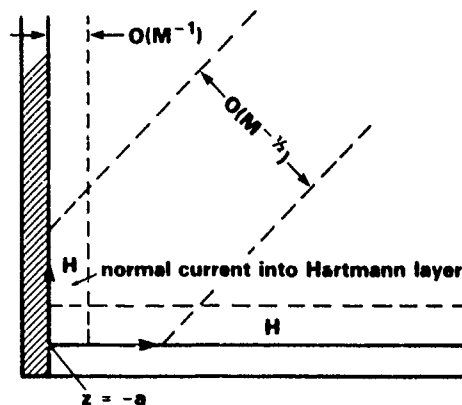


FIG. 7. Hartmann layer H between free-shear layer and insulator at $y = 0$, $z = -a$.

$$Y = M^{1/2}y, \quad y = M^{-1/2}Y, \quad \frac{\partial}{\partial y} = M^{1/2} \frac{\partial}{\partial Y} \quad (27)$$

(see Figs. 6 and 7). The stretching is needed because the Hartmann layer is adjacent to the free-shear layer where variables vary over $O(M^{-1/2})$ distances through the layer. The stretched coordinate normal to the Hartmann layer is

$$Z = M(z + a), \quad z = -a + M^{-1}Z, \quad \frac{\partial}{\partial z} = M \frac{\partial}{\partial Z} \quad (28)$$

The first terms in the series for the solutions to the magneto-hydrodynamic equations are

$$u = M^{1/2}u_H(Y, Z), \quad \phi = \phi_H(Y, Z), \quad (29a)$$

$$j_y = M^{1/2}j_{yH}(Y, Z), \quad j_z = j_{zH}(Y, Z). \quad (29b)$$

The Hartmann layer must match the $O(M^{1/2})$ velocity in the free-shear layer, while the Hartmann layer current density along the insulator is of the same order of magnitude as the velocity $O(M^{1/2})$. The magnetohydrodynamic equations in the Hartmann layer in stretched coordinates can be written as

$$0 = \sin \theta j_{yH} + \frac{\partial^2 u_H}{\partial Z^2}, \quad (30a)$$

$$j_{yH} = -\frac{\partial \phi_H}{\partial Y} - (\sin \theta)u_H, \quad (30b)$$

$$\frac{\partial \phi_H}{\partial Z} = 0 \text{ for } 0 \leq Y < \infty \text{ and } 0 \leq Z < \infty, \quad (30c)$$

$$\frac{\partial j_{yH}}{\partial Y} + \frac{\partial j_{zH}}{\partial Z} = 0. \quad (30d)$$

At the insulating wall $Z = 0$ in the stretched coordinate and the velocity $u_H(Y, Z = 0) = 0$ and the current density $j_{zH}(Y, Z = 0) = 0$. Since the partial derivative of $\phi_{H,0}$ with respect to Z is zero, $\Phi_H = \Phi_H(Y)$. Therefore, the current density can be expressed as

$$j_{yH} = -\frac{d\phi_H(Y)}{dY} - (\sin \theta)u_H(Y, Z). \quad (31)$$

Substituting Eq. (31) into Eq. (30a) results in the partial differential equation

$$\frac{\partial^2 u_H(Y, Z)}{\partial Z^2} - \sin^2 \theta u_H(Y, Z) = (\sin \theta) \frac{d\phi_H(Y)}{dY}. \quad (32a)$$

The solution which satisfies $u_H = 0$ and which does not grow exponentially as $Z \rightarrow \infty$ is

$$\begin{aligned} \phi_{f1} \{ & -a \sin \theta + M^{-1/2}Y \cos \theta + M^{-1}(\sin \theta)Z, -Y \sin \theta + M^{-1/2} \cos \theta Z \} \\ & = \phi_{f1}(-a \sin \theta, -Y \sin \theta) + [M^{-1/2}Y \cos \theta + M^{-1}(\sin \theta)Z] \frac{\partial \phi_{f1}}{\partial \eta}(-a \sin \theta, -Y \sin \theta) \\ & + M^{-1/2} \cos \theta Z \frac{\partial \phi_{f1}}{\partial \zeta}(-a \sin \theta, -Y \sin \theta) + \dots \end{aligned} \quad (39)$$

Only the leading term $\phi_{f1}(-a \sin \theta, -Y \sin \theta)$, enters the matching of the zeroth-order variables. The other terms in the Taylor series expansions of the zeroth order free-shear layer variables enter the matching at higher orders. Physi-

$$u_H(Y, Z) = -\csc \theta \frac{d\phi_H(Y)}{dY} [1 - \exp(-|\sin \theta|Z)], \quad (32b)$$

where the term $|\sin \theta|$ has been used in case θ is negative in the problem. The component of the current density in the y direction is obtained from Eqs. (31) and (32a)

$$j_{yH}(Y, Z) = -\frac{d\phi_H(Y)}{dY} \exp(-|\sin \theta|Z). \quad (33)$$

Using the conservation of charge condition Eq. (30d) in stretched coordinates

$$\frac{\partial j_{zH}}{\partial Z} = \frac{d^2 \phi_H(Y)}{dY^2} \exp(-|\sin \theta|Z) \quad (34)$$

results in the solution for $j_{zH}(Y, Z)$ after integrating from $Z = 0$ to $Z = Z$:

$$j_{zH} = |\csc \theta| \frac{d^2 \phi_H(Y)}{dY^2} [1 - \exp(-|\sin \theta|Z)]. \quad (35)$$

We now need to match the free-shear layer and the Hartmann layer solutions at the boundary. The geometric relationship between the coordinates (x, η, ξ) and (x, y, z) are shown on Fig. 2 and are

$$\eta = z \sin \theta + y \cos \theta, \quad (36a)$$

$$\xi = z \cos \theta - y \sin \theta. \quad (36b)$$

In the free-shear layer and adjacent to the Hartmann layer

$$z = -a + M^{-1}Z, \quad y = M^{-1/2}Y, \quad (37a)$$

$$Z = M(z + a), \quad Y = M^{1/2}y, \quad (37b)$$

and

$$\xi = M^{1/2}(\xi + a \cos \theta). \quad (37c)$$

The coordinate transformations (36a) and (36b) after substituting Eqs. (37a) to (37c) are

$$\eta = -a \sin \theta + M^{-1/2}Y \cos \theta + M^{-1}(\sin \theta)Z, \quad (38a)$$

$$\xi = -a \cos \theta - M^{-1/2}Y \sin \theta + M^{-1}(\cos \theta)Z, \quad (38b)$$

$$\xi = M^{1/2}(\xi + a \cos \theta) = -Y \sin \theta + M^{-1/2}(\cos \theta)Z. \quad (38c)$$

In order to match a free-shear variable, such as $\phi_{f1}(\eta, \xi)$, to the corresponding Hartmann layer variable $\phi_H(Y, Z)$, we substitute the expressions (38a) and (38c) into ϕ_{f1} . We then use a Taylor series to obtain the proper form for an asymptotic expansion, namely powers of M times coefficient functions of Y and Z . This process gives

cally the zeroth-order free-shear layer solution sees the Hartmann layer as a zero thickness layer at the horizontal line $\eta = -a \sin \theta$. In fact, the Hartmann layer has a small $O(M^{-1})$ thickness which would enter the higher order

matching through the $M^{-1/2} \cos \theta Z \partial \phi_{f1} / \partial \zeta$ term, and the layer lies along a sloping line, which would enter through the $(M^{-1/2} Y \sin \theta + M^{-1} \sin \theta Z) \partial \phi_{f1} / \partial \eta$ term.

From the matching principle between the free-shear layer and the Hartmann layer along the insulating wall and adjacent to the free-shear layer, we obtain

$$\phi_H(Y) = \phi_{f1}(-a \sin \theta, -Y \sin \theta). \quad (40)$$

This expression is derived in detail in Appendix C, using the velocity instead of the potential.

From expression (40) the following relationship is obtained:

$$\frac{d^2 \phi_H(Y)}{dY^2} = \sin^2 \theta \frac{\partial^2 \phi_{f1}}{\partial \zeta^2} (-a \sin \theta, -Y \sin \theta), \quad (41)$$

$$\times (\zeta = -Y \sin \theta).$$

The z component of the current density is related to the j_ξ and j_η components of the current density by

$$j_z = \cos \theta j_\xi + \sin \theta j_\eta. \quad (42)$$

To zeroth order the normal current density in the Hartmann layer j_{zH} approaches the normal current density in the free-shear layer

$$j_{zH} = \frac{d^2 \phi_H(Y)}{dY^2} - \cos \theta (M^{-1/2} j_{\xi f1}) + \sin \theta j_{\eta f1}(-a \sin \theta, -Y \sin \theta). \quad (43)$$

Therefore, using Eq. (41) the following relationship holds:

$$\sin \theta j_{\eta f1,0}(-a \sin \theta, -Y \sin \theta) = |\csc \theta| \sin^2 \theta \frac{\partial^2 \phi_{f1,0}}{\partial \zeta^2} (-a \sin \theta, -Y \sin \theta). \quad (44)$$

The current coming out of the Hartmann layer into the free-shear layer equals the tangential second partial derivative of the potential in the free-shear layer and is the fifth boundary condition discussed in Eq. (25f):

$$j_{\eta f1,0}(-a \sin \theta, \zeta) = \operatorname{sgn}(\sin \theta) \frac{\partial^2 \phi_{f1,0}}{\partial \zeta^2} (-a \sin \theta, \zeta). \quad (45)$$

C. Partial differential equation and boundary values for free-shear layer

We shall assume the solutions to the partial differential equation (24) and boundary values (25a)–(25e) to be in the form

$$\phi_{f1,0} = \phi_0 - a \cos \theta + \Phi(t, \zeta), \quad (46a)$$

where

$$t = \eta + a \sin \theta \quad (46b)$$

and

$$\sin \theta > 0 \text{ for } f1, \operatorname{sgn}(\sin \theta) = +1. \quad (46c)$$

$\Phi(t, \zeta)$ is treated as a perturbation which approaches zero as $\zeta \rightarrow -\infty$, see boundary condition (25b). Also $\Phi(t, \zeta)$ approaches zero at the moving perfect conductor [see condition (25c)]. The partial differential in terms of $\Phi(t, \zeta)$ with its five boundary conditions in terms of t, ζ is

$$\frac{\partial^2 \Phi(t, \zeta)}{\partial t^2} = \frac{\partial^4 \Phi(t, \zeta)}{\partial \zeta^4} \text{ for } 0 \leq t \leq \sec \theta, -\infty < \zeta < \infty; \quad (47a)$$

Boundary condition at core C2:

$$\Phi(t, \zeta) \rightarrow (\phi_0 - a \cos \theta)(t \cos \theta - 1), \text{ as } \zeta \rightarrow \infty; \quad (47b)$$

Boundary condition at core C1:

$$\Phi(t, \zeta) \rightarrow 0, \text{ as } \zeta \rightarrow -\infty; \quad (47c)$$

Boundary condition at moving perfect conductor:

$$\Phi(t, \zeta) = 0, \text{ at } t = \sec \theta, \text{ for } -\infty < \zeta < \infty; \quad (47d)$$

Boundary condition at fixed perfect conductor:

$$\Phi(t, \zeta) = -(\phi_0 - a \cos \theta), \text{ at } t = 0 \text{ for } 0 < \zeta < \infty; \quad (47e)$$

Boundary condition at Hartmann layer adjacent to free-shear layer:

$$\frac{\partial^2 \Phi(t, \zeta)}{\partial \zeta^2} + \frac{\partial \Phi(t, \zeta)}{\partial t} = 0, \text{ at } t = 0 \text{ for } -\infty < \zeta < 0; \quad (47f)$$

We solved the partial differential equation and its boundary values in terms of the modified complex Fourier transform¹⁸ in the form

$$\bar{\Phi}(t, k) = \int_{-\infty}^{\infty} \exp(-ik\zeta) \Phi(t, \zeta) d\zeta, \quad (48)$$

where k is generalized to become complex in the lower half-plane (i.e., $k = k_1 - ik_2$), or $\operatorname{Im}(k) < 0$. Accordingly, the modified Fourier inversion formula¹⁸ is written as

$$\Phi(t, \zeta) = \frac{1}{(2\pi)} \int_{-\infty - \pi}^{\infty - \pi} \exp(ik\zeta) \bar{\Phi}(t, k) dk. \quad (49)$$

The inversion contour is in the lower half-plane, along the line $\operatorname{Im}(k) = -\tau$.

The Fourier transform of the partial differential equation is in the form

$$\frac{\partial^2 \bar{\Phi}}{\partial t^2} = k^4 \bar{\Phi}, \text{ for } 0 \leq t \leq \sec \theta, \quad (50)$$

where integration by parts has been used to obtain the above form. The right-hand side requires four integrations by parts with

$$\left(\exp(-ik\zeta) \frac{\partial^n \bar{\Phi}}{\partial \zeta^n}(\eta, \zeta) \right)_{\zeta=-\infty}^{\zeta=\infty} = 0. \quad (51)$$

The upper limit $\zeta \rightarrow \infty$ gives zero because $\operatorname{Im}(k) < 0$; the lower limit $\zeta \rightarrow -\infty$ gives zero because of condition (47c).

Fourier transforming Eq. (47d), we recognize that $\bar{\Phi} = 0$, at $t = \sec \theta$, and assume that the general solution of the Fourier transformed partial differential equation [e.g., Eq. (50)] is

$$\bar{\Phi}(t, k) = A(k) \sinh[k^2(\sec \theta - t)], \quad (52a)$$

where

$$\frac{\partial \bar{\Phi}(t, k)}{\partial t} = -k^2 A(k) \cosh[k^2(\sec \theta - t)] \quad (52b)$$

and

$$\frac{\partial^2 \bar{\Phi}(t, k)}{\partial t^2} = k^4 A(k) \sinh[k^2(\sec \theta - t)]. \quad (52c)$$

The boundary value of Eqs. (47f) can be written in the more general form

$$F(\zeta) = \frac{\partial^2 \Phi}{\partial \zeta^2}(0, \zeta) + \frac{\partial \Phi}{\partial t}(0, \zeta), \quad (53a)$$

where

$$F(\zeta) = \begin{cases} 0, & \text{for } -\infty < \zeta < 0, \\ f(\zeta), & \text{for } 0 < \zeta < \infty, \end{cases} \quad (53b)$$

and $f(\zeta)$ is an unknown function. The Fourier transform of $F(\zeta)$ is expressed as

$$\bar{F}(k) = \frac{\partial \bar{\Phi}}{\partial t}(0, k) - k^2 \bar{\Phi}(0, k). \quad (54)$$

Substituting the general expression for $\bar{\Phi}(t, k)$, Eq. (52a), results in the expression

$$\bar{F}(k) = -k^2 A(k) [\cosh(k^2 \sec \theta) + \sinh(k^2 \sec \theta)], \quad (55a)$$

where

$$A(k) = -\bar{F}(k)/k^2 \exp(k^2 \sec \theta). \quad (55b)$$

Therefore $\bar{\Phi}(t, k)$ can be conveniently expressed as

$$\bar{\Phi}(t, k) = -\bar{F}(k) \sinh[k^2(\sec \theta - t)]/k^2 \exp(k^2 \sec \theta) \quad (56a)$$

$$= -[\bar{F}(k)/2k^2] \{ \exp(-tk^2) - \exp[-k^2(2 \sec \theta - t)] \}, \quad (56b)$$

where $\bar{F}(k)$ is an unknown function.

The convolution theorem can be used to obtain $\Phi(t, \zeta)$

$$\Phi(t, \zeta) = \int_{-\infty}^{\infty} F(\zeta^*) G(t, \zeta - \zeta^*) d\zeta^* \quad (57a)$$

and

$$= \int_0^{\infty} f(\zeta^*) G(t, \zeta - \zeta^*) d\zeta^* \quad (57b)$$

using the definition of $F(\zeta)$ expressed in Eq. (53b).

The Green's function $G(t, \zeta)$ can be obtained by the modified inverse Fourier transform [see Eqs. (57a) and (57b)]:

$$G(t, \zeta) = -\frac{1}{(4\pi)} \int_{-\infty}^{\infty} \{ \exp(-tk^2) - \exp[-k^2(2 \sec \theta - t)] \} \exp(ik\zeta) \frac{dk}{k^2}. \quad (58)$$

There are no poles along the real k axis at $k = 0$, which can be proven by expanding the exponentials in power series and noting that these terms cancel the k^2 term in the denominator. Therefore, the integration of Eq. (58) can be performed with real k . Expanding the exponential (i.e., $e^{iA\zeta} = \cos k\zeta + i \sin k\zeta$) the integration can be changed from $-\infty$ to ∞ to 0 to ∞ by neglecting the odd function or sine term.

$G(t, \zeta)$ was integrated by parts to obtain an integral form which can be simply integrated to exponential and error functions

$$G(t, \zeta) = \frac{1}{\pi} \int_0^{\infty} \{ t \exp(-tk^2) - (2 \sec \theta - t) \times \exp[-k^2(2 \sec \theta - t)] \} \cos k\zeta dk + \frac{\zeta}{(2\pi)} \int_0^{\infty} \{ (\exp(-tk^2) - \exp[-k^2(2 \sec \theta - t)]) \} \left(\frac{\sin k\zeta}{k} \right) dk. \quad (58')$$

It should be noted that $\sin k\zeta/k$ does not produce a singularity as $k \rightarrow 0$, and that integration along real k is still allowable. $G(t, \zeta)$, Eq. (58), was evaluated by using the two integrals

$$\int_0^{\infty} \exp(-tk^2) \cos(k\zeta) dk = (\pi^{1/2}/2) t^{-1/2} \exp(-\zeta^2/4t), \quad (58a)$$

$$\int_0^{\infty} \exp(-tk^2) (\sin k\zeta/k) dk = (\pi/2) \operatorname{erf}[\frac{1}{2} \zeta t^{-1/2}] \quad (58b)$$

to have the form

$$G(t, \zeta) = \frac{1}{2} \pi^{-1/2} \{ t^{1/2} \exp[-\frac{1}{4} \zeta^2 t^{-1}] - (2 \sec \theta - t)^{1/2} \times \exp[-\frac{1}{4} \zeta^2 (2 \sec \theta - t)^{-1}] \} + (\zeta/4) \{ \operatorname{erf}[\frac{1}{2} \zeta t^{-1/2}] - \operatorname{erf}[\frac{1}{2} \zeta (2 \sec \theta - t)^{-1/2}] \}. \quad (58c)$$

Remembering that $\Phi(t, \zeta)$ can be expressed by the convolution integral [see Eq. (57b)]

$$\Phi(t, \zeta) = \int_0^{\infty} f(\zeta^*) G(t, \zeta - \zeta^*) d\zeta^*. \quad (59)$$

We must also satisfy the boundary condition at the fixed conductor

$$\Phi = -(\phi_0 - a \cos \theta), \text{ at } t=0 \text{ for } 0 < \zeta < \infty. \quad (60)$$

Therefore, the following relationship¹⁹ must hold.

$$\int_0^{\infty} f(\zeta^*) G(0, \zeta - \zeta^*) d\zeta^* = -(\phi_0 - a \cos \theta) \text{ for } 0 < \zeta < \infty. \quad (61)$$

Now all the boundary conditions have been accounted for in the problem.

In Eq. (61), we will change coordinates to reduce the integral equation to a form that is independent of $\sec \theta$ and of $(\phi_0 - a \cos \theta)$. The following transformation will be performed:

$$\zeta = 2(2 \sec \theta)^{1/2} Z, \quad \zeta^* = 2(2 \sec \theta)^{1/2} Z^*, \quad (62a)$$

$$d\zeta^* = 2(2 \sec \theta)^{1/2} dZ^*, \text{ where } 0 < \zeta, Z < \infty, \quad (62b)$$

$$f[2(2 \sec \theta)^{1/2} Z] = f(\zeta) = -[(\phi_0 - a \cos \theta)/2 \sec \theta] F(Z). \quad (62c)$$

The integral equations is now in the form

$$\int_0^\infty F(Z^*)\{|Z - Z^*|\operatorname{erfc}(|Z - Z^*|) - \pi^{1/2} \exp[-(Z - Z^*)^2]\}dZ^* = 1 \text{ for } 0 \leq Z < \infty. \quad (63)$$

This equation must be solved for $F(Z)$ in order to solve for the velocity profile directly in the free-shear layer [see, for example, Eqs. (22d) and (23a)]. This work will be reported in the third part to this paper, which is in progress.

D. Characterization of free-shear layers $f1$ and $f2$

For the free-shear layer $f1$ for $0 < \theta < \arctan(2a)$, we will use a coordinate system (x, t, ξ) (see Fig. 4) with the origin at $y = 0$ and $z = -a$, with ξ perpendicular to \mathbf{B} and t parallel to \mathbf{B} . The free-shear layer $f1$ intersects the surface of the moving perfect conductor at $y = 1$ and $z = -a + \tan \theta$, where the conductor's electric potential is $\Phi_{f1} = \phi_0 - a \cos \theta = \phi_m + \sin \theta - a \cos \theta$. Here ϕ_m is the moving conductor's electric potential at the middle of its surface, i.e., ϕ at $y = 1$ and $z = 0$. The potential of the moving conductor's surface is then $\phi = \phi_m + z \cos \theta = \phi_m + \sin \theta + \xi$, at $y = 1$. If $\phi_m = 0$, the potential difference between the moving and fixed electrodes is zero at $z = 0$, while the potential of the moving electrode is greater than or less than that of the fixed conductor for $z > 0$ or $z < 0$, respectively. On the left-hand side of free-shear layer $f1$, the potential in core $C1$ is Φ_{f1} for all t . On the right-hand side of $f1$, the potential in core $C2$ varies linearly from Φ_{f1} at $t = \sec \theta$ to zero at $t = 0$. Therefore, there is a jump in potential across $f1$ and the magnitude of this jump varies linearly from zero at $t = \sec \theta$ to $-\Phi_{f1}$ at $t = 0$. Since the thickness of $f1$ is $O(M^{-1/2})$, $\partial\phi/\partial\xi$ must be large, namely $O(M^{1/2})$, inside $f1$. In the ξ component of ohms law,

$$j_\xi = -\frac{\partial\phi}{\partial\xi} + u. \quad (64)$$

j_ξ is $O(M^{-1/2})$ [see Eq. (22c)], so $u = \partial\phi/\partial\xi = O(M^{1/2})$.

This leads to the conclusion that the velocity in the free-shear layers is much larger than the velocity of the moving wall. Therefore, even though the boundary layer is thin $O(M^{-1/2})$, it involves large velocities, so that the total flow inside the free-shear layers is comparable to that in cores $C1$ and $C2$:

$$\int_{\text{ACROSS } f1} u d\xi \cong -\Phi_{f1} (1 - t \cos \theta). \quad (65)$$

From this equation it can be deduced that if $\Phi_{f1} > 0$, the free-shear layer $f1$ is a high velocity jet in the minus x direction. Conversely, if $\Phi_{f1} < 0$, $f1$ is a jet in the plus x direction. Noting Eq. (65), it is interesting to note that the integral varies linearly from 0 at the moving electrode to a maximum of $-\Phi_{f1}$ at the corner at $z = -a$, $y = 0$. Q_{f1} , the total flow inside $f1$ in plus x direction (i.e., $\Phi_{f1} < 0$), is

$$Q_{f1} = \int_0^{\sec \theta} \int_{\text{ACROSS } f1} u d\xi dt \cong -\frac{1}{2} \Phi_{f1} \sec \theta. \quad (66)$$

Also, for the discussion of free-shear layer $f2$, we will use a similar coordinate system (ξ, t, x) (see Fig. 4). We shall define $\Phi_{f2} = \phi_m + a \cos \theta$ as the potential at the intersection of $f2$ and the surface of the moving electrode, i.e.,

ϕ at $y = 1$ and $z = a$. By the previous arguments for $f1$ it can be shown that the velocity in the free-shear layer is much larger than the velocity of the moving wall. The integral of the velocity across the boundary layer is

$$\int_{\text{ACROSS } f2} u d\xi = -t \Phi_{f2} \cos \theta. \quad (67)$$

If $\Phi_{f2} > 0$, $f2$ is a high velocity jet in the minus x direction. If $\Phi_{f2} < 0$, $f2$ is a jet in the plus x direction.

The integral [Eq. (67)] varies linearly from 0 at the fixed electrode to a maximum of $-\Phi_{f2}$ at the corner $y = 1$, $z = a$. Q_{f2} , the total flow in the plus x direction (i.e., $\Phi_{f2} < 0$), is

$$Q_{f2} = \int_0^{\sec \theta} \int_{\text{ACROSS } f2} u d\xi dt \cong -\frac{1}{2} \Phi_{f2} \sec \theta. \quad (68)$$

The dimensional flow is determined by the definition

$$Q^* = (U_0 L^2) Q. \quad (69)$$

The total dimensionless flow in the x direction equals the total flow in the three core areas Q_{C1} , Q_{C2} , and Q_{C3} and the total flow in the two free-shear layers Q_{f1} and Q_{f2} . The flows in the Hartmann layers of $O(M^{-1})$ will be neglected. Therefore, the total flow Q is expressed as

$$Q = Q_{C1} + Q_{C2} + Q_{C3} + Q_{f1} + Q_{f2} + O(M^{-1}) + \text{Hartmann layers}, \quad (70a)$$

where

$$Q_{f1} = -\frac{1}{2} \Phi_{f1} (\sec \theta), \quad (70b)$$

$$Q_{f2} = -\frac{1}{2} \Phi_{f2} (\sec \theta), \quad (70c)$$

$$Q_{C1} = \frac{1}{2} \tan \theta, \quad (70d)$$

$$Q_{C2} = (2a \cos \theta - \sin \theta) (\frac{1}{2} \cos \theta - \phi_m \tan \theta), \quad (70e)$$

$$Q_{C3} = 0. \quad (70f)$$

After substitution of these expressions and simplification, the total flow in the x direction Q is

$$Q = \cos \theta (a \cos \theta - \frac{1}{2} \sin \theta) - \phi_m (2a \sin \theta + \cos \theta) + O(M^{-1}) + \text{Hartmann layer terms}. \quad (71)$$

Let us now examine the properties of the velocity profiles for no net current flow between the electrodes. The $O(1)$ electric currents in cores $C1$ and $C3$ are blocked by the insulating sides, so that the "active" part of the moving electrode's surface is from $z = -a + \tan \theta$ to $z = a$. For zero net current, the potential at the middle of this active part of the moving electrode must be zero, so that

$$\phi_m = -\frac{1}{2} \sin \theta. \quad (72)$$

Then $\Phi_{f1} = -(a \cos \theta - \frac{1}{2} \sin \theta)$ which is negative because $\tan \theta < 2a$. Therefore, $f1$ is a jet in the plus x direction. Also, $\Phi_{f2} = (a \cos \theta - \frac{1}{2} \sin \theta) = -\Phi_{f1} > 0$, and thus $f2$ is an equal jet in the minus x direction. The total Q is equal to a [see Eq. (70a)].

At this point, it is interesting to note for any ϕ_m , u_{C2} varies linearly with z from

$$u_{C2} = y - \Phi_{f1} (\sin \theta), \text{ at } z = -a + y \tan \theta \quad (73)$$

to

$$u_{C2} = y - \Phi_{f2} (\sin \theta), \text{ at } z = a - (1 - y) \tan \theta. \quad (74)$$

Now we shall plot a typical plot of u_{C2} vs z for a fixed value of y for zero net current (Fig. 8). The jets in the free-shear layers in $f1$ and $f2$ exactly cancel each other [see Eq. (66)]. Note that u_{C2} at position 1 can be greater or less than 1, depending on y and θ (i.e., $u_{C2} > y$). At position 2, u_{C2} can be greater or less than 0, depending on y and θ (i.e., $u_{C2} > y$).

Let us now evaluate the characteristics of the velocity profile in terms of quantity of flow for a net transport current from the moving perfectly conducting electrode to the perfectly conducting stationary electrode. The net transport current is

$$I = (\Delta x) \int_{-a}^a j_y dz < 0, \text{ for } \phi_m > -\frac{1}{2} \sin \theta. \quad (75)$$

ϕ_m is the mean voltage at the moving electrode. As ϕ_m increases from $-\frac{1}{2} \sin \theta$ the jet in the positive x direction inside the region $f1$ (i.e., $\Phi_{f1} = \phi_m + \sin \theta - a \cos \theta < 0$) decreases in magnitude (the quantity of flow Q_{f1} decreases in magnitude). All velocities in core region $C2$ decrease. Also, the jet in the negative x direction inside region $f2$ (i.e., $\Phi_{f2} = \phi_m + a \cos \theta > 0$) increases in magnitude. When ϕ_m reaches the value $(a \cos \theta - \sin \theta)$, then $\Phi_{f1} = 0$, so that there is no jet inside region $f1$, and $u_{C2} = y$, at $z = -a + y \tan \theta$. At this ϕ_m , $\Phi_{f2} = 2a \cos \theta - \sin \theta$, so that the flow in the negative x direction inside region $f2$ is two times what it was for $\phi_m = -\frac{1}{2} \sin \theta$. The total flow Q equals $a - a \cos(2\theta) - (a^2 - \frac{1}{4}) \sin 2\theta$. Finally, as ϕ_m increases further from $a \cos \theta - \sin \theta$, jets in both regions $f1$ and $f2$ are in the negative x direction.

Let us now investigate the velocity profiles for a net transport current from the stationary electrode to the moving electrode as expressed as

$$I = (\Delta x) \int_{-a}^a j_y dz > 0, \text{ for } \phi_m < -\frac{1}{2} \sin \theta. \quad (76)$$

First, ϕ_m decreases from $-\frac{1}{2} \sin \theta$ to larger negative values, with the result that the jet in region $f1$ increases in volume of total flow. All velocities in region $C2$ increase. Also, the jet in the negative x direction in region $f2$ decreases in magnitude. When $\phi_m = -a \cos \theta$, so that $\Phi_{f1} = -(2a \cos \theta - \sin \theta)$, so that the flow in the positive x direction inside $f1$ is two times that for $\phi_m = -\frac{1}{2} \sin \theta$. For this ϕ_m , $\Phi_{f2} = 0$, so there is no jet inside $f2$ and $u_{C2} = y$, at $z = a - (1 - y) \tan \theta$. The total flow

$$Q = a + a \cos(2\theta) + (a^2 - \frac{1}{4}) \sin 2\theta.$$

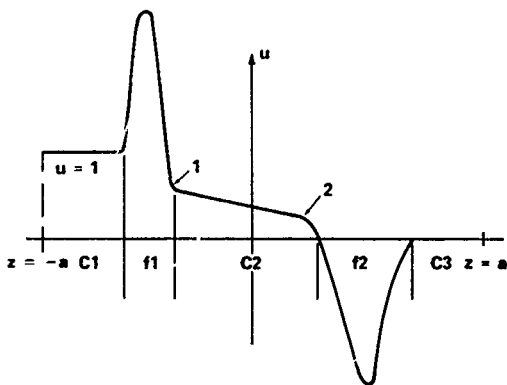


FIG 8 Plot of typical u vs z for fixed value of y for zero net current.

Finally, as ϕ_m decreases further from $-a \cos \theta$, both $f1$ and $f2$ jets are in the positive x direction.

From Eqs. (70a) and (70b), the difference in total volume of flow in regions $f1$ and $f2$ is

$$Q_{f1} - Q_{f2} = \frac{1}{2}(2a - \tan \theta) > 0 \quad (77)$$

so that the difference is independent of ϕ_m .

V. EXPERIMENTAL EVIDENCE FOR FREE-SHEAR LAYERS

Since we have analyzed the free-shear layers mathematically by fundamental magnetohydrodynamic theory and characterized some of the basic properties of these layers, we must ask whether there is any experimental evidence of jets of boundary layer thickness $O(M^{-1/2})$. The answer is yes. Hunt and Malcolm^{13,14} treat theoretically in cylindrical coordinates and experimentally the problem of a circular electrode embedded in an insulating wall in a high external magnetic field in a stationary fluid. They predict a free-shear layer as a jet in the azimuthal direction between the core region and the electrode, and between the core region and the insulating wall. They predict that $v_\theta = O(M^{1/2})$. The free-shear layer is a jet in the θ direction, but the jet is in the $+\theta$ direction for $z > 0$ and the $-\theta$ direction for $z < 0$. ($z = 0$ is midway between the two circular electrodes.) In their work experimental measurements¹⁴ show evidence of these jets.

However, that work is somewhat different from the jets we discuss here, in which each jet must be entirely in the $+x$ or $-x$ direction. For the work herein, the jet goes from zero at the intersection with the perfect conductor to a maximum at the corner where the insulator and other conductor meet. Both cases involve linear variation of velocity along the length of the layer.

VI. TOTAL CURRENT AND POWER LOSSES BETWEEN ELECTRODES IN THE CORES

A. Development of basic theory

We derived the total current between the electrodes (see Figs. 1 and 2) for the core regions. In the core regions $C1$ and $C3$ the current densities $j_{\eta C1}$, $j_{\xi C1}$, $j_{\eta C3}$, and $j_{\xi C3}$ were determined to be zero to $O(1)$, when neglecting terms of $O(M^{-1})$ in the magnetohydrodynamic equations. In the free-shear layers $f1$ and $f2$, the current densities $j_{\eta f1}$ and $j_{\eta f2}$ were determined to be of $O(1)$. But since the thickness of the boundary layer is $O(M^{-1/2})$ the total current is $O(M^{-1/2})$ in the η direction. The current densities in the core $C2$ were derived to be $j_{\xi C2} = 0$, and $j_{\eta C2} = -\cos \theta(\phi_0 + \xi)$ to $O(1)$, neglecting terms to $O(M^{-1})$. Here, ϕ_0 is the nondimensional potential of the perfectly conducting moving wall at $\xi = 0$, in reference to the stationary perfectly conducting wall at the bottom of the channel.

The zeroth order total current I to $O(1)$ carried by the core $C2$ is

$$I = (\Delta x) \int_{-a \cos \theta}^{a \cos \theta - \sin \theta} j_{\eta C2} d\xi, \quad (78)$$

where Δx = nondimensional axial length along channel, I = nondimensional total current in $C2$, $\xi_1 = -a \cos \theta$

(coordinate for corner 2), and $\xi_2 = a \cos \theta - \sin \theta$ (coordinate for corner 3). The total current terms neglected in the two free-shear layers and the two Hartmann layers along the insulating walls are of $O(M^{-1/2})$ and $O(M^{-1})$, respectively.

Integration of the expression for the total nondimensional current I in core $C2$ is

$$I = -(\Delta x) \cos \theta (\phi_m + \frac{1}{2} \sin \theta) (2a \cos \theta - \sin \theta), \quad (79)$$

where ϕ_m is the mean voltage of the moving wall and is defined as $\phi_m = \phi_0 - \sin \theta$. $\phi_m = \phi$ at $y = 1$ and $z = 0$, the potential at the center of the moving wall. The new dimensional quantities with superscripts (*) are defined as

$$I^* = \sigma U_0 B_0 L^2 I, \quad (80)$$

$$\phi_m^* = U_0 B_0 L \phi_m. \quad (81)$$

The other variables were defined previously in the paper.

The total nondimensional zeroth-order total Joulean power loss P_T between the electrodes to $O(M^2)$ in core $C2$ can be derived by integrating the current density squared in the η direction, in core region $C2$:

$$P_T = (\Delta x) M^2 (\sec \theta) \int_{-a \cos \theta}^{a \cos \theta - \sin \theta} (j_{\eta C2})^2 d\xi, \quad (82)$$

where the $\sec \theta$ comes from the integral with respect to η . The total zeroth order Joulean power loss terms neglected in the two free-shear layers and two Hartmann layers along the insulating walls are $O(M^{3/2})$ and $O(M)$, respectively.

The expression for the power loss P_T after integration is

$$P_T = (\Delta x) M^2 \cos \theta (2a \cos \theta - \sin \theta) [\phi_m (\phi_m + \sin \theta) + \frac{1}{3} (a^2 \cos^2 \theta - a \cos \theta \sin \theta + \sin^2 \theta)], \quad (83a)$$

where the dimensional Joulean power loss is defined as

$$P_T^* = (\mu_f U_0^2) P_T. \quad (83b)$$

The current densities in the cores $C1$ and $C3$ were determined to be zero to $O(1)$ and thus do not contribute to the zeroth order total current and zeroth order Joulean power losses.

It should be noted that the expression for P_T , when the magnetic field becomes transverse $\theta = 0$, and no external potential is applied $\phi_0 = 0$; approaches the result obtained by the authors when working the corresponding problem using the infinite series type of mathematical solutions presented by Hughes and Young¹⁰

$$P_T = \frac{2}{3} (\Delta x)^2 M^2 a^3. \quad (84)$$

The nondimensional resistance of the rectangular channel per unit length R in core region $C2$ is defined as the nondimensional length of the resistor L divided by the non-dimensional cross-sectional area A of the resistor

$$R = L/A = 1/(2a - \tan \theta) (\cos^2 \theta) (\Delta x), \quad (85)$$

where $A = (2a - \tan \theta) \cos \theta (\Delta x)$ and $L = \sec \theta$. The dimensional resistance R^* is defined as

$$R^* = (1/L\sigma) R. \quad (86)$$

B. Results and discussion

Figures 9-14 present straight line graphical data for the nondimensional total current per unit channel length in the

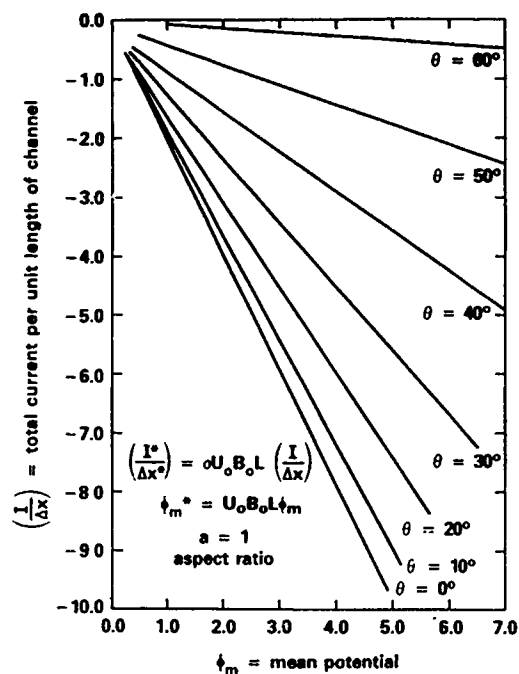


FIG. 9. Total current per unit length of channel vs positive mean potential ϕ_m for aspect ratio $a = 1$.

core $C2$, $(I/\Delta x)$, versus the nondimensional mean voltage at the center of the moving conductor at the top of the rectangular channel ϕ_m . The potential ϕ_m is referenced to the perfect conducting wall at the bottom of the rectangular channel, which is assumed to have the potential $\phi = 0$. Equation (79) is used to numerically calculate the data. Equations (80) and (81) show the parameters used to dimensionalize the nondimensional variables.

Figures 9-11 present straight line plots of positive mean voltage ϕ_m plotted versus total current per unit length $(I/$

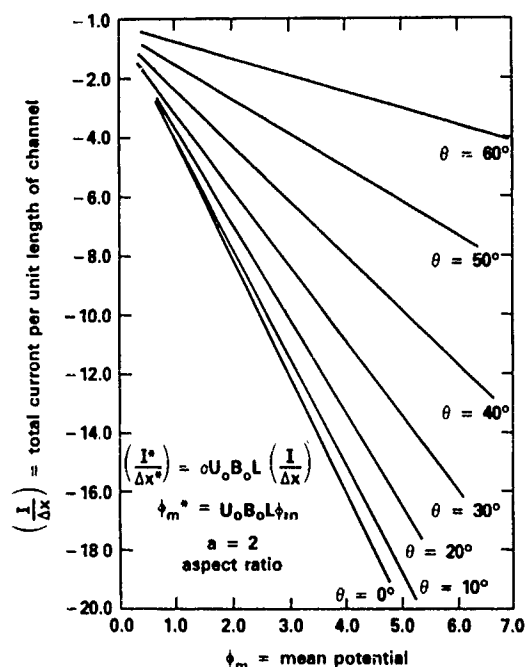


FIG. 10. Total current per unit length of channel vs positive mean potential ϕ_m for aspect ratio $a = 2$.

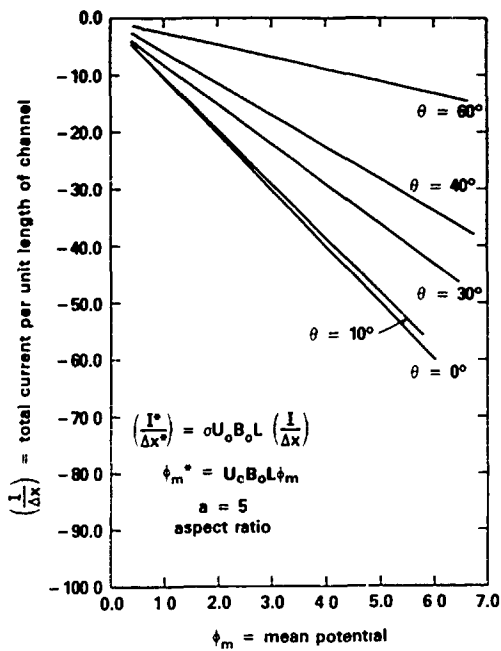


FIG. 11 Total current per unit length of channel vs positive mean potential ϕ_m for aspect ratio $a = 5$

Δx). For the range of variables studied herein the $(I/\Delta x)$ values are all negative quantities. The straight line plots show that for positive mean voltages the total current is flowing from the moving wall to the bottom perfect conductor in the channel in core C 2. Each figure presents data for a particular aspect ratio (i.e., $a = 1, 2, 5$). In each figure the angle θ is placed along each straight line plot where θ shows the external magnetic field angle. The straight line plots show that as the positive mean voltage ϕ_m increases and the external magnetic field angle θ decreases, the total negative current per unit length in the rectangular channel increases for

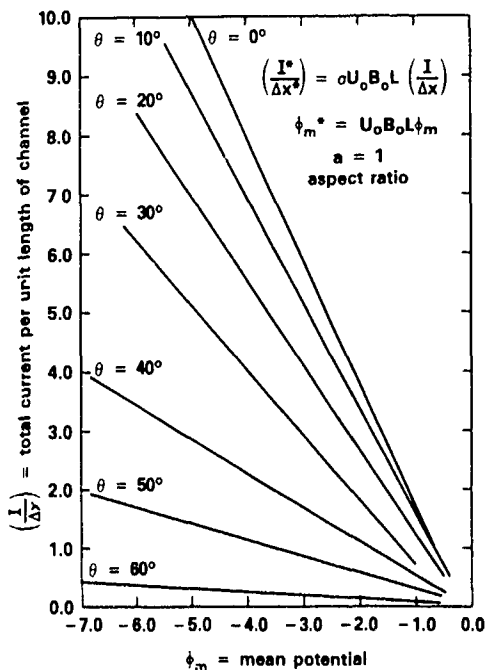


FIG. 12 Total current per unit length of channel vs negative mean potential ϕ_m for aspect ratio $a = 1$

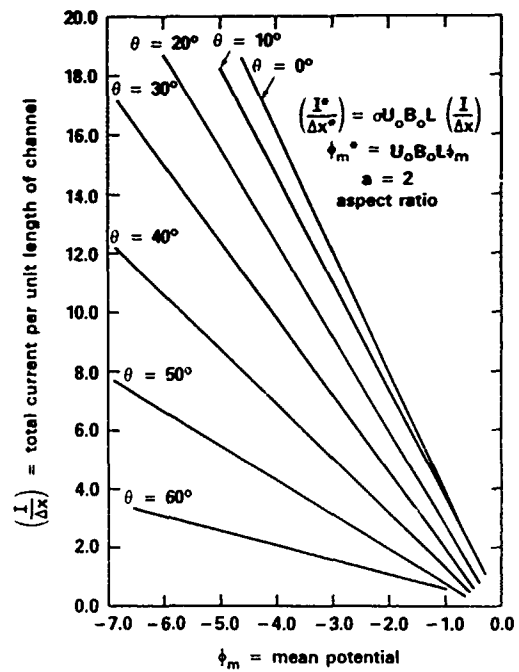


FIG. 13. Total current per unit length of channel vs negative mean potential ϕ_m for aspect ratio $a = 2$.

the range of variables interest. The total current flows from the top moving electrode to the bottom fixed electrode.

Figures 12–14 presents straight line plots of negative voltages ϕ_m plotted against total current pair unit length $(I/\Delta x)$ for core C 2. For the range of variable of interest herein the $(I/\Delta x)$ values are all positive quantities. These straight line plots show that for negative mean voltages the total current is moving from the bottom stationary perfect conductor to the moving perfect conductor at the top of the channel in core C 2. Each figure presents data for a particular channel with a given aspect ratio (i.e., $a = 1, 2, 5$). In each figure the external field angle θ is placed alongside each

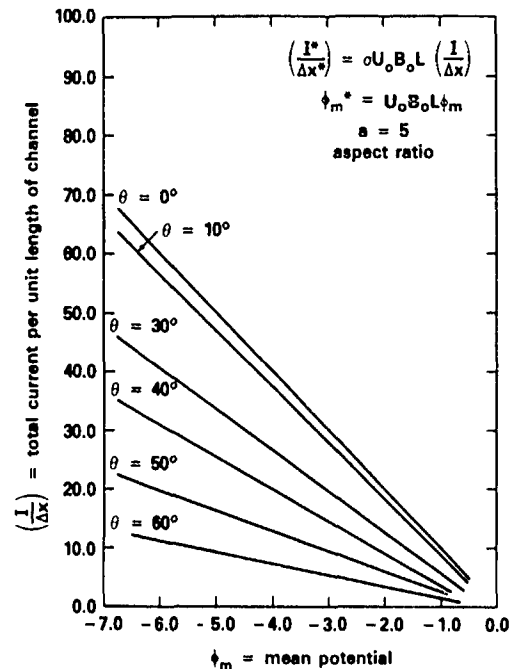


FIG. 14. Total current per unit length of channel vs negative mean potential ϕ_m for aspect ratio $a = 5$

straight line. These plots show that as the negative mean voltage ϕ_m increases, as the aspect ratio of the rectangular duct a increases, and as the external magnetic field angle θ decreases, the total positive total current per unit length of the duct increases for the range of variables of interest.

It is interesting to note at this point that positive mean potentials ϕ_m give a larger absolute value total current per unit length values $|I/\Delta x|$ than the corresponding negative potential in a similar channel with the same $\theta > 0$. Each straight line intersects the $I = 0$ axis at $\phi_m = -\frac{1}{2} \sin \theta$.

In Fig. 15, curves of nondimensional resistance of the duct per unit length R in core $C2$ are plotted versus external magnetic field angle θ . Three curves are shown with aspect ratios of $a = 1, 2,$ and 5 . Each curve has the lowest total resistance at the smallest value of θ and increases as θ increases. The resistance of the duct decreases with aspect ratio a , as would be expected. The nondimensional resistance of the rectangular channel per unit length in core $C2$ is defined as the resistor length L divided by the cross-sectional area A of the resistor and is derived in Eq. (85). The dimensional resistance R per unit length is defined in Eq. (86).

Figures 16 to 19 show the nondimensional Joulean power losses per unit length of channel P_T versus the mean voltage ϕ_m at the center of the moving perfectly conducting wall (i.e., moving electrode) for different external magnetic field angles θ . For both positive and negative potentials the power losses are positive, since heat is lost from the system due to Joulean heating. Power losses for external magnetic field where θ equals zero (i.e., transverse external magnetic field) were reported in an earlier paper by Brown *et al.*¹¹ It should be noted that the power loss value from the negative potential ϕ_m is slightly less than the analogous power loss value from the corresponding positive potential. This is as expected because the positive potential drives a larger absolute value of the total current per unit length of the channel

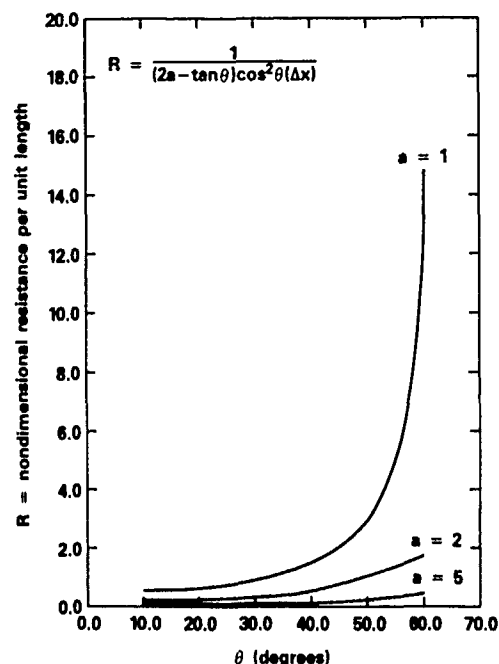


FIG. 15. Nondimensional resistance per unit length of channel vs angle of external, homogeneous magnetic field θ .

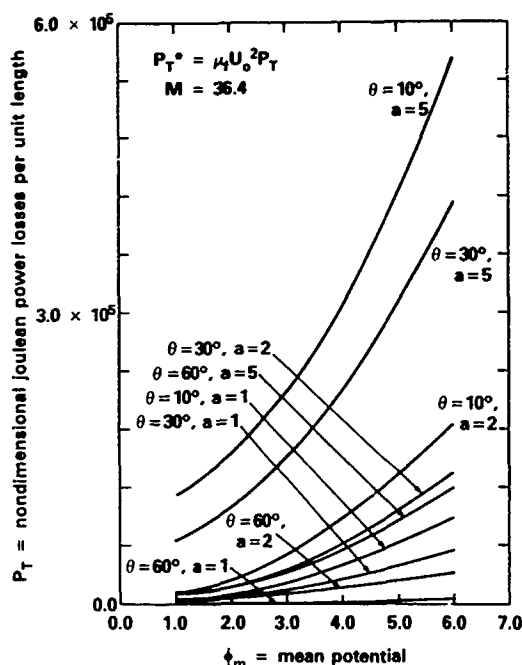


FIG. 16 Nondimensional Joulean power losses per unit length of channel versus positive mean potential ϕ_m for aspect ratios $a = 1, 2,$ and 5 and external magnetic field $\theta = 10^\circ, 30^\circ,$ and 60°

than the analogous negative potential. (See plots of the total currents per unit length of the channel in the preceding part of this section.)

VII. DISCUSSION AND CONCLUSIONS

Fully developed viscous liquid-metal flows in a rectangular channel (duct flow) with insulating side walls that are skewed to a high, homogeneous external magnetic field were studied. A perfectly conducting moving top wall with an

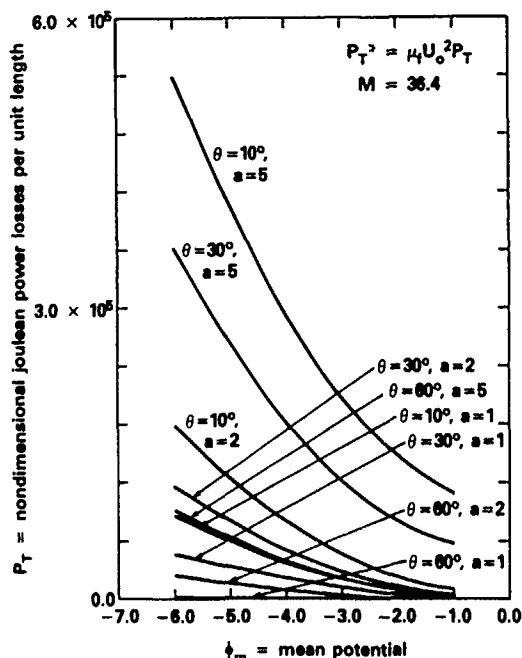


FIG. 17. Nondimensional Joulean power losses per unit length of channel vs negative potential ϕ_m for aspect ratios $a = 1, 2,$ and 5 and external magnetic field angles $\theta = 10^\circ, 30^\circ,$ and 60° .

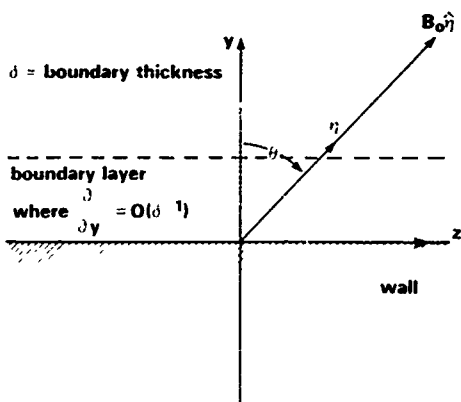


FIG. 18. Wall with the unit normal $\hat{\eta}$ at an angle θ to the external magnetic field direction

external potential and a stationary perfectly conducting bottom wall at zero potential act as electrodes and are also skewed to the external magnetic field. The angles of the external magnetic field \mathbf{B}_0 is in the range of values $0 < \theta < \arctan 2a$. The flow in the channel is characterized by high Hartmann number M , high interaction parameter N , low magnetic Reynolds number R_m , channel aspect ratio a , and external magnetic field angle θ .

In this work, since the Hartmann number is always assumed large (i.e., $M \gg 1$), it was determined by magnetohydrodynamic theory that the channel could be divided into subregions shown in Fig. 3. In the three channel core subregions C 1, C 2, and C 3 the first partial derivatives $\partial/\partial \xi$ and $\partial/\partial \eta$ are of $O(1)$. The six Hartmann layers, $h 1-h 6$, along the sides of the duct are of $O(M^{-1})$ thickness and have $O(M)$ normal derivatives. $f 1$ and $f 2$ are two free-shear layers (or interior regions) which have unique characteristics. The free-shear layers separate the three core regions from each other. A free-shear layer lies along the magnetic field lines through the appropriate channel corner and is driven by a current density singularity at this corner (see Figs. 4-6). The layers have $O(M^{-1/2})$ thickness. The first partial derivatives are of order $\partial/\partial \xi = O(M^{1/2})$ and $\partial/\partial \eta = O(1)$.

The general mathematical solutions in the cores were obtained from the basic magnetohydrodynamic equations (7b) and (7c) in the core if the term of $O(M^{-2})$ is neglected. The method of singular perturbation expansion and matched asymptotic expansions at the boundaries between

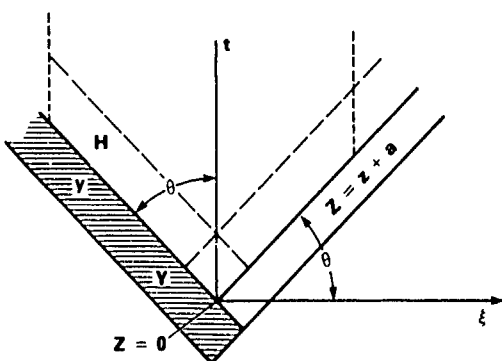


FIG. 19 Geometry of free-shear layer at $z = -a$.

the Hartmann layer and core region is applied to the complex system of coupled equations to obtain the core solutions in the different core regions to zeroth order. It is assumed that the physically realizable functions in the core $u_c(x;M)$ can be expanded at high Hartmann number M as

$$u_c(x;M) = u_{c0}(x) + (1/M)u_{c1}(x) + (1/M^2)u_{c2}(x) + \dots, \quad (87)$$

where x is an independent variable. The function $u_b(x;M)$ can be expanded at high Hartmann number M in the Hartmann layer as

$$u_b(X;M) = u_{b0}(X) + (1/M)u_{b1}(X) + (1/M^2)u_{b2}(X) + \dots, \quad (88)$$

where X is a stretched coordinate. The zeroth order terms are $u_{c0}(x)$ and $u_{b0}(X)$, and the first-order terms are $(1/M)u_{c1}(x)$ and $(1/M)u_{b1}(X)$.

To zeroth order in the core C 1 the velocity $u_{c1,0} = 1$ throughout the region. The velocity is the same as the moving wall throughout this core region. The two components of the current density to zeroth order $j_{\xi c1,0}$ and $j_{\eta c1,0}$ are both equal to zero. Also the potential to zeroth order throughout the core C 1 is $\phi_{c1,0} = \phi_0 + \xi$ throughout the core area. To zeroth order in core C 2 the current density follows the external magnetic field \mathbf{B}_0 and therefore $j_{\xi c2,0} = 0$, and $j_{\eta c2,0} = -\cos \theta(\phi_0 + \xi)$ [see Eq. (17a)]. The zeroth order potentials $\phi(\eta, \xi)$ and $u(\eta, \xi)$ are functions of η and ξ [see Eqs. (7b) and (7c)]. It should be noted that to zeroth order there is a jump on u_{c2} across each Hartmann layer at the top and bottom wall [see Eq. (17e)]. In core C 3 to zeroth order $u_{c3,0}$ is zero throughout the subregion. Thus, the core C 3 flow has no velocity throughout the subregion. Both components of the current density in C 3, $j_{\eta c3,0}$ and $j_{\xi c3,0}$ are zero as in core subregion C 1. To zeroth order the potential $\phi_{c3,0}$ is also zero throughout the region. It was not necessary at this point in the work to obtain the Hartmann layer solutions adjacent to each core region to solve for the core region flow profiles to zeroth order.

The fundamental mathematical theory was developed for the free-shear layers $f 1$ and $f 2$ in the rectangular channel. The free-shear layers in regions $f 1$ and $f 2$ in coordinates (x, t, ξ) are shown in Fig. 4. The corner region of the free-shear layer $f 1$ between the insulating wall and the perfect conductor is at $(t = 0, \xi = -a \cos \theta)$. The free-shear layer $f 2$ has the corner region between the insulating wall and the perfect conductor at $(t = \sec \theta, \xi = a \cos \theta - \sin \theta)$. In this work we developed the fundamental mathematical theory for shear layer $f 1$: the theory for shear layer $f 2$ can be performed in an analogous manner. Alty¹² previously studied this problem of the free-shear layer in a rectangular channel with all stationary walls, but his free-shear layer solution is wrong.

The basic fourth order, partial differential equation for the potential to zeroth order in $f 1$, $\Phi(t, \xi)$, [Eq. (47a)] in the free-shear layer was derived. The solution to the partial differential equation fits five different boundary conditions [see Eqs. (47b)-(47e)]. The partial differential equation was solved in this work by using the mathematical technique of the complex Fourier transform. The mathematical solu-

tion to the problem using this technique evolves into an integral equation which can be solved numerically for the zeroth-order velocity profile in shear layer $f1$. The numerical solution of the integral equation will be presented in a future paper. From the fundamental theory for the free-shear layer the basic characteristics of the free-shear layer were determined and discussed in detail. There has been experimental verification of a similar, but not exactly the same, type of free-shear layer as presented herein, reported by Hunt and Malcolm.¹³

The basic theory was derived to calculate to zeroth order the total current per unit length of the channel in core $C2$ due to an external potential applied across the electrodes (i.e., perfect conducting walls). Also, the expressions for the power losses per unit length of the channel were derived to zeroth order for core $C2$. The derived expressions are dependent on channel aspect ratio a , external magnetic field angle θ , and Hartmann number M . No current is carried in cores $C1$ and $C3$ to zeroth order. The total current per unit length terms neglected in the two free-shear layers and the two Hartmann layers along the insulating walls are of $O(M^{-1/2})$ and $O(M^{-1})$, respectively.

In this paper Figs. 9–14 show linear plots of the mean voltage ϕ_m at the center of the perfectly conducting moving wall versus total current per unit length of the channel ($I/\Delta x$). The potential ϕ_m is referenced to the perfect conducting wall at the bottom of the channel, which is assumed to have a potential of $\phi = 0$. The linear plots show that for the range of variables studied for positive mean voltage ϕ_m , the total current per unit length is negative. The total current is thus flowing from the moving wall to the bottom perfect conductor in the duct in core $C2$. Similar linear plots show that for negative mean voltages ϕ_m the total current is positive and is flowing from the bottom stationary conducting wall to the top moving conducting wall in core $C2$.

The following general conclusions can be drawn from this range of calculated data. The plots show that as the positive mean voltage ϕ_m increases, as the aspect ratio of channel a increases, and as the external magnetic field angle θ decreases, the total negative current per unit length increases. The total current is flowing from the top moving electrode to the bottom moving electrode. The plots also show that as the negative mean voltage ϕ_m increases, as the aspect ratio of the duct increases, and as the external magnetic field angle θ decreases, the total positive current per unit length increases. The total current is flowing from the bottom to the top electrode. It should be noted at this point that positive mean potential ϕ_m gives a larger absolute value total current per unit length value, $|(I/\Delta x)|$, than the corresponding negative potentials in a similar channel.

Figure 15 shows a plot of nondimensional resistance per unit length of channel versus angle of the external, homogeneous magnetic field B_0 . For this data the conclusion is reached that the resistance of the channel increases with increasing external magnetic field θ and decreasing channel aspect ratio a , as would be expected.

Nondimensional Joulean power losses per unit length of channel versus mean potential ϕ_m for different external magnetic field angles θ and aspect ratios a are plotted in Figs.

16 and 17. For limited data, power losses increase with increasing positive potential or decreasing negative potential ϕ_m and with decreasing external magnetic field angle θ .

For fully developed flow, we assume that there is only one component of velocity $u\hat{x}$ and that all variables are independent of x and time t^* . Therefore, the inertial term in the Navier–Stokes Eq. (1a),

$$N^{-1} \left[\left(\frac{\partial v}{\partial t^*} \right) + (v \cdot \nabla) v \right]$$

is identically equal to zero for any value of the interaction parameter N . Fully developed flow is always a mathematically correct solution of the governing equations, but it may not actually occur in the real duct flow. Under certain circumstances, the fully developed flow is unstable with respect to a small, three-dimensional, time varying disturbance. The disturbance grows until a different stable flow is realized. In the actual flow, all three components of velocity are nonzero and the flow variables depend on both x and t^* . This flow may involve a coherent structure, such as a series of vortices, or a chaotic structure, such as turbulence. In magnetohydrodynamic flows, the magnetic field strongly affects the instability and the structure of the periodic flow.

For the present problem, the largest velocities occur in the free-shear layers $f1$ and $f2$, so that inertial effects will first become significant in these layers. The key inertial parameter for these layers is $\alpha = M^{1/2} N^{-1/3}$. If $\alpha < 1$, then the electromagnetic body force overwhelms inertial effects, the inertial terms in Eq. (1a) are negligible, even in the high velocity free-shear layers, and fully developed flow is realized. This corresponds to the statement that low Reynolds number flows are stable in ordinary hydrodynamics. We can increase α by increasing U_0 or by decreasing B_0 . At some critical value of α , fully developed flow becomes unstable and there is a transition to a periodic flow. For α slightly above α_c , there is a velocity fluctuation wave in the free-shear layer. This wave propagates with a definite wavelength and wave speed around the circumference of the current collector which is modeled here. At first, this wave would represent a propagating undulation in the free-shear layer. As α is increased further, the undulations grow and become a series of vortices whose axes are parallel to \mathbf{B} in the plane of the free-shear layer. The vortices are convected around the circumference of the current collector. The vortices provide significant momentum transport in the ξ direction. This momentum transport causes the free-shear layer to become thicker and its maximum mean velocity to become smaller. The layer thickness grows from $M^{-1/2}$ to $N^{-1/3}$, while the mean u decreases from $M^{1/2}$ to $N^{1/3}$. However, inertial effects are still negligible in the core regions, which involve much smaller velocities, so that the present core solutions still apply. The core velocities and potentials are the same, so that the jump in potential across each free-shear layer is the same. The relationship $u_j = \partial\phi_j/\partial\xi$ for each free-shear layer comes from ohms law, so it is unchanged. The new periodic, inertial free-shear layers with $O(N^{-1/3})$ thickness must have the same total flow at each $t = \text{constant}$ level as the original $M^{-1/2}$ thickness layers.

In the free-shear layers for fully developed flow, there is

a large viscous dissipation because the velocity gradient $\partial u_f / \partial \xi = O(M)$. After transition to the periodic, inertial free-shear layer structure, the viscous dissipation in the mean velocity is much smaller since

$$\frac{\partial u_f}{\partial \xi} = O(N^{2/3}) \ll O(M).$$

However, the mean flow also loses energy to the vortices through the Reynolds stress. The vortices receive energy from the mean flow and lose it to viscous dissipation and to electromagnetic damping (Joulean dissipation). An infinitely long vortex with rotation around a straight magnetic field line represents a generator on open circuit: The radial component of $\mathbf{v} \times \mathbf{B}$ is exactly cancelled by the radial electric field, so that there is no current and no electromagnetic damping. However, in the present problem, each magnetic field line intersects one or two perfect conductors. These perfect conductors provide a short circuit for the vortex generator. Electric current circulates through the conductor and vortex and strongly damps the vortex. If α is increased further, nonlinear vortex interactions lead to a wide spectrum of vortex sizes, i.e., to turbulence. However, the turbulence is two-dimensional since any eddy whose axis is not parallel to \mathbf{B} is strongly damped.⁸ The value of α when each transition occurs depends critically on the geometry and conductivity of the duct walls.

ACKNOWLEDGMENTS

The authors wish to express their appreciation for the helpful discussions and encouragement given by Dr. F. J. Young, Scientific Division, Frontier Timber Co., Bradford, PA 16701. We would also like to express our appreciation for the support given by the IR/IED program at the David Taylor Research Center, Bethesda, MD 20084-5000.

APPENDIX A: THICKNESS OF LAYERS IN FULLY DEVELOPED MAGNETOHYDRODYNAMIC CHANNEL FLOWS

The discussion herein presents a fundamental general magnetohydrodynamic mathematical treatment for determining the order of magnitude of boundary layer thickness in fully developed laminar, magnetohydrodynamic channel flows.

Equations for fully developed magnetohydrodynamic channel flows with a uniform magnetic field are as follows:

$$j_\xi = M^{-2} \left(\frac{\partial^2 u}{\partial \eta^2} + \frac{\partial^2 u}{\partial \xi^2} \right), \quad (\text{A1a})$$

$$j_\eta = -\frac{\partial \phi}{\partial \eta}, \quad (\text{A1b})$$

$$j_\xi = -\frac{\partial \phi}{\partial \xi} + u, \quad (\text{A1c})$$

$$\frac{\partial j_\eta}{\partial \eta} + \frac{\partial j_\xi}{\partial \xi} = 0. \quad (\text{A1d})$$

Here (x, η, ξ) are Cartesian coordinates with the velocity u in the x direction and the magnetic field in the η direction. Introduce Eq. (A1c) for the u in Eq. (A1a) to obtain

$$j_\xi = M^{-2} \left(\frac{\partial^3 \phi}{\partial \eta^2 \partial \xi} + \frac{\partial^3 \phi}{\partial \xi^3} + \frac{\partial^2 j_\xi}{\partial \eta^2} + \frac{\partial^2 j_\xi}{\partial \xi^2} \right). \quad (\text{A2})$$

Now we differentiate Eq. (A2) with respect to ξ :

$$\frac{\partial j_\xi}{\partial \xi} = M^{-2} \left(\frac{\partial^4 \phi}{\partial \eta^2 \partial \xi^2} + \frac{\partial^4 \phi}{\partial \xi^4} + \frac{\partial^3 j_\xi}{\partial \eta^2 \partial \xi} + \frac{\partial^3 j_\xi}{\partial \xi^3} \right). \quad (\text{A3})$$

Substitute Eq. (A1b) into Eq. (A1d) to obtain

$$\frac{\partial j_\xi}{\partial \xi} = -\frac{\partial j_\eta}{\partial \eta} = \frac{\partial^2 \phi}{\partial \eta^2}. \quad (\text{A4})$$

Substitute Eq. (A4) for each j_ξ into Eq. (A3)

$$\begin{aligned} \frac{\partial^2 \phi}{\partial \eta^2} &= M^{-2} \left(\frac{\partial^4 \phi}{\partial \eta^2 \partial \xi^2} + \frac{\partial^4 \phi}{\partial \xi^4} + \frac{\partial^4 \phi}{\partial \eta^4} + \frac{\partial^4 \phi}{\partial \eta^2 \partial \xi^2} \right), \\ \frac{\partial^2 \phi}{\partial \eta^2} &= M^{-2} \nabla^4 \phi. \end{aligned} \quad (\text{A5})$$

Now let us consider a wall in which the unit normal $\hat{\mathbf{y}}$ is at an angle θ to the magnetic field direction (see Fig. 18). The unit vector $\hat{\boldsymbol{\eta}}$, the first derivative $\partial / \partial \eta$, and the second derivative can be written as in terms of Cartesian coordinates

$$\hat{\boldsymbol{\eta}} = \cos \theta \hat{\mathbf{y}} + \sin \theta \hat{\mathbf{z}}, \quad (\text{A6a})$$

$$\frac{\partial}{\partial \eta} = \cos \theta \frac{\partial}{\partial y} + \sin \theta \frac{\partial}{\partial z}, \quad (\text{A6b})$$

$$\frac{\partial^2}{\partial \eta^2} = \cos^2 \theta \frac{\partial^2}{\partial y^2} + 2 \sin \theta \cos \theta \frac{\partial^2}{\partial y \partial z} + \sin^2 \theta \frac{\partial^2}{\partial z^2}. \quad (\text{A6c})$$

Therefore in (x, y, z) coordinates, Eq. (A5) is expressed as

$$\begin{aligned} \cos^2 \theta \frac{\partial^2 \phi}{\partial y^2} + 2 \sin \theta \cos \theta \frac{\partial^2 \phi}{\partial y \partial z} + \sin^2 \theta \frac{\partial^2 \phi}{\partial z^2} \\ = M^{-2} \left(\frac{\partial^4 \phi}{\partial y^4} + 2 \frac{\partial^4 \phi}{\partial y^2 \partial z^2} + \frac{\partial^4 \phi}{\partial z^4} \right). \end{aligned} \quad (\text{A7})$$

Here it noted that ∇^4 is unchanged by rotating the axis. Equation (A7) is a fourth order elliptic equation so that two boundary conditions must be described at each boundary. For a magnetohydrodynamic problem, the velocity is usually $u = 0$ and either the potential ϕ is given at a perfect conductor or j_y could be given at a finite conductor as $j_y = C(\partial^2 \phi / \partial z^2)$ where $C = (\sigma_w t / \sigma L)$ is the wall conductance ratio, where σ_w and t are the conductivity and thickness of the wall, respectively. Therefore, let us assume that there are two boundary conditions at the wall at $y = 0$. Now consider the asymptotic solution as $M \rightarrow \infty$. Unless some derivative becomes very large ϕ is governed by the "reduced equation":

$$\cos^2 \theta \frac{\partial^2 \phi}{\partial y^2} + 2 \sin \theta \cos \theta \frac{\partial^2 \phi}{\partial y \partial z} + \sin^2 \theta \frac{\partial^2 \phi}{\partial z^2}. \quad (\text{A8})$$

The reduced equation is only second order, so it cannot satisfy both boundary conditions at $y = 0$. Therefore, there must be a boundary layer adjacent to the wall where the normal derivative $\partial / \partial y$ is sufficiently large that at least one of the fourth-order derivatives on the right-hand side of Eq. (A7) is comparable to the second-order derivatives on the left-hand side. Then, near the wall, the governing equation again becomes fourth order and can satisfy both boundary conditions at $y = 0$. The core region is obviously governed by the "reduced equation."

We now change y to stretched boundary layer coordinates.

$$Y = \delta^{-1}y, \quad (\text{A9a})$$

$$y = (\delta)Y, \quad (\text{A9b})$$

$$\frac{\partial}{\partial y} = \frac{dY}{dy} \frac{\partial}{\partial Y} = \delta^{-1} \frac{\partial}{\partial Y}. \quad (\text{A9c})$$

Equation (A7) is expressed in stretched boundary layer coordinates as

$$\begin{aligned} & \cos^2 \theta (\delta^{-2}) \frac{\partial^2 \phi}{\partial Y^2} + 2 \sin \theta \cos \theta (\delta^{-1}) \frac{\partial^2 \phi}{\partial Y \partial z} \\ & + \sin^2 \theta \frac{\partial^2 \phi}{\partial z^2} \\ & = M^{-2} \left((\delta^{-4}) \frac{\partial^4 \phi}{\partial Y^4} + 2(\delta^{-3}) \frac{\partial^4 \phi}{\partial Y^2 \partial z^2} + \frac{\partial^4 \phi}{\partial z^4} \right). \end{aligned} \quad (\text{A10})$$

The first term on the right-hand side of Eq. (A10) is always much larger than the other two terms. There are three cases for various δ . In case I, $\cos \theta$ is not small [i.e., $0 \leq \theta \leq \theta_0 < (\pi/2)$], so the magnetic field has a finite component normal to the wall. Then $\delta = M^{-1}$ and the basic governing equation is

$$\cos^2 \theta \frac{\partial^2 \phi}{\partial Y^2} = \frac{\partial^4 \phi}{\partial Y^4}. \quad (\text{A11})$$

This is the governing equation for all Hartmann layers for walls where there is a finite normal component of \mathbf{B} . The basic solutions are

$$\begin{aligned} & A_1(z), A_2(z)Y, A_3(z)\exp(-|\cos \theta|Y), \\ & A_4(z)\exp(+|\cos \theta|Y), \end{aligned}$$

where the $A_i(z)$ are arbitrary functions. Thus, all Hartmann layer solutions are composed of linear combinations of these four solutions.

In case II the angle $\theta = \pi/2$ and the magnetic field is exactly parallel to the wall. Then $\delta = M^{-1/2}$, and the governing equation is of the mathematical form

$$\frac{\partial^2 \phi}{\partial z^2} = \frac{\partial^4 \phi}{\partial Y^4}. \quad (\text{A12})$$

This is the governing equation for "side layers." These are boundary layers on walls parallel to the magnetic field, and it is the governing equation for free-shear (or interior) layers that lie along the magnetic field, such as the free-shear layers being studied within this paper.

Case III deals with the problem when $\cos \theta = \alpha M^{-1/2}$ and $\delta = M^{-1/2}$, where α is an $O(1)$ parameter in the problem. Then the governing Eq. (A10) becomes

$$\alpha^2 \frac{\partial^2 \phi}{\partial Y^2} + 2\alpha \frac{\partial^2 \phi}{\partial Y \partial z} + \frac{\partial^2 \phi}{\partial z^2} = \frac{\partial^4 \phi}{\partial Y^4}. \quad (\text{A13})$$

This is the equation for a wall that is nearly, but not exactly, parallel to the magnetic field. The governing equation for case III becomes that for case II as $\alpha \rightarrow 0$ and becomes that for case I as $\alpha \rightarrow \infty$, if we redefine δ .

APPENDIX B: MATCHING PRINCIPLE BETWEEN HARTMANN LAYER AND CORE REGION

The matching principle was originally stated by Lagerstrom^{20,21} in the early 1960s, which was proven to be rigorous by O'Malley^{22,23} in the late 1960s. The principle states that

$$n \text{ inner}(m \text{ outer}) = m \text{ outer}(n \text{ inner}) \quad (\text{B1})$$

where outer = core, and inner = boundary layer. We will illustrate with an example 2-inner (2-outer) = 2-outer (2-inner) where ($n = m = 2$).

The outer (core) expansion is

$$u_C(x; M) = u_{C0}(x) + M^{-1}u_{C1}(x) + M^{-2}u_{C2}(x) + \dots, \quad (\text{B2a})$$

2-outer = truncated after first two terms.

Thus,

$$2\text{-outer} = u_{C0}(x) + M^{-1}u_{C1}(x). \quad (\text{B2b})$$

Now, inner (n outer) = n outer rewritten in inner (boundary layer) variables so that

$$\text{inner}(2\text{-outer}) = u_{C0}(M^{-1}X) + M^{-1}u_{C1}(M^{-1}X). \quad (\text{B3})$$

This is not a legitimate asymptotic expansion because the coefficient functions $u_{Ci}(M^{-1}X)$ depend on M . We must change this to asymptotic expansion before we go on.

$$\text{For } X \text{ fixed, } M^{-1}X \rightarrow 0 \text{ as } M \rightarrow \infty. \quad (\text{B4})$$

Therefore, we use expansions for small argument, i.e., Taylor series:

$$\begin{aligned} u_{C0}(M^{-1}X) &= u_{C0}(0) + M^{-1}X \frac{du_{C0}(0)}{dx} \\ &+ \frac{1}{2} M^{-2}X^2 \frac{d^2u_{C0}(0)}{dx^2} \\ &+ \frac{1}{6} M^{-3}X^3 \frac{d^3u_{C0}(0)}{dx^3}. \end{aligned} \quad (\text{B5})$$

Also expanding $u_{C1}(M^{-1}X)$ in a Taylor series results in the following expansion for the truncated series

$$\begin{aligned} & \text{inner}(2\text{-outer}) \\ &= u_{C0}(0) + M^{-1} \left(u_{C1}(0) + X \frac{du_{C0}(0)}{dx} \right) \\ &+ M^{-2} \left(X \frac{du_{C1}(0)}{dX} + \frac{1}{2} X^2 \frac{d^2u_{C0}(0)}{dx^2} \right). \end{aligned} \quad (\text{B6})$$

This is now a valid asymptotic expansion in the form

$$\sum_i f_i(X)M^{-i}. \quad (\text{B7})$$

Therefore,

2-inner (2-outer) = truncated after second term,
2-inner (2-outer)

$$= u_{C0}(0) + M^{-1} \left(u_{C1}(0) + X \frac{du_{C0}(0)}{dx} \right). \quad (\text{B8a})$$

The inner expansion can be expressed as

$$\text{inner} = u_{b0}(X) + M^{-1}u_{b1}(X) + M^{-2}u_{b2}(X),$$

$$2\text{-inner} = u_{b0}(X) + M^{-1}u_{b1}(X),$$

$$\text{outer (2-inner)} = u_{b0}(Mx) + M^{-1}u_{b1}(Mx). \quad (\text{B8b})$$

This is not a legal expansion. Thus, we need to know how $u_{b1}(X)$ behaves as $X \rightarrow \infty$.

In general, we have solution forms from Hartmann boundary layer equations, so we know how the solution behaves. Assume, for some $\alpha > 0$

$$u_{b0}(X) \rightarrow A_0 + A_c \exp(-\alpha X) \text{ as } X \rightarrow \infty \quad (\text{B9})$$

and

$$u_{b1}(x) \rightarrow A_1 + B_1 X + B_c \exp(-\alpha X) \text{ as } X \rightarrow \infty.$$

By inspection the following relationships can be obtained for the Hartmann layer equations:

$$\lim_{X \rightarrow \infty} (u_{b0}) = A_0, \quad (\text{B10a})$$

$$\lim_{X \rightarrow \infty} \left(\frac{du_{b1}}{dX} \right) = B_1, \quad (\text{B10b})$$

$$\lim_{X \rightarrow \infty} (u_{b1} - B_1 X) = A_1. \quad (\text{B10c})$$

Note as $X \rightarrow \infty$, $\exp(-\alpha X) \ll X^{-n}$ for any n . The expansion in terms of these expressions is

outer (2-inner)

$$= A_0 + A_c \exp(-\alpha Mx) + M^{-1}[A_1 + B_1 Mx + B_c \exp(-\alpha Mx)]. \quad (\text{B11})$$

Since $\exp(-\alpha Mx) = \exp(-\alpha X) \rightarrow 0$ as $X \rightarrow \infty$ 2 outer (2-inner) = $A_0 + B_1 x + M^{-1}A_1$ + asymptotically exponentially small terms.

Using the matching principle [Eq. (B1)] as $X \rightarrow \infty$ in the boundary layer we obtain

$$A_0 + B_1 M^{-1}X + M^{-1}A_1 = u_{c0}(0) + M^{-1}u_{c1}(0) + M^{-1}X \frac{du_{c0}(0)}{dx}. \quad (\text{B12})$$

Therefore, the zeroth and first order matching conditions between the core region and Hartmann layer are

$$A_0 = u_{c0}(0) = \lim_{X \rightarrow \infty} [u_{b0}(X)], \quad (\text{B13a})$$

$$A_1 = u_{c1}(0) = \lim_{X \rightarrow \infty} [u_{b1}(X) - B_1 X], \quad (\text{B13b})$$

$$B_1 = \frac{du_{c0}(0)}{dx} = \lim_{X \rightarrow \infty} \frac{du_{b1}(X)}{dX}. \quad (\text{B13c})$$

APPENDIX C: MATCHING PRINCIPLE BETWEEN THE FREE-SHEAR LAYER AND HARTMANN LAYER

The free-shear layer is separated from each wall by a Hartmann layer with $O(M^{-1})$ thickness. Since the free-shear layer is $O(M^{-1/2})$ thickness and $M^{-1} \ll M^{-1/2}$, these Hartmann layers appear to the free-shear layer to have zero thickness. That is, the free-shear layer solution applies to

within an arbitrarily small distance from a wall and then there is a jump across a zero thickness layer to satisfy the wall conditions. When we stretch the normal coordinate to the wall by M , we can look at the structure of the jump across the "zero-thickness" layer which has been stretched to have $O(1)$ thickness. However, since $M \gg M^{1/2}$ the Hartmann layer sees the free-shear layer to be at infinity. Specifically, the value which the free-shear layer "sees" at an arbitrarily small distance from the wall appears to the Hartmann layer's stretched coordinate to be infinitely far from the wall.

The free-shear layer "sees" horizontal boundaries at $t = 0$ and $t = \sec \theta$, even though walls are not horizontal here.

The coordinate transformations are (see Figs. 2 and 4)

$$(z + a) = \xi \cos \theta + t \sin \theta, \quad (\text{C1a})$$

$$y = t \cos \theta - \xi \sin \theta, \quad (\text{C1b})$$

$$t = y \cos \theta + (z + a) \sin \theta, \quad (\text{C1c})$$

$$\xi = (z + a) \cos \theta - y \sin \theta. \quad (\text{C1d})$$

Let us now consider the matching between the free-shear layer and insulated Hartmann layer. The stretched coordinates are

$$Y = M^{1/2}y, \quad y = M^{-1/2}Y \quad (\text{C2a})$$

$$Z = M(z + a), \quad z = -a + M^{-1}Z. \quad (\text{C2b})$$

The Hartmann layer solution can be expressed as

$$u_H = M^{1/2}u_{H0}(Y, Z) + u_{H1}(Y, Z). \quad (\text{C3})$$

The free-shear layer coordinate and stretched coordinate are, respectively,

$$t = t, \quad \xi = M^{1/2}\xi. \quad (\text{C4})$$

The velocity in the free-shear layer can be expressed as

$$u_{f1} = 2\text{-outer} = M^{1/2}u_{f1}^{(0)}(t, \xi) + u_{f1}^{(1)}(t, \xi) \quad (\text{C5})$$

For inner (2-outer), we need t and ξ in terms of Y and Z . Note that t can be expressed in terms of y and z as

$$t = y \cos \theta + (z + a) \sin \theta. \quad (\text{C6})$$

Substituting Eqs. (C2a) and (C2b) for stretched coordinates results in the expression

$$t = \cos \theta (M^{-1/2}Y) + \sin \theta (M^{-1}Z). \quad (\text{C7a})$$

Also, ξ is expressed as

$$\begin{aligned} \xi &= M^{1/2}\xi = M^{1/2}(M^{-1}Z \cos \theta - M^{-1/2}Y \sin \theta) \\ &= (\cos \theta M^{-1}Z - Y \sin \theta). \end{aligned} \quad (\text{C7b})$$

Now the free-shear layer velocity u_{f1} can be expressed as

inner (2-outer)

$$\begin{aligned} &= M^{1/2}u_{f1,0}^{(0)}[(\cos \theta M^{-1/2}Y + \sin \theta M^{-1}Z), \\ &(\cos \theta M^{-1/2}Z - Y \sin \theta)] + u_{f1,1}^{(1)}[(\quad), (\quad)] + \dots \end{aligned} \quad (\text{C8})$$

The terms inner and outer are defined in Appendix B. Next we need to use a double Taylor series expansion:

$$u_{f1}^{(0)}(t, \zeta) = u_{f1}^{(0)}(0, -Y \sin \theta) + t \frac{\partial u_{f1}^{(0)}}{\partial t}(0, -Y \sin \theta) + (\zeta + Y \sin \theta) \frac{\partial u_{f1}^{(0)}}{\partial \zeta}(0, -Y \sin \theta), \quad (C9a)$$

where

$$(\zeta + Y \sin \theta) = \cos \theta M^{-1/2} Z. \quad (C9b)$$

Substituting in Eq. (C8) results in the expression

$$\begin{aligned} 2\text{-inner}(2\text{-outer}) = & M^{1/2} \left(u_{f1}^{(0)}(0, -Y \sin \theta) + (\cos \theta M^{-1/2} Y + \sin \theta M^{-1} Z) \frac{\partial u_{f1}^{(0)}}{\partial t}(0, -Y \sin \theta) \right. \\ & \left. + (\cos \theta M^{-1/2} Z) \frac{\partial u_{f1}^{(0)}}{\partial \zeta}(0, -Y \sin \theta) + \dots \right) + u_{f1}^{(1)}(0, -Y \sin \theta) + (\cos \theta M^{-1/2} Y \\ & + \sin \theta M^{-1} Z) \frac{\partial u_{f1}^{(1)}}{\partial t}(0, -Y \sin \theta) + \cos \theta M^{-1/2} Z \frac{\partial u_{f1}^{(1)}}{\partial \zeta}(0, -Y \sin \theta) + \dots \end{aligned} \quad (C10)$$

Keeping only $M^{1/2}$ and $O(1)$ terms for 2-inner (2-outer expression):

$$\begin{aligned} 2\text{-inner}(2\text{-outer}) = & M^{1/2} u_{f1}^{(0)}(0, -Y \sin \theta) + \cos \theta Y \frac{\partial u_{f1}^{(0)}}{\partial t}(0, -Y \sin \theta) \\ & + \cos \theta Z \frac{\partial u_{f1}^{(0)}}{\partial \zeta}(0, -Y \sin \theta) + u_{f1}^{(1)}(0, -Y \sin \theta). \end{aligned} \quad (C11)$$

When we do the matching all conditions on u_{f1} will be at $t = 0$, so it sees a horizontal wall

$$1\text{-inner}(1\text{-outer}) = 1\text{-outer}(1\text{-inner}): \quad \lim_{Z \rightarrow \infty} u_{H0}(Y, Z) = u_{f1}^{(0)}(0, -Y \sin \theta). \quad (C12)$$

¹H. O. Stevens, M. J. Superczynski, T. J. Doyle, J. H. Harrison, and H. Messinger, *IEEE Trans. Magn.* **13**, 269 (1977).

²T. J. Doyle, J. H. Harrison, and A. Chaikin, "Navy Superconductive Machinery Program," Soc. in Star Symposium, Naval Arch. Mar. Eng. Spring Meeting, New London Ct., paper 20, pp. 1-7; Society of Naval Architects and Marine Engineers, New York, NY 10048 (April 26-29, 1978) (unpublished).

³J. T. Eriksson, *Acta Polytech. Scand. Electr. Eng. Ser.* **48**, 1 (1948).

⁴H. O. Stevens and M. J. Cannell, "Acyclic Superconductive Generator Development 400-Horsepower Generator Design," David Taylor Naval Ship Research and Development Center, Report No. DTNSRDC/PAS-81/14, Bethesda, MD (Oct. 1981) (unpublished).

⁵R. L. Rhodenizer, "Development of Solid and/or Liquid Metal Collectors for Acyclic Machines," Final Report, Task 4 and 5, General Electric Co., Contract No. N00024-68-C-5415 (30 Sep. 1971), pp. 7-35 (unpublished).

⁶J. L. Johnson, G. T. Hummert, and A. R. Keeton, *IEEE Trans. Power Appar. Syst.* **PAS-95**, 1234 (1976).

⁷G. S. S. Ludford and J. S. Walker, in *MHD Flow and Turbulence II*, edited by H. Branover and A. Yakhot (Israel Universities Press, Jerusalem, Israel, 1980), pp. 83-95.

⁸H. Branover, *Magnetohydrodynamic Flow in Ducts* (Wiley, New York, 1978).

⁹J. C. R. Hunt and J. A. Shercliff, *Annu. Rev. Fluid Mech.* **3**, 37 (1971).

¹⁰W. F. Hughes and F. J. Young, *The Electromagnetodynamics of Fluids* (Wiley, New York, 1966).

¹¹S. H. Brown, J. Reilly, and N. A. Sondergaard, *J. Appl. Phys.* **62**, 386 (1987).

¹²C. J. N. Alty, *J. Fluid Mech.* **48**, 429 (1971).

¹³J. C. R. Hunt and D. G. Malcolm, *J. Fluid Mech.* **33**, 775 (1968).

¹⁴D. G. Malcolm, *J. Fluid Mech.* **41**, 531 (1970).

¹⁵J. C. R. Hunt and K. Stewartson, *J. Fluid Mech.* **38**, 225 (1969).

¹⁶L. D. Landau and E. M. Lifshitz, *Fluid Mechanics* (Pergamon, Addison-Wesley, Reading, MA, 1959).

¹⁷L. C. S. Utrecht, *Math. Appl. Sci.* **2**, 531 (1980).

¹⁸L. P. Cook, G. S. S. Ludford, and J. S. Walker, *Proc. Camb. Philos. Soc.* **72**, 13 (1972).

¹⁹P. S. Morse and H. Feshbach, *Methods of Theoretical Physics (Part I)*, (McGraw-Hill, New York, 1953), pp. 453-469.

²⁰P. A. Lagerstrom, *Lecture Notes, Institut Henri Poincare, Paris* (1961) (unpublished).

²¹P. A. Lagerstrom and R. G. Casten, *SIAM Rev.* **14**, 63 (1972).

²²R. E. O'Malley, Jr., *SIAM Rev.* **13**, 425 (1971).

²³R. E. O'Malley, Jr., *Arch. Ration. Mech. Anal.* **40**, 209 (1971).

Further studies of liquid-metal flows and power losses in ducts with a moving conducting wall and a skewed magnetic field

John S. Walker

University of Illinois at Urbana-Champaign, Urbana, Illinois 61801

Samuel H. Brown and Neal A. Sondergaard

David Taylor Research Center, Bethesda, Maryland 20084-5000

(Received 22 February 1988; accepted for publication 7 April 1988)

In a previous paper the authors initiated studies of fully developed laminar liquid-metal flows, currents, and power losses in a rectangular channel with a moving perfectly conducting wall and with a skewed homogeneous external magnetic field for high Hartmann numbers, high interaction parameters, low magnetic Reynolds numbers, and different aspect ratios. The channel had insulating side walls that were skewed to the external magnetic field, while the perfectly conducting moving top wall with an external potential and the stationary perfectly conducting bottom wall at zero potential acted as electrodes. These electrodes were also skewed to the external magnetic field. A mathematical solution was obtained for high Hartmann numbers by dividing the flow into three core regions, two free shear layers, and six Hartmann layers along the channel walls. The free shear layers were treated rigorously and in detail with fundamental magnetohydrodynamic theory. The previous work, however, left the solution for the velocity profiles in terms of a complex integral equation which was not solved. In the present work the integral equation is solved numerically by the method of quadratures to give the velocity profiles, viscous dissipation and Joulean losses in the free shear layers. In addition, expressions for the viscous dissipation in the six Hartmann layers are presented. The best approximation to the viscous dissipation in the channel is the sum of the $O(M^{3/2})$ contributions from the two free shear layers, the $O(M^{3/2})$ contributions from the two Hartmann layers separating the free shear layers from the insulators, and the $O(M)$ contributions from three of the Hartmann layers separating core regions from the walls. The best approximation to the Joulean power losses in the channel is the sum of the $O(M^2)$ contribution from the central core region which carries an $O(1)$ current between the electrodes and the $O(M^{3/2})$ contributions from the free shear layers. The expressions for the viscous dissipation and Joulean losses in each region involve the products of universal constants, electrical potentials and geometric factors. The theoretical magnetohydrodynamic model presented here was developed to provide data to help in the design of liquid-metal current collectors.

I. INTRODUCTION

Advanced homopolar electrical machinery is being developed for many new applications.¹⁻⁶ These advanced homopolar machines require current collectors for transporting high current at low voltages between rotating and stationary members of the machines with minimal losses and maximal operational stability. Therefore, liquid metals are often used in the sliding electric contact region, instead of more conventional brush technology. Generally, these machines have large magnetic fields in the region of the current collector, which produce Lorentz forces on the liquid metal which can increase power losses and lead to flow instabilities. Thus, to obtain current collector design parameters, one is interested in liquid-metal channel flow problems with applied external magnetic fields and with boundary conditions containing combinations of moving and fixed, conducting, or insulating walls. These boundary conditions then approximately correspond to a rotor, stator, or sidewall of the current collector and the liquid metal corresponds to the sliding electric contact.

In contrast to the rather extensive magnetohydrodynamic (MHD) duct flow literature,⁷⁻⁹ investigations treating moving conducting walls, such as discussed by Hughes and Young,¹⁰ are rare. Brown, Reilly, and Sondergaard¹¹ have studied fully developed, viscous liquid-metal flows and power losses in a rectangular channel with a moving conducting wall in a uniform, external magnetic field for moderate Hartmann numbers. The rectangular channel had insulating side walls parallel to the magnetic field and a perfectly conducting moving top wall and stationary bottom wall perpendicular to the field. A previous paper¹² by the authors treated rigorously and comprehensively this same problem with two major differences. The homogeneous transverse magnetic field was changed to a high strength, skewed magnetic field, and an external potential was applied to the conducting moving wall, thus making the channel transport current. Skewed magnetic fields are present at the collectors in some machine designs and external potentials on the electrodes correspond to the generated or motored voltage of the machines. These changes complicate the channel problem by

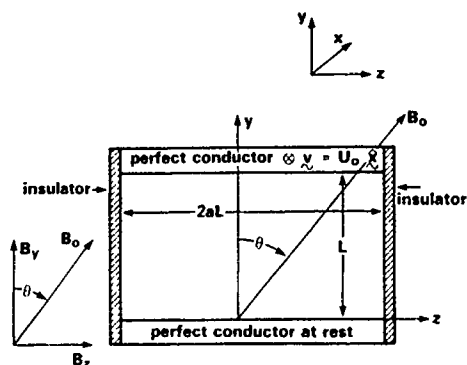


FIG 1 Rectangular channel with skewed external magnetic field and with moving and stationary perfect conductors

removing symmetry. The present paper should be considered as part two of the previous paper.¹²

The purpose of the previous paper¹² was to present comprehensive, two-dimensional analytical solutions for the flow velocity and electrical potential in different regions of the channel (see Fig. 1). In the three core regions, the singular perturbation problem for the velocity and electric potential was solved to zero order using matched asymptotic expansions. The solutions in the three core regions enabled the investigation of the influence on the velocity and electrical potential of the insulating sidewalls and an external skewed high magnetic field. Furthermore, analytic expressions were derived for the quantities of technical interest in the cores to zero order. These quantities were the load currents between the electrodes (i.e., moving and stationary conducting walls), Joulean and viscous dissipation, and channel resistance with skew angle. The parameters of variation were applied skewed external magnetic field, fluid electrical conductivity and viscosity, and channel aspect ratio.

The fundamental magnetohydrodynamic theory for the two free shear layers was also derived to zero order. However, the expressions for the velocity and electrical potential were left in a form requiring the solution of an integral equation.

The work begun in our earlier paper¹² is combined and completed here. We have calculated the velocity profile, viscous dissipation, and Joulean power losses in the free shear layers by numerically solving the integral equation with the method of quadratures. Furthermore, analytic expressions for the velocity profiles and viscous dissipation in the six Hartmann layers in the channel are presented.

In treating the magnetohydrodynamic flow due to electric current between two circular electrodes embedded in two parallel insulators with a transverse magnetic field, Alty¹¹ and Hunt and Malcolm^{14,15} treated a similar free shear layer, but their approach is quite different from ours.

II. NONDIMENSIONAL MAGNETOHYDRODYNAMIC EQUATIONS

The nondimensional magnetohydrodynamic equations for laminar duct flow in an external, homogeneous magnetic

field at an angle θ with the vertical can be written as

$$N^{-1}(\mathbf{v} \cdot \nabla) \mathbf{v} = -\nabla P + \mathbf{j} \times \hat{\mathbf{b}} + M^{-2} \nabla^2 \mathbf{v}, \quad (1a)$$

$$\mathbf{j} = -\nabla \phi + \mathbf{v} \times \hat{\mathbf{b}}, \quad (1b)$$

$$\nabla \cdot \mathbf{v} = 0, \quad (1c)$$

$$\nabla \cdot \mathbf{j} = 0, \quad (1d)$$

where

$$N = \text{interaction parameter, the ratio of ponderomotive force to inertial force} = \sigma B_0^2 L / \rho U_0; \quad (2a)$$

$$M = \text{Hartmann number, the positive square root of the ratio of the ponderomotive force to the viscous force} = LB_0(\sigma/\mu_f)^{1/2}; \quad (2b)$$

$$\mathbf{v} = \text{fluid velocity vector normalized by } U_0 = \mathbf{v}^*/U_0; \quad (2c)$$

$$P = \text{pressure normalized by } \sigma U_0 B_0^2 L = P^*/\sigma U_0 B_0^2 L; \quad (2d)$$

$$\mathbf{j} = \text{electric current density vector normalized by } \sigma U_0 B_0 = \mathbf{j}^*/\sigma U_0 B_0; \quad (2e)$$

$$\phi = \text{electrical potential normalized by } U_0 B_0 L = \phi^*/U_0 B_0 L; \quad (2f)$$

$$\nabla = \text{gradient normalized by } L = L \nabla^*; \quad (2g)$$

$$\hat{\mathbf{b}} = \text{unit vector parallel to external magnetic field } \mathbf{B}_0 (\mathbf{B}_0 = B_0 \hat{\mathbf{b}}); \quad (2h)$$

$$(\hat{\mathbf{x}}, \hat{\mathbf{y}}, \hat{\mathbf{z}}) = \text{unit vectors in Cartesian coordinates (see Fig. 1),}$$

$$\hat{\mathbf{b}} = \cos \theta \hat{\mathbf{y}} + \sin \theta \hat{\mathbf{z}}; \quad (2i)$$

where an asterisk denotes a dimensional quantity. Here σ and μ_f are the electrical conductivity and viscosity of the liquid metal, while L is the distance between the perfectly conducting electrodes, U_0 is the velocity of the moving perfectly conducting top, and B_0 is the strength of the external magnetic field.

It is assumed during this work that the magnetic Reynolds number $R_m = U_0 L \sigma \mu$ (i.e., ratio of induced magnetic field to external magnetic field) is much less than one, where μ is the liquid's magnetic permeability.

In the Cartesian system of dimensional coordinates (see Fig. 1), the (x, y, z) coordinates are normalized by L . The perfectly conducting sliding wall is at a constant velocity of $U_0 \hat{\mathbf{x}}$ at $y = 1$, the stationary perfectly conducting wall is positioned at $y = 0$. The insulating walls are at $z = \pm a$, where $2a$ is the aspect ratio of the channel. The external magnetic field angle θ is represented in terms of the field components as

$$\theta = \arctan(B_z/B_y), \quad (3a)$$

and the magnitude of the external magnetic field in terms of the field components is

$$B_0 = (B_y^2 + B_z^2)^{1/2}. \quad (3b)$$

Equation (1a) is the dimensionless Navier Stokes equation with an external ponderomotive body force $\mathbf{j} \times \hat{\mathbf{b}}$. Equation (1b) is the dimensionless expression for the electric current density induced in the channel. Equation (1c) is the dimensionless expression for the fluid incompressibility.

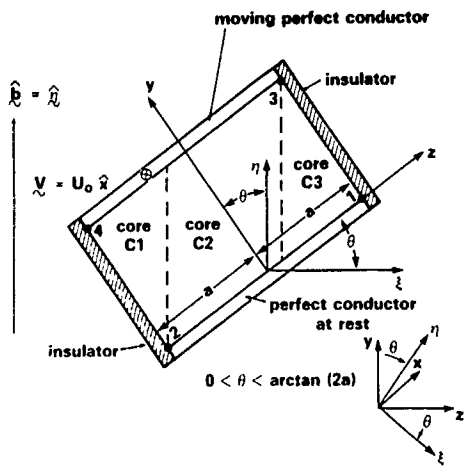


FIG 2 Rectangular channel with coordinate systems (x, y, z) and (x, η, ξ)

Equation (1d) represents the conservation of charge.

A new rotated nondimensional coordinate system (x, η, ξ) is defined with the η axis parallel to the external field \mathbf{B}_0 . Therefore, the unit vectors $\hat{\eta}$ and \hat{b} are identical (see Fig. 2), and \hat{x} is the unit vector in the axial direction along the channel. In our new rotated, right-handed coordinate system, the straight lines describing the top, bottom, left, and right walls are represented by the following equations:

$$\eta = \sec \theta + (\tan \theta) \xi \quad \text{for } -a \cos \theta - \sin \theta \leq \xi \leq a \cos \theta - \sin \theta, \quad (4a)$$

$$\eta = (\tan \theta) \xi \quad \text{for } -a \cos \theta \leq \xi \leq a \cos \theta, \quad (4b)$$

$$\eta = -a \csc \theta - (\cot \theta) \xi \quad \text{for } -a \cos \theta - \sin \theta \leq \xi \leq -a \cos \theta, \quad (4c)$$

$$\eta = a \csc \theta - (\cot \theta) \xi \quad \text{for } a \cos \theta - \sin \theta \leq \xi \leq a \cos \theta. \quad (4d)$$

It should be noted that the unit vectors in the two systems have the following relationships:

$$\hat{z} = \sin \theta \hat{\eta} + \cos \theta \hat{\xi}, \quad (5a)$$

$$\hat{y} = \cos \theta \hat{\eta} - \sin \theta \hat{\xi}, \quad (5b)$$

In our rotated coordinate system (x, η, ξ) the physically realizable variables for fully developed flow¹⁶ can be expressed as

$$\mathbf{v} = u(\eta, \xi) \hat{x}, \quad (6a)$$

$$P = P(\eta, \xi) \quad (\text{no axial pressure gradient}), \quad (6b)$$

$$\phi = \phi(\eta, \xi), \quad (6c)$$

$$\mathbf{j} = j_\eta(\eta, \xi) \hat{\eta} + j_\xi(\eta, \xi) \hat{\xi}. \quad (6d)$$

Substituting these variables into Eqs. (1a)–(1d) results in the following system of magnetohydrodynamic equations in terms of velocity and electrical potential. The electrical potential and flow velocity are variables that can be measured experimentally.

$$j_z = M^{-2} \left(\frac{\partial^2 u}{\partial \eta^2} + \frac{\partial^2 u}{\partial \xi^2} \right), \quad (7a)$$

$$j_\eta = -\frac{\partial \phi}{\partial \eta}, \quad j_\xi = -\frac{\partial \phi}{\partial \xi} + u, \quad (7b)$$

$$\frac{\partial j_\eta}{\partial \eta} + \frac{\partial j_\xi}{\partial \xi} = 0, \quad (7c)$$

and P is a constant.

Here we assume that the Hartmann number M is large. For $M \gg 1$, the interior of the channel is subdivided into three core regions with all $O(1)$ derivatives, two free shear layers which have $O(M^{-1/2})$ thicknesses and which separate adjacent core regions, and Hartmann layers which have $O(M^{-1})$ thicknesses and which separate cores or free shear layers from adjacent walls. In each core region,

$$j_\xi = 0, \quad j_\eta = j_\eta(\xi), \quad \phi = \psi(\xi) - \eta j_\eta(\xi), \quad u = \frac{\partial \phi}{\partial \xi}, \quad (8)$$

neglecting $O(M^{-2})$ terms. The jump in electrical potential or normal current density across a Hartmann layer is $O(M^{-1})$. The integration functions $j_\eta(\xi)$ and $\psi(\xi)$ in each core are determined by the electric potential of either perfect conductor or by the boundary condition $j_z = 0$ at either insulator, neglecting $O(M^{-1})$ terms. This completely determines the core solutions, which we presented in our previous paper.¹² The electrical potentials in adjacent cores are not equal at $\xi = -a \cos \theta$ and at $\xi = a \cos \theta - \sin \theta$, and the free shear layers at these planes must accommodate these jumps in the electrical potential. The dimensionless potentials at the fixed and moving conductors are zero and $(\phi_0 + \xi)$, respectively.

III. FREE SHEAR LAYER ANALYSIS

The free shear layer in region $f1$ is shown in Fig. 3. The potential at the left is

$$\phi_{c1} = \phi_0 - a \cos \theta, \quad (9a)$$

and the potential at the right is

$$\phi_{c2} = \cos \theta (\phi_0 - a \cos \theta) (\eta + a \sin \theta). \quad (9b)$$

The width of the layer is $O(M^{-1/2})$ and the top and bottom are at $\eta = \sec \theta - a \sin \theta$ and $\eta = -a \sin \theta$, respectively.

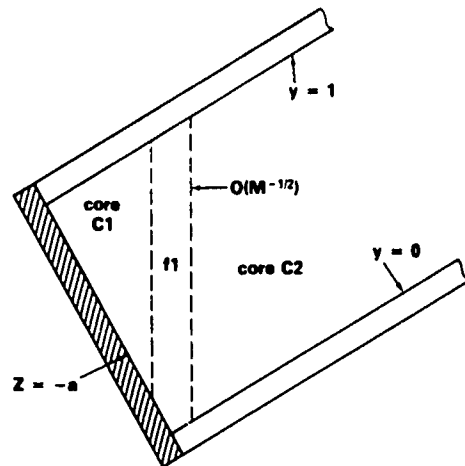


FIG. 3. Free shear layer $f1$ separating cores $c1$ and $c2$

We shall work out the fundamental mathematical theory for shear layer $f1$; the theory for shear layer $f2$ can be performed in an analogous manner. In order to develop the theory for $f1$, the stretched coordinate ξ will be defined as

$$\xi = M^{1/2}(\zeta + a \cos \theta), \quad \zeta = -a \cos \theta + M^{-1/2} \xi, \quad (10a)$$

$$\frac{\partial}{\partial \xi} = \frac{d\xi}{d\zeta} \frac{\partial}{\partial \zeta} = M^{1/2} \frac{\partial}{\partial \zeta}. \quad (10b)$$

The fundamental magnetohydrodynamic Eqs. (7a)–(7c) in the free shear layer $f1$ for fully developed flow in stretched coordinate ξ and regular coordinate η are

$$j_{\xi}(\eta, \xi) = \frac{1}{M^2} \left(\frac{\partial^2 u}{\partial \eta^2} + M \frac{\partial^2 u}{\partial \xi^2} \right), \quad (11a)$$

$$j_{\eta}(\eta, \xi) = -\frac{\partial \phi}{\partial \eta}(\eta, \xi),$$

$$j_{\xi} = -M^{1/2} \frac{\partial \phi}{\partial \xi}(\eta, \xi) + u(\eta, \xi), \quad (11b)$$

$$\frac{\partial j_{\eta}}{\partial \eta} + M^{1/2} \frac{\partial j_{\xi}}{\partial \xi} = 0.$$

The first terms in the series solutions in the free shear layer $f1$ are

$$j_{\eta}(\eta, \xi) = j_{\eta f1,0}(\eta, \xi), \quad (12a)$$

$$j_{\xi}(\eta, \xi) = M^{-1/2} j_{\xi f1,0}(\eta, \xi),$$

$$\phi(\eta, \xi) = \phi_{f1,0}(\eta, \xi), \quad (12b)$$

$$u(\eta, \xi) = M^{1/2} u_{f1,0}(\eta, \xi),$$

neglecting the $O(M^{-1/2})$, $O(M^{-1})$, $O(M^{-1/2})$, and $O(1)$ terms, respectively.

From the magnetohydrodynamic Eqs. (11a) and (11b), the following relationships can be developed:

$$u_{f1,0} = \frac{\partial \phi_{f1,0}}{\partial \xi}, \quad j_{\eta f1,0} = -\frac{\partial \phi_{f1,0}}{\partial \eta}, \quad (13a)$$

$$j_{\xi f1,0} = \frac{\partial^3 \phi_{f1,0}}{\partial \xi^3}, \quad \frac{\partial^2 \phi_{f1,0}}{\partial \eta^2} = \frac{\partial^4 \phi_{f1,0}}{\partial \xi^4}. \quad (13b)$$

The mathematical solutions to the differential Eq. (13a) and the boundary values of Eqs. (9a) and (9b) are assumed to be in the form

$$\phi_{f1,0} = \phi_0 - a \cos \theta + \Phi(t, \xi), \quad (14a)$$

where

$$t = \eta + a \sin \theta, \quad (14b)$$

and

$$\sin \theta > 0 \text{ for } f1, \quad \text{sign}(\sin \theta) = +1. \quad (14c)$$

Here $\Phi(t, \xi)$ is treated as a perturbing term which approaches zero as $\xi \rightarrow -\infty$ [see boundary value Eq. (9a)]. Also $\Phi(t, \xi)$ approaches zero at the moving perfect conductor. The partial differential Eq. (13b) in terms of $\Phi(t, \xi)$ with its five boundary conditions in terms of t and ξ is

$$\frac{\partial^2 \Phi}{\partial t^2} = \frac{\partial^4 \Phi}{\partial \xi^4} \text{ for } 0 < t < \sec \theta, \quad -\infty < \xi < \infty, \quad (15a)$$

where the boundary condition from matching core $c2$ is

$$\Phi \rightarrow (\phi_0 - a \cos \theta)(t \cos \theta - 1) \text{ as } \xi \rightarrow \infty, \quad (15b)$$

the boundary condition from matching core $c1$ is

$$\Phi \rightarrow 0 \text{ as } \xi \rightarrow -\infty, \quad (15c)$$

the boundary condition at the moving perfect conductor is

$$\Phi = 0 \text{ at } t = \sec \theta \text{ for } -\infty < \xi < \infty, \quad (15d)$$

the boundary condition at the fixed perfect conductor is

$$\Phi = -(\phi_0 - a \cos \theta) \text{ at } t = 0 \text{ for } 0 < \xi < \infty, \quad (15e)$$

and the boundary condition at the Hartmann layer separating the free shear layer from the insulating wall is

$$\frac{\partial^2 \Phi}{\partial \xi^2} + \frac{\partial \Phi}{\partial t} = 0 \text{ at } t = 0 \text{ for } -\infty < \xi < 0. \quad (15f)$$

The boundary conditions at the perfect conductors apply because the jumps in electrical potential across the Hartmann layers between the free shear layer and perfect conductors are $O(M^{-1})$. The boundary condition Eq. (15f) is obtained by matching the solution in the Hartmann layer between the free shear layer and the insulating wall.¹² Physically, this Hartmann layer must match the $O(M^{1/2})$ free shear layer velocity $u_{f1,0}$ at $t = 0$, and must satisfy the no-slip condition at the insulating wall. This jump in velocity involves a very large gradient in the viscous shear stress inside this Hartmann layer, i.e., $\partial \tau_{xz} / \partial z$ is large. The term τ_{xz} represents the x component of the surface force per unit area along the x - y plane. An $O(M^{1/2})$ tangential current density j_y inside this Hartmann layer provides the electromagnetic body force to balance this large shear stress gradient. The total Hartmann layer current in the y direction at each point along the insulating wall is proportional to the free shear layer velocity $u_{f1,0}$ evaluated at $t = 0$. Since this velocity varies along the insulator, the total current inside the Hartmann layer must vary as well. An increase in current must be drawn from the free shear layer, while a decrease implies a current into the free shear layer from the Hartmann layer. In the boundary condition (15f), the term $\partial^2 \Phi / \partial \xi^2$ represents the tangential variation of $u_{f1,0}$ at $t = 0$ since $u_{f1,0} = \partial \Phi / \partial \xi$. The term $\partial \Phi / \partial t$ represents the electric current from the Hartmann layer into the free shear layer or vice versa, since $j_{\eta} = -\partial \Phi / \partial t$.

By using the techniques of complex Fourier transform, the convolution theorem can be used to obtain $\Phi(t, \xi)$:

$$\Phi = \int_{-\infty - i\tau}^{\infty - i\tau} \hat{f}(\zeta^*) G(t, \xi - \zeta^*) d\zeta^*$$

$$= \int_0^{-i\tau} f(\zeta^*) G(t, \xi - \zeta^*) d\zeta^*, \quad (16a)$$

where

$$\hat{f}(\zeta) = \frac{\partial^2 \Phi}{\partial \xi^2}(0, \zeta) + \frac{\partial \Phi}{\partial t}(0, \zeta) = \begin{cases} 0 & \text{for } -\infty < \zeta < 0, \\ f(\zeta) & \text{for } 0 < \zeta < \infty. \end{cases} \quad (16b)$$

In the previous work¹² the Green function was evaluated to have the form

$$\begin{aligned}
G(t, \zeta) &= (\zeta/4) \{ \operatorname{erf}(\frac{1}{2}\zeta t^{-1/2}) \\
&\quad - \operatorname{erf}[\frac{1}{2}\zeta(2 \sec \theta - t)^{-1/2}] \} \\
&\quad + \frac{1}{2}\pi^{-1/2} \{ t^{1/2} \exp(-\frac{1}{2}\zeta^2 t^{-1}) \\
&\quad - (2 \sec \theta - t)^{1/2} \exp[-\frac{1}{2}\zeta^2(2 \sec \theta - t)^{-1}] \}. \quad (17)
\end{aligned}$$

This solution satisfies the governing equation and all boundary conditions except the condition (15f).

Remembering that $\Phi(t, \zeta)$ can be expressed by the convolution integral [Eq. (16a)] and must also satisfy the boundary condition at the fixed perfect conductor

$$\Phi = -(\phi_0 - a \cos \theta) \quad \text{at } t=0, \quad \text{for } 0 < \zeta < \infty, \quad (18)$$

the following relationship must hold:

$$\begin{aligned}
\int_0^\infty f(\zeta^*) G(0, \zeta - \zeta^*) d\zeta^* &= -(\phi_0 - a \cos \theta) \\
\text{for } 0 < \zeta < \infty. \quad (19)
\end{aligned}$$

In this equation, we change coordinates to reduce the integral equation to a form that is independent of $\sec \theta$ and of $(\phi_0 - a \cos \theta)$.

$$\begin{aligned}
\int_0^\infty F(Z^*) \{ |Z - Z^*| \operatorname{erfc}(|Z - Z^*|) \\
- \pi^{-1/2} \exp[-(Z - Z^*)^2] \} dZ^* &= 1 \\
\text{for } 0 < Z < \infty, \quad (20a)
\end{aligned}$$

where

$$\zeta = 2(2 \sec \theta)^{1/2} Z, \quad \zeta^* = 2(2 \sec \theta)^{1/2} Z^*, \quad (20b)$$

$$d\zeta^* = 2(2 \sec \theta)^{1/2} dZ^*, \quad 0 < \zeta, Z < \infty, \quad (20c)$$

$$f(\zeta) = f[2(2 \sec \theta)^{1/2} Z] = -\frac{(\phi_0 - a \cos \theta)}{2 \sec \theta} F(Z). \quad (20d)$$

This integral equation is solved numerically in detail here in order to determine the velocity profile directly in the free shear layer. We did not solve it in the previous paper.¹²

The velocity of the free shear layer is represented to zero order by [see Eq. (12b)]

$$u = M^{1/2} u_{f1,0}(\eta, \zeta), \quad (21a)$$

where the stretched coordinate ζ is defined as

$$\zeta = M^{1/2}(\xi + a \cos \theta). \quad (21b)$$

Here $u_{f1,0}$ is related to the zero-order potential function by

$$\begin{aligned}
u_{f1,0} &= \frac{\partial \phi_{f1,0}}{\partial \zeta} = \frac{\partial \Phi}{\partial \zeta}(t, \zeta) \\
\text{for } 0 \leq t \leq \sec \theta, \quad -\infty < \zeta < \infty. \quad (22)
\end{aligned}$$

The function $u_{f1,0}$ can be represented as

$$u_{f1,0} = \int_0^\infty f(\zeta^*) \frac{\partial G}{\partial \zeta}(t, \zeta - \zeta^*) d\zeta^*, \quad (23a)$$

where

$$\begin{aligned}
\frac{\partial G}{\partial \zeta}(t, \zeta) &= \frac{1}{4} \{ \operatorname{erf}(\frac{1}{2}\zeta t^{-1/2}) \\
&\quad - \operatorname{erf}[\frac{1}{2}\zeta(2 \sec \theta - t)^{-1/2}] \} \quad (23b)
\end{aligned}$$

was obtained from $G(t, \zeta)$ by partial differentiation [see Eq. (17)]. By using the identities

$$\operatorname{erf}(x) = \operatorname{sgn}(x) \operatorname{erf}(|x|), \quad \operatorname{erf}(x) = 1 - \operatorname{erfc}(x),$$

we obtain the expression

$$\begin{aligned}
u_{f1,0}(t, \zeta) &= \frac{1}{4} \int_0^\infty f(\zeta^*) \operatorname{sgn}(\zeta - \zeta^*) \\
&\quad \times \{ \operatorname{erfc}[\frac{1}{2}|\zeta - \zeta^*|(2 \sec \theta - t)^{-1/2}] \\
&\quad - \operatorname{erfc}[\frac{1}{2}|\zeta - \zeta^*|t^{-1/2}] \} d\zeta^*, \quad (24a)
\end{aligned}$$

where

$$f(\zeta) = -\frac{1}{2}(\phi_0 - a \cos \theta) \cos \theta F[\frac{1}{2}\zeta(2 \sec \theta)^{-1/2}]. \quad (24b)$$

Substituting

$$Z = \frac{1}{2}\zeta(2 \sec \theta)^{-1/2} \leftrightarrow \zeta = 2(2 \sec \theta)^{1/2} Z, \quad (25a)$$

$$Z^* = \frac{1}{2}\zeta^*(2 \sec \theta)^{-1/2} \leftrightarrow \zeta^* = 2(2 \sec \theta)^{1/2} Z^*, \quad (25b)$$

$$T = \frac{1}{2} \cos \theta t \leftrightarrow t = 2 \sec \theta T. \quad (25c)$$

into Eq. (24a) results in the expression for $u_{f1,0}$:

$$u_{f1,0} = (\phi_0 - a \cos \theta) (\cos \theta)^{1/2} U(T, Z), \quad (26a)$$

where

$$\begin{aligned}
U &= (2)^{-3/2} \int_0^\infty F(Z^*) \operatorname{sgn}(Z - Z^*) \\
&\quad \times \{ \operatorname{erfc}(|Z - Z^*|T^{-1/2}) - \operatorname{erfc} \\
&\quad \times [|Z - Z^*|(1 - T)^{-1/2}] \} dZ^*. \quad (26b)
\end{aligned}$$

It remains to solve the integral equation for $F(Z^*)$ for $0 \leq Z^* < \infty$ and to substitute this solution into the integral expression for $U(T, Z)$. The universal velocity function $U(T, Z)$ for $0 \leq T \leq 0.5$ and $-\infty < Z < \infty$ is independent of all parameters in the problem. For a particular set of values for θ and ϕ_0 , expression (26a) scales this universal velocity function into the $O(M^{1/2})$ free shear layer velocity $u_{f1,0}$.

The solution of the integral equation involves a Dirac delta function at $Z^* = 0$. The Hartmann layers on the insulator and perfect conductor intersect to form an $O(M^{-1}) \times O(M^{-1})$ corner region at $y = 0, z = -a$, as shown in Fig. 4. As noted in part a of this figure, the potential changes from 0 to $(\phi_0 - a \cos \theta)$ over a very small distance $\Delta y = O(M^{-1/2})$ at $z = -a$. This is the same as the jump in ϕ across the free shear layer at $t = 0$, but in the free shear layer this potential difference is balanced by the large induced electric field $(u_{f1,0} \hat{x}) \times \hat{b}$. Inside the Hartmann layer adjacent to the insulator, u must decrease from $u_{f1,0}$ to 0, so that locally the large potential gradient is not balanced by the induced electric field. This leads to a large electric current leaving the fixed perfect conductor through the $O(M^{-1}) \times O(M^{-1})$ corner region. Part of this current continues in the y direct to become the j_y in the insulating wall Hartmann layer which balances the large viscous shear gradient here. The rest of this current enters the free shear layer directly. Since the corner region has $O(M^{-1})$ dimensions, while the free shear layer has a much larger $O(M^{-1/2})$ thickness, the free shear layer sees the current from the corner region as a point source of electric current at $t = 0$ and $\zeta = 0$. Since F is the rescaled value of

$$\frac{\partial^2 \Phi}{\partial \zeta^2} + \frac{\partial \Phi}{\partial t} \quad (27)$$

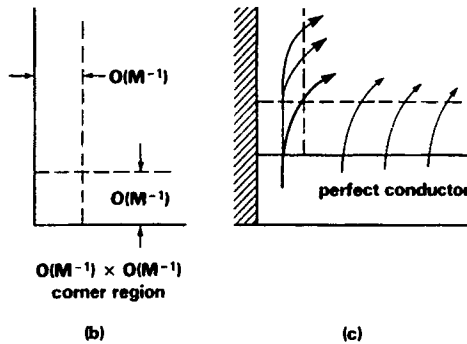
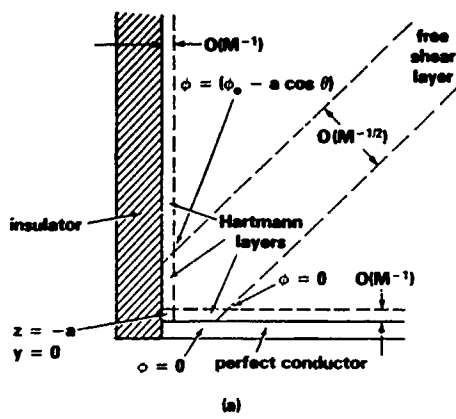


FIG. 4. Hartmann layers which separate the free shear layer f_1 from the walls at the corner, the $O(M^{-1}) \times O(M^{-1})$ corner region and the electric current flowing through the corner region into the free shear layer.

at $t = 0$, and $j_y = -\partial\Phi/\partial t$ is the current which sees a source at $Z = 0$, then

$$F(Z^*) = I_0 \delta(Z^* - \epsilon) + \hat{F}(Z^*), \quad (28)$$

where $0 < \epsilon \leq 1$ is included to avoid any ambiguity in the integral of δ from $Z^* = 0$ to ∞ . Here I_0 represents the magnitude of the electric current flowing from the corner region to the free shear layer and is determined by the condition that $\hat{F}(Z^*)$ is bounded at $Z^* = 0$. In other words, I_0 is chosen to remove all singular behavior from the modified integral equation

$$\int_0^\infty \hat{F}(Z^*) \{ |Z - Z^*| \operatorname{erfc}(|Z - Z^*|) - \pi^{-1/2} \exp[-(Z - Z^*)^2] \} dZ^* = 1 + I_0 [\pi^{-1/2} \exp(-Z^2) - Z \operatorname{erfc}(Z)]. \quad (29)$$

This integral equation is solved numerically using the following steps. The integral from $Z^* = 0$ to ZN is approximated by a trapezoidal rule and with a step size $\Delta Z^* = H$. For the integral from $Z^* = ZN$ to ∞ , we assume that $\hat{F}(Z^*) = \hat{F}(ZN)$ and carry out the integration explicitly. The integral from ZN to ∞ is then added to the coefficient of $\hat{F}(ZN)$ from the trapezoidal rule quadrature formula. The integral equation is evaluated at $Z = iH$, for $i = 0$ to $n = ZN/H$, i.e., at $Z = 0, H, 2H, \dots, ZN$. This gives $n + 1$ simultaneous linear algebraic equations for the unknowns $\hat{F}_j = \hat{F}(jH)$ for $j = 0$ to n . This set of simultaneous equations

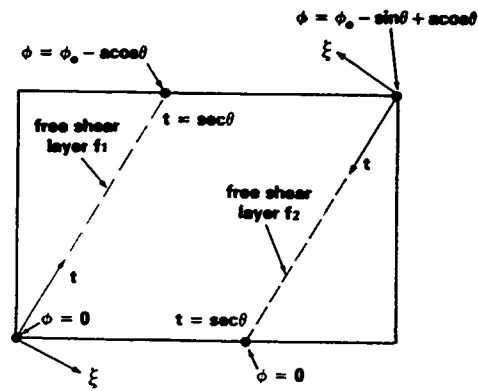


FIG. 5. Local (t, ξ) coordinates for each layer f_1 and f_2 . (1) Origin is at the corner of conductor and insulator, (2) t is parallel to the magnetic field; (3) at corner, perfect conductor lies in $\xi > 0$ and insulator lies in $\xi < 0$, and (4) ξ is the regular, unstretched coordinate.

is solved using Gauss elimination with partial pivoting. The value of I_0 is adjusted until $\hat{F}_0 = \hat{F}(0)$ is clearly the finite continuation of $\hat{F}_1 = \hat{F}(H)$ and $\hat{F}_2 = \hat{F}(2H)$. The values of \hat{F}_0 for two successive values of I_0 were used to predict the next guess for I_0 . This process converges quickly to $I_0 = -1$. This test is quite sensitive because $I_0 = -0.98$ gives a very large positive value of \hat{F}_0 and $I_0 = -1.02$ gives a very large negative value of \hat{F}_0 . For $I_0 = -1.00$, $\hat{F}_0 = -1.48$, $\hat{F}_1 = -1.51$, and $\hat{F}_2 = -1.54$, with $H = 0.03$. The values of H, ZN , and n were varied over a wide range of values to test the accuracy of the trapezoidal rule quadrature. The results for $H = 0.03, ZN = 1.2$, and $n = 40$ were the results used to compute U , but were essentially identical to the values for the other similar sets of H, ZN , and n .

The expression for $U(T, Z)$ is evaluated in a comparable series of steps. We substitute $F(Z^*) = -\delta(Z^* - \epsilon) + \hat{F}(Z^*)$. We use a trapezoidal rule quadrature for $0 \leq Z^* \leq ZN$. We take $\hat{F}(Z^*) = \hat{F}_n$ for $Z^* > ZN$ and integrate for this range explicitly.

IV. GENERALIZED FREE SHEAR LAYER SOLUTIONS

A. Free shear layer f_1

We have defined ϕ_1 to equal $(\phi_0 - a \cos \theta)$ in free shear layer f_1 (see Figs. 5 and 6). The change in potential across the layer is

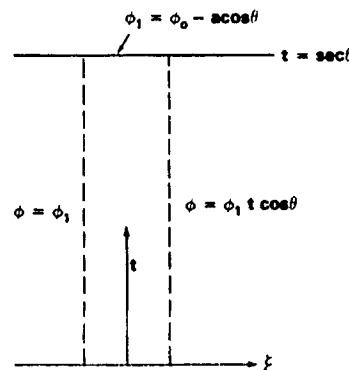


FIG. 6. Free shear layer f_1 .

$$\Delta\phi(t) = \phi(Z \rightarrow \infty) - \phi(Z \rightarrow -\infty), \quad (30a)$$

where the stretched coordinate Z is defined as

$$\xi = 2M^{-1/2}(2 \sec \theta)^{1/2}Z, \quad (30b)$$

$$Z = \frac{1}{2} M^{1/2} (2 \sec \theta)^{-1/2} \xi, \quad (30c)$$

where (t, ξ) are local Cartesian coordinates with the origin at the corner. Therefore,

$$\Delta\phi(t) = \phi_1(t \cos \theta - 1), \quad (31)$$

so that $\Delta\phi(t)$ varies from $-\phi_1$ at $t = 0$ to 0 at $t = \sec \theta$. The velocity in the free shear layer $f1$ is expressed as

$$u = M^{1/2} \phi_1 (\cos \theta)^{1/2} U(T, Z), \quad (32)$$

where t has been defined as $t = T(2 \sec \theta)$ in Eq. (25c). $T = 0$ at the corner of the insulator and perfect conductor and $T = 0.5$ at the other conductor. The range of T is $0 \leq T \leq 0.5$, which is inconvenient, but it eliminates several square roots of two from the equations.

When $Z \rightarrow \infty$ the stretched coordinate approaches the core between two perfect conductors. When $Z \rightarrow -\infty$, the coordinate approaches the core between the conductor and the insulator. $U(T, Z)$ is independent of ϕ_0 , θ , and a .

B. Free shear layer $f2$

In free shear layer $f2$, ϕ_2 was defined to equal

$$\phi_2 = (\phi_0 + a \cos \theta - \sin \theta)$$

(see Figs. 5-7). The jump in potential across the layer is

$$\Delta\phi(t) = \phi(Z \rightarrow \infty) - \phi(Z \rightarrow -\infty), \quad (33a)$$

where the stretched coordinate Z is defined as

$$\xi = 2M^{-1/2}(2 \sec \theta)^{1/2}Z, \quad (33b)$$

$$Z = \frac{1}{2} M^{1/2} (2 \sec \theta)^{-1/2} \xi, \quad (33c)$$

so that

$$\Delta\phi(t) = -\phi_2(t \cos \theta - 1). \quad (33d)$$

The velocity in the free shear layer $f2$ is expressed as

$$u = -M^{1/2} \phi_2 (\cos \theta)^{1/2} U(T, Z). \quad (34)$$

The definitions for T, Z , and U are the same as those given previously.

C. Generalized expression for velocity in free shear layers

The change in potential $\Delta\phi(t)$ across the generalized layer is (see Fig. 8)

$$\Delta\phi(t) = \phi(Z \rightarrow \infty) - \phi(Z \rightarrow -\infty), \quad (35)$$

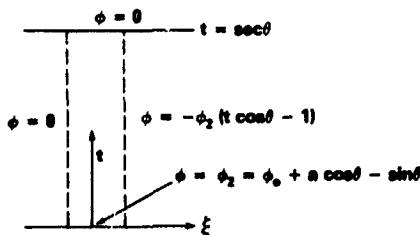


FIG. 7. Free shear layer $f2$.

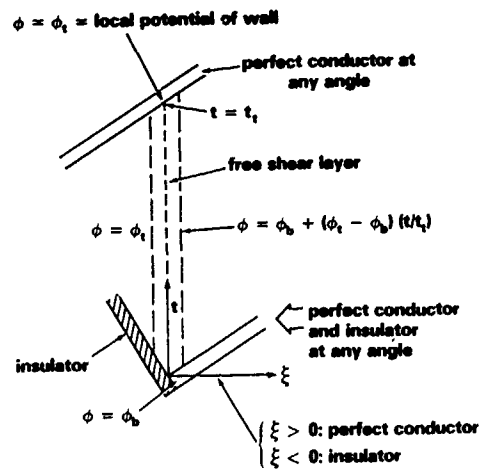


FIG. 8. Generalized notation for free shear layer.

where Z is the stretched coordinate. Then

$$\begin{aligned} \Delta\phi(t) &= \phi_b + (\phi_i - \phi_b)(t/t_i) - \phi_i \\ &= (\phi_i - \phi_b) [(t/t_i) - 1], \end{aligned} \quad (36a)$$

and the velocity u in the free shear layer is

$$u = M^{1/2} (\phi_i - \phi_b) (t_i)^{-1/2} U(T, Z), \quad (36b)$$

where

$$t = 2t_i T \leftrightarrow T = t/2t_i, \quad (36c)$$

and the stretched coordinate Z is defined as

$$\xi = 2M^{-1/2} (2t_i)^{1/2} Z \leftrightarrow Z = \frac{1}{2} M^{1/2} (2t_i)^{-1/2} \xi. \quad (36d)$$

As $Z \rightarrow \infty$, the stretched coordinate approaches the core between the two perfect conductors, and as $Z \rightarrow -\infty$ it approaches the core between the conductor and the insulator.

The function $U(T, Z)$ was defined as before. The results for U are presented in Fig. 9. Since inside the free shear layer

$$u = \frac{\partial \phi}{\partial \xi}, \quad \xi = M^{1/2} \xi, \quad (37)$$

and since $\phi = 0$ at $t = 0$, for $\xi > 0$, then $u = 0$ at $t = 0$, for $\xi > 0$. As $T \rightarrow 0$, the velocity profile becomes skewed to negative Z with $u \rightarrow 0$ for $Z > 0$. The volume flux inside the free

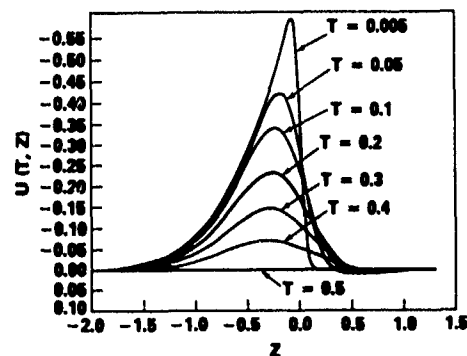


FIG. 9. Rescaled free shear layer velocity profiles $U(T, Z)$.

shear layer is proportional to $(\sec \theta - t)$, so it is 0 at $t = \sec \theta$ or $T = 0.5$, and maximum at $t = T = 0$ where $u = 0$ for $\zeta > 0$. As T increases from 0, the profile settles toward a nearly symmetric one with its center at $Z = -0.3$.

V. VISCOUS DISSIPATION AND JOULEAN POWER LOSSES

A. Free shear layers

The nondimensional viscous dissipation in the total channel can be found by solving the following integral in the different regions (see Fig. 10):

$$P_{T\mu} = \frac{P_{T\mu}^*}{\mu_f U_0^2} = \int_{-a}^a \int_0^1 \left[\left(\frac{\partial u}{\partial y} \right)^2 + \left(\frac{\partial u}{\partial z} \right)^2 \right] dy dz. \quad (38)$$

The contributions of the core regions are of order $O(1)$, the contributions of the Hartmann layers between the cores and the walls are of $O(M)$, the contributions of the two free shear layers are of order $O(M^{3/2})$, and the contributions of the two Hartmann layers between the free shear layers and the insulating walls are of $O(M^{3/2})$.

The nondimensional viscous dissipation in free shear layer $f1$ is expressed as

$$P_{T\mu f1} = M^{3/2} \int_0^{\sec \theta} \int_{-\infty}^{\infty} \left(\frac{\partial u_{f1,0}}{\partial \zeta} \right)^2 d\zeta dt, \quad (39a)$$

where

$$u_{f1,0}(t, \zeta) = (\phi_0 - a \cos \theta) (\cos \theta)^{1/2} U(T, Z) \quad (39b)$$

and

$$\frac{\partial u_{f1,0}}{\partial \zeta} = (2)^{-3/2} (\phi_0 - a \cos \theta) \cos \theta \frac{\partial U}{\partial Z}(T, Z). \quad (39c)$$

Since $d\zeta = 2(2 \sec \theta)^{1/2} dZ$ and $dt = 2 \sec \theta dT$, the viscous dissipation in $f1$ can be expressed as

$$P_{T\mu f1} = M^{3/2} (\phi_0 - a \cos \theta)^2 (\cos \theta)^{1/2} (P_{\mu f}), \quad (40a)$$

where

$$P_{\mu f} = (2)^{-1/2} \int_0^{1/2} \int_{-\infty}^{\infty} \left(\frac{\partial U}{\partial Z} \right)^2 dZ dT. \quad (40b)$$

We introduce Eq. (26b) for $U(T, Z)$, and expression (28) for $F(Z^*)$. We use the identities

$$\frac{\partial}{\partial Z} (|Z|) = \text{sgn}(Z), \quad \frac{\partial}{\partial Z} [\text{sgn}(Z)] = 2\delta(Z). \quad (41)$$

Finally we introduce the numerical results for $\hat{F}(Z^*)$ and evaluate the integral with respect to Z^* with the same trapezoidal rule quadrature to obtain a value for $P_{\mu f}$. $P_{\mu f}$ is a universal constant for all free shear layers of this type and equals 0.0918. The dimensionless viscous dissipation for free shear layer $f1$ is written as

$$P_{T\mu f1} = M^{3/2} \phi_1^2 (\cos \theta)^{1/2} (P_{\mu f}), \quad (42)$$

where $\phi_1 = (\phi_0 - a \cos \theta)$.

The dimensionless viscous dissipation for free shear layer $f2$ is derived from analogous arguments as

$$P_{T\mu f2} = M^{3/2} \phi_2^2 (\cos \theta)^{1/2} (P_{\mu f}), \quad (43)$$

where $\phi_2 = (\phi_0 + a \cos \theta - \sin \theta)$.

Also the viscous dissipation for a generalized free shear layer using the generalized formulation for the free shear layers can be expressed as [Eqs. (36)]

$$P_{T\mu f} = M^{3/2} (\phi_i - \phi_b)^2 (t_i)^{-1/2} (P_{\mu f}), \quad (44)$$

where $P_{\mu f}$ is again the universal constant 0.0918.

B. Viscous dissipation in the Hartmann layers

Let $P_{T\mu H1}$ be the dimensionless viscous dissipation for the Hartmann layer between the free shear layer $f1$ and the insulator at $z = -a$ and let $P_{T\mu H2}$ be the dimensionless viscous dissipation for the Hartmann layer between the free

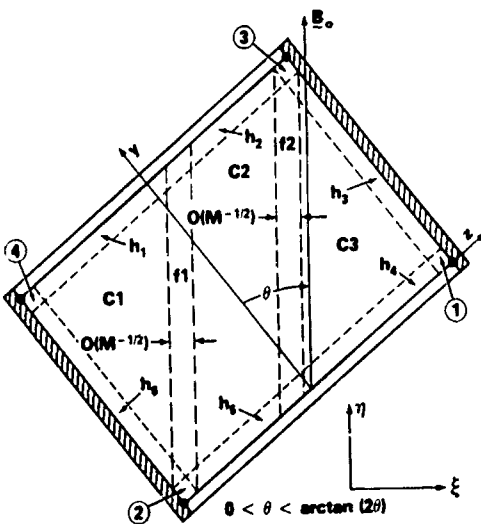


FIG. 10. Subregions in magnetohydrodynamic channel flow at high external magnetic fields

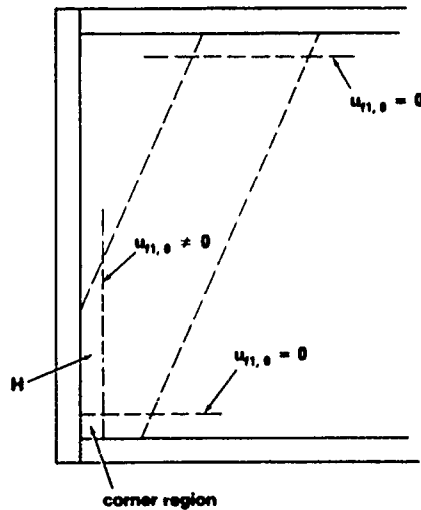


FIG. 11. Hartmann layer adjacent to free shear layer $f1$. The $O(M^{1/2})$ free shear layer velocity $u_{f1,0}$ is zero at $t = \sec \theta$ for all ζ and at $t = 0$ for $\zeta > 0$. There are no $O(M^{1/2})$ velocities in the Hartmann layers between the free shear layer and the perfect conductors, so that $P_{T\mu} = O(M^{1/2})$ in these layers.

shear layer $f2$ and the insulator at $z = a$.

In a previous paper,¹² we found the zero-order velocity in the Hartmann layer H (see Fig. 11) to have the form

$$u = M^{1/2} u_{f1,0}(0, -Y \sin \theta) \times [1 - \exp(-|\sin \theta| \Xi)], \quad (45)$$

where

$$Y = M^{1/2} y \quad \text{and} \quad \Xi = M(z + a) \quad (46)$$

are the stretched tangential and normal coordinates for this Hartmann layer, respectively. Here $\zeta = -Y \sin \theta$ in the free shear layer at $t = 0$. In the Hartmann layer

$$\frac{\partial u}{\partial z} = M^{3/2} u_{f1,0}(0, -Y \sin \theta) |\sin \theta| \times \exp(-|\sin \theta| \Xi), \quad (47)$$

while $\partial u / \partial y$ is only $O(M)$. We introduce the result Eq. (47) into expression (38) for the dimensionless viscous dissipation, where

$$dy = M^{-1/2} dY, \quad dz = M^{-1} d\Xi, \quad (48)$$

for this Hartmann layer. The ranges of integration for both Y and Ξ are from 0 to ∞ . The integral with respect to Ξ can be carried out explicitly since it only involves $\exp(-2|\sin \theta| \Xi)$. The result is an expression for the dimensionless viscous dissipation in this Hartmann layer,

$$P_{\mu H1} = \frac{1}{2} M^{3/2} |\sin \theta| \int_0^\infty [u_{f1,0}(0, -Y \sin \theta)]^2 dY. \quad (49)$$

Substituting $\zeta = -Y \sin \theta$, or $dY = -\csc \theta d\zeta$, noting that $\sin \theta$ is positive for this Hartmann layer, and reversing the limits of integration gives

$$P_{\mu H1} = \frac{1}{2} M^{3/2} \int_{\zeta}^0 [u_{f1,0}(0, \zeta)]^2 d\zeta. \quad (50)$$

Note that the expression is independent of the angle of the insulator relative to the free shear layer. The integral involves only the free shear layer solution which depends on only two parameters: the jump in ϕ , namely $\phi_1 = (\phi_0 - a \cos \theta)$, and the length of the layer $t_1 = \sec \theta$. Changing the variables from $u_{f1,0}$ to U and from ζ to Z gives

$$P_{\mu H1} = M^{3/2} \phi_1^2 (\cos \theta)^{1/2} (P_{\mu H}), \quad (51a)$$

where

$$P_{\mu H} = (2)^{1/2} \int_{-\infty}^0 [U(0, Z)]^2 dZ. \quad (51b)$$

$P_{\mu H}$ was calculated numerically from Eq. (26b) and the value is 0.197 26, which is more than double the value for the free shear layer.

$U(0, Z)$ has a discontinuity or step at $Z = 0$ from roughly -0.7 to 0, as shown in Fig. 12. The corner region which is $O(M^{-1}) \times O(M^{-1})$ must match this discontinuity. Hunt and Stewartson¹⁶ give the solution inside the corner region. In this region $u = O(M^{1/2})$, $\partial u / \partial y = O(M^{1/2})$, and $\partial u / \partial z = O(M^{3/2})$, so that

$$\left[\left(\frac{\partial u}{\partial y} \right)^2 + \left(\frac{\partial u}{\partial z} \right)^2 \right] = O(M^1). \quad (52)$$

However, $dy = O(M^{-1})$ and $dz = O(M^{-1})$ in expression

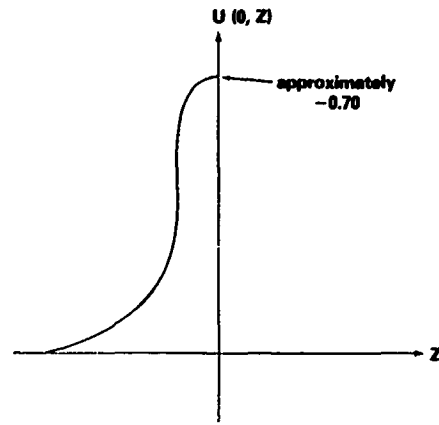


FIG 12. Sketch of $U(T, Z)$ at $T = 0$.

(38) for the viscous dissipation, so that the contribution to P_{μ} from the corner region is only $O(M^1)$. This contribution represents a small correction to the viscous dissipation in the Hartmann layer between the insulator and free shear layer $f1$.

The only $O(M^{3/2})$ contributions to the viscous dissipation arise from the two free shear layers and the $O(M^{-1}) \times O(M^{-1/2})$ Hartmann layers separating the free shear layers from the adjacent insulators. Summing both free shear layers and their Hartmann layers gives the following expression for the $O(M^{3/2})$ viscous dissipation

$$P_{T\mu} = M^{3/2} (\phi_1^2 + \phi_2^2) (\cos \theta)^{1/2} (P_{\mu f} + P_{\mu H}), \quad (53)$$

where $P_{\mu f} = 0.0918$ and $P_{\mu H} = 0.197 26$.

The coefficient $(P_{\mu f} + P_{\mu H}) = 0.2891$ of the $O(M^{3/2})$ dimensionless viscous dissipation is relatively small. With the assumption that $M \gg 1$, we have so far assumed that the $O(M)$ contributions to the viscous dissipation are negligible compared to the $O(M^{3/2})$ leading term in the asymptotic expansion. In actual homopolar devices, M has a moderately large value, for example, 50, so that $M^{3/2}$ is not much larger than M . If the coefficient of the $O(M)$ term is larger than $(P_{\mu f} + P_{\mu H})$, then the $O(M)$ term might be as large as the $O(M^{3/2})$ term for actual values of M , such as 50. There are four contributions to the $O(M)$ dimensionless viscous dissipation:

(1) The $O(M)$ correction or perturbation in the free shear layers.

(2) The $O(M)$ correction or perturbation in the Hartmann layers separating the free shear layers from the insulators.

(3) The viscous dissipation in the $O(M^{-1}) \times O(M^{-1})$ corner regions at $y = 0, z = \pm a$, associated with the jump in $U(0, Z)$ from -0.7 to 0.

(4) The viscous dissipation in the Hartmann layers between the core regions and the walls where there is a jump in the $O(1)$ velocity across the Hartmann layer.

The first three contributions to the $O(M)$ dissipation are all proportional to the free shear layer solution. We will assume that this proportionality leads to coefficients which are comparable to $(P_{\mu f} + P_{\mu H})$, so that these contributions are indeed $O(M^{-1/2})$ smaller. On the other hand, the Hart-

mann layers adjacent to the core regions involve a contribution that is related to the potentials in the perfect conductors and not to those in the free shear layers. In particular, the viscous dissipations in the Hartmann layers adjacent to the two perfect conductors increase as the aspect ratio of the channel, $2a$, increases. Real current collectors have large values of $2a$, for example, 25, so that the $O(M)$ Hartmann layer contribution may be larger than the $O(M^{3/2})$ free shear layer contribution.

The Hartmann layers adjacent to the cores are numbered $h 1$ to $h 6$ in Fig. 10. The core solutions were presented in a previous paper.¹² Hartmann layers $h 1$, $h 3$, and $h 4$ involve no jumps in the $O(1)$ velocity u , and their viscous dissipation is at most $O(1)$. For Hartmann layers $h 2$, $h 5$, and $h 6$, the velocity varies exponentially from the core value to the wall value (0 or 1). The velocities inside these Hartmann layers are

$$u_{h6} = 1 - \exp[-M|\sin\theta|(z+a)], \quad (54a)$$

$$u_{h2} = u_{c2}(y=1)\{1 - \exp[M|\cos\theta|(y-1)]\} + 1, \quad (54b)$$

$$u_{h5} = u_{c2}(y=0)\{1 - \exp[-M|\cos\theta|y]\}. \quad (54c)$$

In core $c2$, ϕ is determined by the potentials of the perfect conductors and $u = \partial\phi/\partial\xi$. Integrating the viscous dissipation per unit volume over each of the Hartmann layers $h 6$, $h 2$, and $h 5$ gives

$$P_{\mu h6} = \frac{1}{2} M \sin\theta, \quad (55a)$$

$$P_{\mu h2} = P_{\mu h5} = \frac{1}{6} M \sin^2\theta(\phi_2^3 - \phi_1^3), \quad (55b)$$

where again $\phi_1 = \phi_0 - a \cos\theta$, and

$$\phi_2 = \phi_0 + a \cos\theta - \sin\theta = \phi_1 + \Delta\phi, \quad (55c)$$

$$\Delta\phi = 2a \cos\theta - \sin\theta > 0, \quad (55d)$$

for $0 < \tan\theta < 2a$. Therefore, the viscous dissipation in the free shear layers and adjacent Hartmann layers H is proportional to

$$\phi_2^3 - \phi_1^3 = 2\phi_1^2(\Delta\phi) + (\Delta\phi)^3, \quad (56)$$

while the viscous dissipation in the Hartmann layers adjacent to the core $c2$ is proportional to

$$\phi_2^3 - \phi_1^3 = (\Delta\phi)[3\phi_1^2 + 3\phi_1(\Delta\phi) + (\Delta\phi)^2]. \quad (57)$$

The quantity $(\Delta\phi)$ can be moderately large. For example, for $2a = 25$ and $\theta = 45^\circ$, $(\Delta\phi) = 17$, which can make the Hartmann layer dissipation comparable to that of the free shear layers for modest values of M . Therefore, the best approximation to the viscous dissipation would be the sum of the $O(M^{3/2})$ contribution from the free shear layers and Hartmann layers H and of the $O(M)$ contribution from the Hartmann layers $h 6$, $h 2$, and $h 5$.

C. Joulean power losses

In addition to viscous dissipation, there are Joulean power losses due to the flow of electric current through the electrically resistive liquid metal. The Joulean power losses are given by

$$P_{Tj} = \frac{P_{Tj}^*}{\mu_f U_0^2} = M^2 \int_{-a}^a \int_0^1 (j_y^2 + j_z^2) dy dz. \quad (58)$$

In the core regions $c1$ and $c3$, $j_\eta = O(M^{-1})$; in the core region $c2$, $j_\eta = O(1)$; and in all three core regions, $j_\xi = O(M^{-2})$. Therefore, the contributions to the Joulean power losses are $O(M^2)$ for the core region $c2$ and $O(1)$ for the core regions $c1$ and $c3$. In a previous paper,¹² we presented the expression for the Joulean losses in the core region $c2$, namely

$$P_{Tj c2} = \frac{1}{3} M^2 (\cos\theta) (\phi_2^3 - \phi_1^3). \quad (59)$$

Equation (59) assumes that $j_\eta = -\cos\theta(\phi_0 + \xi)$ everywhere in the parallelogram defined by $(\tan\theta)\xi \leq \eta \leq (\tan\theta)\xi + \sec\theta$, for $-a \cos\theta \leq \xi \leq a \cos\theta - \sin\theta$, and that $j = 0$ everywhere in the two triangles for $\xi \leq -a \cos\theta$ and for $\xi \geq a \cos\theta - \sin\theta$. In reality, the $O(1)$ current density deviates from these values inside the free shear layers $f1$ and $f2$ and in the Hartmann layers $h 2$ and $h 5$, so that these viscous layers contribute corrections, either additions or subtractions, to the Joulean power losses based on the core solutions.

The current lines do not actually end exactly at $\xi = -a \cos\theta$ and at $\xi = a \cos\theta - \sin\theta$. Instead, the current lines fringe an $O(M^{-1/2})$ distance beyond these lines inside the free shear layers. Thus the cross-sectional area of the effective conductor between the two electrodes is the $O(1)$ area of the core region $c2$ plus the $O(M^{-1/2})$ areas of the two free shear layers $f1$ and $f2$. The $O(M^{-1/2})$ additional current inside the two free shear layers contributes an $O(M^{3/2})$ additional Joulean power loss. The steps to determine the free shear layer contribution exactly parallel the steps to determine the $O(M^{3/2})$ viscous dissipation due to the free shear layers. The total addition due to both free shear layers is

$$P_{Tj f} = 0.6692 M^{3/2} (\cos\theta)^{1/2} (\phi_1^2 + \phi_2^2). \quad (60)$$

The additional Joulean power losses due to the extra fringing current inside the free shear layers is more than twice the viscous dissipation in the free shear layers and associated Hartmann layers, as given by Eq. (53).

In the Hartmann layers $h 2$ and $h 5$, the current lines from the core region $c2$ must bend in order to enter the perfect conductors at right angles. This bend in the current lines makes the current density in the Hartmann layer less than that in the core. Since Eq. (59) assumes that the core solution applies all the way to the perfect conductors, it slightly overestimates the Joulean power losses very near the conductors. The $O(M)$ correction due to both the Hartmann layers $h 2$ and $h 5$ is given by

$$P_{Tj h} = -M(\sin\theta)^2 \cos\theta(\phi_2^3 - \phi_1^3). \quad (61)$$

The best estimate of the Joulean power losses is given by the sum of Eqs. (59)–(61).

VI. CONCLUSIONS

In a rectangular duct having insulating sides, a moving perfectly conducting top wall, a stationary perfectly conducting bottom wall, and a strong, skewed magnetic field, there are free shear or interior layers lying along the two magnetic field lines through opposite corners of the cross section. These free shear layers separate pairs of inviscid core regions and must match different electrical potentials in the

adjacent cores. These layers involve very large, $O(M^{1/2})$ dimensionless velocities, while the core velocities are only $O(1)$. These high velocity sheet jets can be in either the plus or the minus x direction, i.e., with or opposite to the moving wall's direction. The direction of flow in each free shear layer depends on the sign of the electrical potential at the point where the layer intersects the moving conductor, that is, on the signs of ϕ_1 and ϕ_2 . These values depend on the direction of the load current: if there is a significant load current from the stator to the rotor, then both ϕ_1 and ϕ_2 are negative; if there is a significant current from the rotor to the stator, then both ϕ_1 and ϕ_2 are positive; if there is no load current, then ϕ_1 is negative and ϕ_2 is positive.

The boundary value problem for the free shear layers was reduced to an integral equation in a previous paper.¹² The numerical solution of this integral equation is presented here. The velocity profiles in the free shear layers are also presented here. These profiles are reduced to a universal function $U(T, Z)$ for all similar shear layers. The scaling for any particular shear layer depends on only two parameters: the jump in the electrical potential across the layer at the corner where the insulator and conductor meet, i.e., ϕ_1 and ϕ_2 for free shear layers $f1$ and $f2$ here, and the length of the free shear layer along the magnetic field line, i.e., $\sec \theta$ here.

Since there are large velocities inside very thin regions, the free shear layers and adjacent Hartmann layers involve large viscous dissipation. Their contributions to the dimensionless viscous dissipation are $O(M^{3/2})$, while those of the cores are only $O(1)$. We have also computed the $O(M)$ viscous dissipation in the Hartmann layers between the cores and the walls. Finally we determined the contributions to the Joulean power losses from the core region $c2$, from the free shear layers $f1$ and $f2$, and from the Hartmann layers $h2$ and $h5$.

Here we assumed that the flow is laminar. Very strong magnetic fields would completely eliminate turbulence and instability in the laminar flow. However, in actual homopolar devices, the magnetic field is strong enough to make the turbulence two-dimensional, but is not strong enough to eliminate turbulence completely or to eliminate instabilities which lead to vortices aligned with the magnetic field. The two-dimensional turbulence or aligned vortices would be strongest in the free shear layer because of the large velocity gradients here. The effects of this turbulence or vorticity would be to increase the thickness of the free shear layer, to reduce the maximum free shear layer velocity proportionately, and to reduce the viscous dissipation considerably. Two-dimensional turbulence or aligned vortices in a strong magnetic field involve relatively little dissipation, unlike three-dimensional turbulence. Therefore, the present expressions for the viscous dissipation should provide conservative overestimations.

ACKNOWLEDGMENTS

We wish to express our appreciation for the helpful discussions and encouragement given by Dr. F. J. Young, Scientific Division, Frontier Timber Co., Bradford, PA 16701. We are also grateful for the support of the Independent Research/Independent Exploratory Development (IR/IED)

program at the David Taylor Research Center, Bethesda, MD 20084-5000, sponsored by the office of the Chief of Naval Research, Director of Naval Research.

APPENDIX: HUNT AND STEWARTSON'S INTEGRAL EQUATION FOR A SIMILAR FREE SHEAR LAYER

The integral equation of interest in the present paper is a Fredholm integral equation of the first kind

$$\int_0^\infty F(Z^*) \{ |Z - Z^*| \operatorname{erfc}(|Z - Z^*|) - \pi^{-1/2} \exp[-(Z - Z^*)^2] \} dZ^* = 1. \quad (A1)$$

Hunt and Stewartson's¹⁶ integral equation has the form

$$g(\rho) = (2\pi)^{-1/2} \int_0^\infty g(t) \exp[-\frac{1}{2}(t - \rho)^2] dt. \quad (A2)$$

Equation (A1) can be reduced to Eq. (A2) by three steps: integration by parts, differentiation with respect to Z and rescaling Z and Z^* by $(2)^{1/2}$. Substituting the expressions

$$G(Z^*) = \int_0^{Z^*} F(\hat{Z}) d\hat{Z}, \quad \frac{dG(Z^*)}{dZ^*} = F(Z^*) \quad (A3)$$

into the inhomogeneous integral Eq. (A1) and integrating by parts gives the equivalent form:

$$\int_0^\infty G(Z^*) \operatorname{sgn}(Z - Z^*) \operatorname{erfc}(|Z - Z^*|) dZ^* = 1. \quad (A4)$$

Differentiation with respect to Z gives

$$G(Z) = \pi^{-1/2} \int_0^\infty G(Z^*) \exp[-(Z - Z^*)^2] dZ^*. \quad (A5)$$

If we now introduce the change of variables

$$Z = \rho(2)^{-1/2}, \quad Z^* = t(2)^{-1/2}, \quad G[\rho(2)^{-1/2}] = A g(\rho) \quad (A6)$$

into the integral Eq. (A5), then we obtain Hunt and Stewartson's integral Eq. (A2). Here A is an arbitrary multiplicative constant since their integral equation is homogeneous. The integral Eq. (A1) has a unique solution, but one must recognize that $F(Z)$ has a singularity at $Z = 0$ and must adjust the strength of the singularity I_0 to obtain a numerical solution which gives a bounded \hat{F} at $Z = 0$. The integral Eq. (A2) does not have a unique solution. Hunt and Stewartson¹⁶ made the solution unique with the condition

$$\frac{dg(\rho)}{d\rho} \rightarrow 1 \quad \text{as } \rho \rightarrow \infty, \quad (A7)$$

which they derived by matching the adjacent core solution. No such condition is needed here, and $F \rightarrow -2$ automatically as $Z \rightarrow \infty$, which is equivalent to condition (A7).

¹H. O. Stevens, M. J. Superczynski, T. J. Doyle, J. H. Harrison, and H. Messinger, IEEE Trans. Magn. MAG-13, 269 (1977).

²T. J. Doyle, J. H. Harrison, and A. Chaikin, in *Star Symposium*, Naval Arch. Mar. Eng. Spring Meeting, April 26-29, 1978, New London, CT (Society of Naval Architects and Marine Engineers, New York, 1978), paper 20, pp. 1-7.

³Jarl-Thure Eriksson, in *Electrical Engineering Series*, edited by M. Luukkala (The Finnish Academy of Technical Sciences, Helsinki, Finland, 1948), Vol. 48.

- ⁴H. O. Stevens and M. J. Cannell, "Acyclic Superconductive Generator Development 400-Horsepower Generator Design," David Taylor Naval Ship Research and Development Center, Report No. DTNSRDC/PAS-81/14, Bethesda, MD (Oct., 1981).
- ⁵R. L. Rhodenizer, "Development of Solid and/or Liquid Metal Collectors for Acyclic Machines," Final Report, Task 4 and 5, General Electric Co., Contract No. N00024-68-C-5415 (30 Sept. 1971), pp. 7-35.
- ⁶J. L. Johnson, G. T. Hummert, and A. R. Keeton, IEEE Trans. Power Appar. Syst. PAS-95, 1234 (1976).
- ⁷G. S. S. Ludford and J. S. Walker, in *MHD Flow and Turbulence II*, edited by H. Branover and A. Yakhot (Israel Universities, Jerusalem, 1980), pp. 83-95.
- ⁸H. Branover, *Magnetohydrodynamic Flow in Ducts* (Wiley, New York, 1978).
- ⁹J. C. R. Hunt and J. A. Shercliff, Ann Rev. Fluid Mech 3, (1971).
- ¹⁰W. F. Hughes and F. J. Young, *The Electromagnetodynamics of Fluids* (Wiley, New York, 1966).
- ¹¹S. H. Brown, P. J. Reilly, and N. A. Sondergaard, J. Appl. Phys. 62, 386 (1987).
- ¹²J. S. Walker, S. H. Brown, and N. A. Sondergaard, J. Appl. Phys. 64, 48 (1988).
- ¹³C. J. N. Alty, J. Fluid Mech. 48, 429 (1971).
- ¹⁴J. C. R. Hunt and D. G. Malcolm, J. Fluid Mech. 33, 775 (1968).
- ¹⁵D. G. Malcolm, Ph.D. thesis, University of Warwick, 1968.
- ¹⁶J. C. R. Hunt and K. Stewartson, J. Fluid Mech. 38, 225 (1969).
- ¹⁷L. D. Landau and E. M. Lifshitz, *Fluid Mechanics* (Pergamon, Addison-Wesley, Reading, MA, 1959).
- ¹⁸L. C. S. Utrecht, Math. Appl. Sci. 2, 531 (1980).
- ¹⁹L. P. Cook, G. S. S. Ludford, and J. S. Walker, Proc. Camb. Philos. Soc. 72, 117 (1972).
- ²⁰P. S. Morse and H. Feshbach, *Methods of Theoretical Physics (Part I)* (McGraw-Hill, New York, 1953), pp. 453-469

INITIAL DISTRIBUTION

Copies		Center Distribution		
		Copies	Code	Name
12	DTIC			
1	Dr. Ralph Burton	10	012.3	
	Mr. Gaines Burton	1	2702	
	Burton Technologies Incorp.	2	271	
	4940 B. North Boulevard	1	2710	
	Raleigh, North Carolina 27606	3	2711	
20	Dr. John S. Walker	20	2712	
	University of Illinois	1	5211	Knox
	at Urbana-Champaign	10	5211	Reports Control
	Department of Mechanical and	1	522.1	TIC (C)
	Industrial Engineering	1	522.2	TIC (A)
	144 Mechanical Engineering Building	2	5231	
	1206 West Green St.			
	Urbana, Illinois 61801			